

Random Subset Averaging*

Wenhao Cui

School of Economics and Management, Beihang University

and

Jie Hu [†]

Yau Mathematical Sciences Center, Tsinghua University

December 30, 2025

Abstract

We propose a new ensemble prediction method, Random Subset Averaging (RSA), tailored for settings with many covariates, particularly in the presence of strong correlations. RSA constructs candidate models via binomial random subset strategy and aggregates their predictions through a two-round weighting scheme, resulting in a structure analogous to a two-layer neural network. All tuning parameters are selected via cross-validation, requiring no prior knowledge of covariate relevance. We establish the asymptotic optimality of RSA under general conditions, allowing the first-round weights to be data-dependent, and demonstrate that RSA achieves a lower finite-sample risk bound under orthogonal design. Simulation studies demonstrate that RSA consistently delivers superior and stable predictive performance across a wide range of sample sizes, dimensional settings, sparsity levels and correlation structures, outperforming conventional model selection and ensemble learning methods. An empirical application to financial return forecasting further illustrates its practical utility.

Keywords: Ensemble learning; Random subset; Mallows criterion; Model uncertainty; High correlation

*We thank Yuhong Yang for useful comments. We also benefit a lot from the discussion with Jiandong Wang. Wenhao Cui gratefully acknowledges financial support from the National Natural Science Foundation of China (NSFC, 72473006, 72103014). Jie Hu's research is supported by the Postdoctoral Fellowship Program and China Postdoctoral Science Foundation under Grant Number BX20240182.

[†]Correspondence should be addressed to Jie Hu: <hujie_86@163.com>.

1 Introduction

Forecasting with limited sample sizes and many covariates poses significant challenges, especially when the number of covariates K grows with the sample size N as $K = CN^\alpha$, where $C > 0$ and $\alpha \in [0, 1]$. This setting encompasses low-dimensional ($\alpha = 0$), moderately high-dimensional ($0 < \alpha < 1$), and high-dimensional cases ($\alpha = 1, C > 1$). As K increases, including all covariates becomes impractical due to the curse of dimensionality, which inflates estimation error and weakens forecast performance. On the other hand, omitting relevant covariates risks information loss and degrades predictive accuracy. These difficulties are compounded by strong correlations among covariates, commonly observed in applications such as gene expression analysis, asset returns, and macroeconomic forecasting. While high correlation undermines parameter estimation due to near-singular design matrices, it can enhance forecast accuracy by enabling redundant covariates to serve as substitutes. The central question is how to leverage correlation structures effectively for prediction without succumbing to the adverse effects of multicollinearity when many covariates are available.

To address this challenge, we propose the Random Subset Averaging (RSA) method, a two-layer ensemble approach designed to improve both predictive accuracy and stability. RSA combines a binomial random subset strategy with a two-round weighting scheme to construct and aggregate multiple candidate models. In the first layer, RSA independently generates multiple predictions from candidate models of varying sizes, constructed using the binomial random subset strategy. In the second layer, these predictions are grouped and aggregated using convex weights. The final prediction is then obtained through a second-round convex aggregation across these groups. The binomial random subset strategy helps mitigate multicollinearity among covariates, producing well-conditioned design matrices with high probability, while maintaining sufficient model complexity to reduce misspecification bias. The two-round weighting scheme effectively balances model complexity and predictive

performance, yielding asymptotically optimal predictions. Overall, RSA is flexible, robust and performs well across a wide range of dimensional settings and correlation structures, with tuning parameters selected by cross validation.

Several existing approaches have attempted to address similar forecasting challenges, but each comes with its limitations. Model selection methods aim to identify a single best model using criteria such as AIC (Akaike 1974) and BIC (Schwarz 1978). However, these criteria typically ignore uncertainty in the selection process (Yuan & Yang 2005) and often overfit in high-dimensional settings (Bogdan et al. 2015, Chen & Chen 2008). Even their high-dimensional extensions (Owrang & Jansson 2018, Gohain & Jansson 2023, Pluntz et al. 2025) generally require a preliminary screening step, which introduces additional selection variability and further compromises robustness.

Variable selection methods, such as Lasso (Tibshirani 1996), Adaptive Lasso (Zou 2006), SCAD (Fan & Li 2001), and MCP (Zhang 2010), also target a single model by shrinking many coefficients toward zero. While these techniques are effective when the true model is sparse, they tend to underfit in the presence of dense signals. Moreover, their performance is highly sensitive to the choice of tuning parameters, resulting in unstable variable selection (Nan & Yang 2014) and volatile predictions, particularly when covariates are highly correlated.

To reduce the risk of relying on a single model, ensemble learning has emerged as a powerful alternative that combines multiple models to improve predictive accuracy and stability. A prominent class of ensemble methods originates from machine learning, including feature bagging (Ho 1998), random forests (Breiman 2001) and random subset regression (Elliott et al. 2013, Boot & Nibbering 2019). These methods construct base learners using random subspaces or data partitions, and aggregate their predictions, typically with equal weights, to enhance generalization. While computational efficient and well-suited for high-dimensional problems, these methods may exhibit systematic bias when the fixed subset

size misaligns with the true model complexity. Additionally, equal-weighted aggregation can be suboptimal, motivating efforts to design convex-weighted ensembles that better exploit model heterogeneity (Liang et al. 2011, Zhang et al. 2016).

From a statistical perspective, model averaging offers a complementary ensemble strategy aimed at mitigate model uncertainty by combining forecasts from a set of candidate models. These methods are particularly effective in dense settings (Peng & Yang 2022), but often rely on a known or well-ordered variable inclusion structure (Hansen 2007), which is rarely available in practice. Efforts to impose such orderings using solution paths from variable selection methods (Zhang et al. 2019) are vulnerable to selection instability, while non-nested averaging approaches (Wan et al. 2010) offer limited practical guidance for constructing meaningful candidate models.

The proposed RSA method addresses several key limitations of existing approaches. First, it provides a data-driven procedure for constructing non-nested candidate models, directly tackling the lack of guidance in current methods and eliminating the need for prior knowledge of variable ordering. Second, by allowing model sizes to vary across submodels, RSA reduces bias arising from fixed-size model misspecification, a common shortcoming of random subspace methods. Third, RSA employs a structured two-round convex weighting scheme that adaptively downweights weak predictors and enhances both forecast accuracy and stability, offering a principled alternative to equal-weighted ensembles. Finally, RSA is computationally efficient and inherently parallelizable, as submodels training within each layer can be easily distributed across processors. Collectively, these properties enable RSA to achieve strong predictive performance without incurring excessive computational burden.

The remainder of this study is organized as follows. Section 2 introduces RSA and explores its theoretical properties. Section 3 presents simulations to evaluate the finite-sample performance of RSA. The empirical analysis appears in Section 4, and Section 5 concludes

the study.

2 Random Subset Averaging and Its Properties

In Section 2.1, we present the RSA method for ensemble-based prediction. Section 2.2 analyses its theoretical properties, while Section 2.3 compares RSA to existing methods in an orthogonal setting to highlight its advantages.

2.1 The Random Subset Averaging Estimator

We consider a homoscedastic linear regression model throughout this study:

$$y_i = \mu_i + e_i, \text{ where } i = 1, 2, \dots, N, \text{ and } \mu_i = \sum_{j=1}^K \beta_j x_{ij} = x_i^\top \beta, \quad (2.1)$$

where $x_i = (x_{i1}, \dots, x_{iK})^\top$ and $\beta = (\beta_1, \dots, \beta_K)^\top$ are both K -dimensional column vectors. The number of regressors K are allowed to grow with the sample size N , e.g., $K = CN^\alpha, C > 0, \alpha \in [0, 1]$. The response variable y_i is real-valued, and we assume $E(e_i | x_i) = 0$ and $E(e_i^2 | x_i) = \sigma^2$. The model in Eq. (2.1) encompasses a broad class of commonly used statistical frameworks, including linear least squares regression and nonparametric series regression. Eq. (2.1) can also be expressed in matrix form as $Y = X\beta + e$, where Y is an $N \times 1$ response vector, X is an $N \times K$ design matrix, and the error term e satisfies $E(e | X) = 0$ and $E(ee^\top | X) = \sigma^2 I_N$.

RSA is an ensemble learning method designed to improve both prediction accuracy and stability. It combines a binomial random subset strategy with a two-round weighting scheme to address challenges arising from high dimensionality and strong correlations among covariates. This leads to a two-layer architecture, conceptually analogous to a shallow neural network, as illustrated in Figure 1. In the first layer, multiple predictions are generated

from models built on randomly selected subsets of covariates. In the second layer, disjoint subgroups of these predictions are aggregated using convex weights to produce a set of intermediate predictions. These are then further combined through a second round of convex weighting to yield the final prediction. The complete procedure is outlined below.

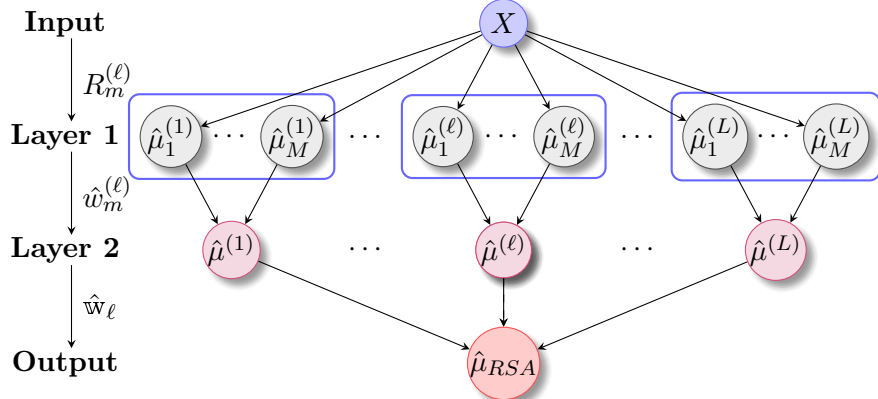


Figure 1: Graphical Illustration of RSA.

Design of the first layer. To fix ideas, let $R = \text{diag}(r_1, \dots, r_K)$ be a random selection matrix, where each r_j is an independent Bernoulli random variable with selection probability $p_j \in [0, 1]$. The resulting candidate model is given by $Y = XR\beta_R + U$, where XR represents a randomly selected subset of the original K covariates. The selection probabilities p_j can, in principle, vary across covariates to reflect prior beliefs or empirical relevance. However, determining optimal covariate-specific probabilities is a nontrivial task and is left for future work. For simplicity, we adopt a common selection probability p in both simulations and empirical analyses, yielding an expected subset size of Kp . This random selection acts as a form of dimension reduction, particularly valuable in high-dimensional settings.

Relying on a single selection matrix R for forecasting can result in unstable and potentially misspecified predictions, especially when important covariates are omitted. To address this issue, we independently generate random selection matrices $R_m^{(\ell)}$ for $m = 1, \dots, M$ and $\ell = 1, \dots, L$, thereby constructing L groups of M candidate models. The corresponding design matrices $XR_m^{(\ell)}$ are non-nested and vary in dimensionality, which helps reduce the

risk of model misspecification. Conventional ensemble methods aggregate predictions across all ML models simultaneously. In contrast, RSA adopts a hierarchical approach: it first averages predictions across the M models within each group ℓ , and then aggregates the resulting L group-level predictions. This two-layer structure enhances robustness across diverse scenarios, as shown in our simulations and empirical study. For each design matrix $XR_m^{(\ell)}$, the first-layer output is defined as its best linear prediction of Y , given by

$$\hat{\mu}_m^{(\ell)} = XR_m^{(\ell)} \hat{\beta}_{R_m^{(\ell)}} = XR_m^{(\ell)} (R_m^{(\ell)} X^\top X R_m^{(\ell)})^{-} R_m^{(\ell)} X^\top Y, \quad (2.2)$$

where A^{-} denotes the Moore–Penrose generalized inverse of matrix A .

Design of the second layer. Each element in the second layer is formed as a convex combination of the M predictions within group ℓ :

$$\hat{\mu}^{(\ell)} = \sum_{m=1}^M \hat{w}_m^{(\ell)} \hat{\mu}_m^{(\ell)}, \quad (2.3)$$

where the weights $\hat{w}_m^{(\ell)}$, for $m = 1, \dots, M$, may be either data-dependent or deterministic, and satisfy the constraint $\sum_{m=1}^M \hat{w}_m^{(\ell)} = 1$.

A simple choice is uniform weighting, $\hat{w}_m^{(\ell)} = 1/M$, which corresponds to naive averaging. More generally, this framework allows for data-driven weighting schemes such as Mallows model averaging, where the weights are obtained by solving the optimization problem

$$(\hat{w}_1^{(\ell)}, \dots, \hat{w}_M^{(\ell)}) = \arg \min_{(w_1, \dots, w_M) \in H_M} \left\| Y - \sum_{m=1}^M w_m \hat{\mu}_m^{(\ell)} \right\|^2 + 2\sigma^2 \sum_{m=1}^M w_m k_m^{(\ell)}, \quad (2.4)$$

where the weight set is defined as $H_M \equiv \{w \in [0, 1]^M : \sum_{m=1}^M w_m = 1\}$. Here, $k_m^{(\ell)}$ denotes the number of selected covariates in model m of group ℓ , which equals the trace of the projection matrix $P_{XR_m^{(\ell)}}$, with $P_A = A(A^\top A)^{-} A^\top$ for any matrix A .

Design of the output layer. To reduce the variability caused by randomness in model construction, we introduce a second-round aggregation step in the final prediction. Given the L group-level predictions $\hat{\mu}^{(\ell)}$ from the second layer, the final RSA estimator is formed as a convex combination:

$$\hat{\mu}_{RSA} = \sum_{\ell=1}^L \hat{w}_\ell \hat{\mu}^{(\ell)}, \quad (2.5)$$

where the weights are obtained by minimizing a Mallows criterion:

$$(\hat{w}_1, \dots, \hat{w}_L) = \arg \min_{(w_1, \dots, w_L) \in H_L} \left\| Y - \sum_{\ell=1}^L w_\ell \hat{\mu}^{(\ell)} \right\|^2 + 2\sigma^2 \sum_{\ell=1}^L w_\ell k^{(\ell)}, \quad (2.6)$$

with the feasible set defined as $H_L \equiv \{w \in [0, 1]^L : \sum_{\ell=1}^L w_\ell = 1\}$. Here, $k^{(\ell)} = \sum_{m=1}^M \hat{w}_m^{(\ell)} k_m^{(\ell)}$ denotes the effective model dimension associated with $\hat{\mu}^{(\ell)}$.

The second-round aggregation enhances robustness by stabilizing predictions, particularly in sparse settings where only a small subset of covariates is informative. In such cases, the individual predictors $\hat{\mu}_m^{(\ell)}$ may be weak or unstable, and the additional averaging step helps mitigate variability in the final prediction.

Remark 2.1. The proposed RSA method shares conceptual similarities with several well-established ensemble learning techniques, including dropout in neural networks, stacking, and random forests with feature bagging. Like dropout, which randomly deactivates neurons during training to implicitly average over subnetworks, RSA introduces randomness through covariate subsetting and performs explicit aggregation across multiple predictors. However, RSA differs by employing a structured two-round convex weighting scheme, making the aggregation process both tractable and broadly applicable to a wide class of base learners. Compared to stacking, which combines heterogeneous models trained on the same feature set, RSA promotes diversity through random covariate subspaces while maintaining a shared model structure. This distinction enables RSA to systematically capture variable

interactions and mitigate overfitting in high-dimensional settings. RSA also resembles random forests in its use of feature-level randomness, but it applies convex weighting rather than majority voting or unweighted averaging. In essence, RSA can be viewed as a general-purpose, structured ensemble method that draws on the strengths of dropout, stacking, and feature bagging, while offering greater flexibility and theoretical transparency through its two-layer architecture.

2.2 Asymptotic Optimality of Random Subset Averaging

In this section, we establish the asymptotic optimality of the RSA estimator defined in Eq. (2.5). A key difference from existing methods is that RSA permits data-dependent weighting in its first-round aggregation, so the final estimator is not necessarily linear. This additional flexibility improves performance but also complicates the derivation of theoretical guarantees.

Before presenting the theoretical results, we first introduce the necessary notations. Our analysis focuses on the squared L_2 loss function, $\mathcal{L}_N(\mathbf{w}) = (\hat{\mu}_{RSA}(\mathbf{w}) - \mu)^\top (\hat{\mu}_{RSA}(\mathbf{w}) - \mu)$, and its associated risk function, $\mathcal{R}_N(\mathbf{w}) = E[\mathcal{L}_N(\mathbf{w})|X, R]$, where the expectation is taken conditional on the full set of covariates X and all random selection matrices $R = \{R_m^{(\ell)} : m = 1, \dots, M, \ell = 1, \dots, L\}$. Further, we assume that the first-round weights $\hat{w}^{(\ell)} = (\hat{w}_1^{(\ell)}, \dots, \hat{w}_M^{(\ell)})^\top$ converge in probability to a deterministic (data-independent) limit $w^{(\ell)} = (w_1^{(\ell)}, \dots, w_M^{(\ell)})^\top$. Recall the RSA estimator with any second-round weights \mathbf{w} is expressed as:

$$\hat{\mu}_{RSA}(\mathbf{w}) = \sum_{\ell=1}^L \mathbf{w}_\ell \hat{\mu}^{(\ell)} = \sum_{\ell=1}^L \mathbf{w}_\ell \sum_{m=1}^M \hat{w}_m^{(\ell)} P_{X R_m^{(\ell)}} Y,$$

We define the asymptotic counterpart $\tilde{\mu}_{RSA}(\mathbf{w})$ by replacing the random weights $\hat{w}^{(\ell)}$ with

their probability limits $w^{(\ell)}$:

$$\tilde{\mu}_{RSA}(\mathbf{w}) = \sum_{\ell=1}^L \mathbf{w}_\ell \sum_{m=1}^M w_m^{(\ell)} P_{X R_m^{(\ell)}} Y.$$

The corresponding squared L_2 loss and risk functions are:

$$\tilde{\mathcal{L}}_N(\mathbf{w}) = (\tilde{\mu}_{RSA}(\mathbf{w}) - \mu)^\top (\tilde{\mu}_{RSA}(\mathbf{w}) - \mu), \quad \tilde{\mathcal{R}}_N(\mathbf{w}) = E [\tilde{\mathcal{L}}_N(\mathbf{w}) | X, R].$$

Theorem 2.1. *Let $\xi_N = \inf_{\mathbf{w} \in H_L} \tilde{\mathcal{R}}_N(\mathbf{w})$ and assume the following conditions hold:*

1. $E(e_i^4 | x_i) < \infty$.
2. $E[\|\hat{w}^{(\ell)} - w^{(\ell)}\|^4 | X, R] = O(r_{N,M}^4)$ for all $\ell = 1, \dots, L$.
3. $\xi_N^{-1} r_{N,M}^2 L M N \rightarrow 0$, $\xi_N^{-1} r_{N,M} L \sqrt{M N} \rightarrow 0$, and $\xi_N^{-1} L^2 \rightarrow 0$.

Then, we have

$$\frac{\mathcal{L}_N(\hat{\mathbf{w}})}{\inf_{\mathbf{w} \in H_L} \mathcal{L}_N(\mathbf{w})} \xrightarrow{p} 1.$$

Remark 2.2. Theorem 2.1 establishes the asymptotic optimality of the RSA estimator by showing that it achieves the asymptotically minimal loss. The validity of this result hinges on the condition $E[\|\hat{w}^{(\ell)} - w^{(\ell)}\|^4 | X, R] = O(r_{N,M}^4)$, where the rate $r_{N,M}$ depends on the estimation method for the first-round weights. For example, if the weights are obtained via simple averaging, i.e., $\hat{w}_m^{(\ell)} = w_m^{(\ell)} = 1/M$ for all $m = 1, \dots, M$, then the deviation vanishes, so $E[\|\hat{w}^{(\ell)} - w^{(\ell)}\|^4 | X, R] = 0$. In this case, $r_{N,M}$ can be chosen arbitrarily small, and condition (3) in Theorem 2.1 simplifies to $\xi_N^{-1} L^2 \rightarrow 0$, which imposes restrictions only on the number of disjoint groups. On the other hand, if the weights $\hat{w}_m^{(\ell)}$ are estimated using a parametric model, the standard convergence rate implies $r_{N,M} = M^{1/2} N^{-1/2}$. Consequently,

condition (3) becomes $\xi_N^{-1}LM^2 \rightarrow 0$ and $\xi_N^{-1}L^2 \rightarrow 0$, thereby placing additional constraints on the number of candidate models within each group.

Remark 2.3. In practice, we recommend estimating the first-round weights by optimizing the Mallows criterion in Eq. (2.4), since doing so implicitly guarantees asymptotic optimality for both $\hat{\mu}^{(\ell)}$ and $\hat{\mu}_{RSA}$. This optimization is equivalent to a constrained OLS problem. When the true parameter lies in the interior of the constraint set, the resulting estimator converges at the usual rate $\sqrt{M/N}$; if the constraint is binding, the convergence rate is even faster (see Remark 2.2 and Liew (1976)). Consequently, the condition $\xi_N^{-1}LM^2 \rightarrow 0$ implies $\left(\xi_N^{(\ell)}\right)^{-1}M^2 \rightarrow 0$ for each $\ell = 1, \dots, L$, where $\xi_N^{(\ell)} = \inf_{w \in H_M} E \left[\left\| \hat{\mu}^{(\ell)}(w) - \mu \right\|^2 | X, R \right]$ is the minimal risk in group ℓ . This implication holds because ξ_N , the global minimal model averaging risk, satisfies $\xi_N \leq \xi_N^{(\ell)}$. Together with Condition (1), this ensures the asymptotic optimality of each $\hat{\mu}^{(\ell)}$ as shown in Zhang (2021). Therefore, when both rounds employ Mallows criterion weighting, Theorem 2.1 establishes the asymptotic optimality of the full two-round convex weighting procedure.

Remark 2.4. As demonstrated in Remark 2.3, Theorem 2.1 establishes the asymptotic optimality of the two-round Mallows model averaging procedure. Moreover, the theorem remains valid and can be extended to a multi-round Mallows model averaging framework. However, from a practical standpoint, adding additional rounds increases computational cost at a polynomial rate. Therefore, we focus on the two-round procedure in this study. On the other hand, the proposed method is amenable to parallel implementation, which can substantially improve computational efficiency.

Remark 2.5. The performance of the proposed RSA estimator largely depends on the tuning parameters (p, M, L) . The parameter p governs the expected model size, with approximately Kp variables selected per candidate model, thereby directly controlling model complexity. The parameters M and L specify the number of candidate models and

the number of groups, respectively. We select (p, M, L) via 5-fold CV over a predefined grid, choosing the combination that yields the best predictive accuracy. Simulation results indicate that p plays the most critical role, as it determines the complexity of each candidate model. In contrast, M and L have a comparatively minor effect on RSA's performance, provided they are set to moderately large values (e.g., $L = 30$ in our simulations). See the heatmap figures in the supplementary materials for an illustration.

2.3 Risk Comparison under Orthogonal Covariates

In this section, we assess the performance of RSA in a simple setting and compare it with nested model averaging (MA), random projection regression (RPR), and random subset regression (RSR). Specifically, we consider the linear model

$$y_i = \sum_{j=1}^K \beta_j x_{ij} + e_i = x_i^\top \beta + e_i, \text{ for } i = 1, 2, \dots, N,$$

where the covariates are orthogonalized so that $X^\top X = NI_K$, and the error terms satisfy $E(e_i|x_i) = 0$ and $E(e_i^2|x_i) = \sigma^2$. For convenience, we arrange the covariates such that $|\beta_j|$ forms a non-increasing sequence of positive values, with $\sum_{j=1}^K \beta_j^2 < \infty$. This setting has been extensively studied in Peng & Yang (2022) and Peng et al. (2024) in the context of nested model averaging.

Under this setup, the following theorem characterizes the minimal squared L_2 risk of RSA when $M, L \rightarrow \infty$. We consider two scenarios: one in which $p_j = p$ is fixed across all covariates, and another in which p_j varies across covariates to reflect their relative importance. Throughout, we use the notation $A \asymp B$ to indicate that there exist positive constants C_1 and C_2 such that $C_1 A \leq B \leq C_2 A$ as $M, L \rightarrow \infty$.

Theorem 2.2. *Let $\xi_N = \inf_{w \in H_L} \tilde{\mathcal{R}}_N(w)$ denote the minimal squared L_2 risk. Under the*

orthogonal setup, when the selection probability is constant across covariates (i.e., $p_j = p$ for all j), we have

$$\xi_N \asymp \frac{K\sigma^2 \sum_{k=1}^K N\beta_k^2}{\sum_{k=1}^K N\beta_k^2 + K\sigma^2}.$$

Moreover, if the probabilities p_j are allowed to vary across covariates, the minimal risk becomes

$$\xi_N \asymp \sum_{k=1}^K \frac{N\beta_k^2 \sigma^2}{N\beta_k^2 + \sigma^2}.$$

Theorem 2.2 establishes an asymptotically valid lower bound for $\xi_N = \inf_{\mathbf{w} \in H_L} \tilde{\mathcal{R}}_N(\mathbf{w})$ as $M, L \rightarrow \infty$, while remaining applicable for any finite sample size N . In what follows, we compare the bound provided by Theorem 2.2 with those of several commonly used methods. Within the considered framework, most of these methods can be represented by the following parsimonious model:

$$y_i = x_i^\top R\beta_R + u_i,$$

where R is typically a data-driven random selection matrix that varies depending on the specific approach. For instance, model selection methods typically define R as a selection matrix that identifies the best subset of covariates according to a chosen information criterion. In principal component regression, R corresponds to the $K \times P$ matrix of principal component loadings associated with the top P eigenvalues. The nested model averaging method restricts R to sequentially select the first covariate, the first two, and so on, up to all covariates. Predictions based on each such R are then averaged, with weights determined by specific optimality criteria. The RPR method constructs the matrix R by independently drawing each entry from a standard normal distribution, scaled by $1/\sqrt{P}$, i.e., $R_{ij} \sim N(0, 1/P)$ for $1 \leq i \leq K$ and $1 \leq j \leq P$. The RSR method (Elliott et al. 2013,

Boot & Nibbering (2019) defines R as a $K \times P$ random selection matrix that selects P predictors uniformly at random from the original K covariates. Notably, P is fixed in their setting, and predictions are averaged using equal weights. The following lemma provides lower bounds for the nested model averaging, RPR, and RSR methods under the given setup.

Lemma 2.3. *Under the orthogonal setup, let ξ_N^{MA} , ξ_N^{RPR} , and ξ_N^{RSR} denote the minimal squared L_2 risks associated with MA, RPR, and RSR, respectively. Then we have the following results:*

$$\xi_N^{MA} = \sigma^2 + \sum_{j=2}^K \frac{N\beta_j^2\sigma^2}{N\beta_j^2 + \sigma^2}, \quad \xi_N^{RPR} = \xi_N^{RSR} = \frac{K\sigma^2 \sum_{j=1}^K N\beta_j^2}{\sum_{j=1}^K N\beta_j^2 + K\sigma^2},$$

where the minimum of ξ_N^{RPR} and ξ_N^{RSR} is achieved at $P = \frac{K \sum_{j=1}^K N\beta_j^2}{K\sigma^2 + \sum_{j=1}^K N\beta_j^2}$.

Lemma 2.3 extends Theorem 1 in Peng & Yang (2022), which compares nested model averaging with model selection. In addition to generalizing their result, the lemma provides explicit optimal risk bounds for both RPR and RSR, serving as benchmarks for evaluating the asymptotic risk of RSA. When the selection probability p_j is fixed across covariates, Theorem 2.2 and Lemma 2.3 together show that RSA asymptotically matches the performance of RPR and RSR:

$$\xi_N \asymp \xi_N^{RPR} = \xi_N^{RSR} = \frac{K\sigma^2 \sum_{j=1}^K N\beta_j^2}{\sum_{j=1}^K N\beta_j^2 + K\sigma^2}.$$

However, the performance of RSA can be further enhanced by allowing p_j to vary across covariates:

$$\xi_N \asymp \sum_{k=1}^K \frac{N\beta_k^2\sigma^2}{N\beta_k^2 + \sigma^2} \leq \xi_N^{RPR} = \xi_N^{RSR},$$

where this result is a direct consequence of Jensen's inequality. Moreover, RSA attains

strictly lower asymptotic risk than nested model averaging:

$$\xi_N \asymp \sum_{k=1}^K \frac{N\beta_k^2\sigma^2}{N\beta_k^2 + \sigma^2} < \xi_N^{MA} = \sigma^2 + \sum_{j=2}^K \frac{N\beta_j^2\sigma^2}{N\beta_j^2 + \sigma^2}.$$

The extent of improvement depends on the residual variance σ^2 and the size of the leading coefficients, particularly $|\beta_1|$. For fixed σ^2 , a smaller $|\beta_1|$ yields a lower asymptotic risk of RSA relative to MA, underscoring the advantage of RSA under weak covariate signals. These results demonstrate that, with properly chosen selection probabilities, RSA can outperform both nested model averaging and random subspace methods.

The asymptotic properties of nested model averaging are further analysed in [Peng et al. \(2024\)](#), where it is shown to achieve full asymptotic optimality under additional parameter conditions (see [Peng et al. \(2024\)](#) for a formal definition). Taken together, these findings underscore the strengths of RSA: it offers comparable or better asymptotic performance while providing greater flexibility in model construction.

Remark 2.6. The superior performance of RSA can alternatively be interpreted through its connection to shrinkage estimators, particularly the ridge regression estimator. In the orthogonal setting, the OLS estimator is given by $\hat{\beta} = \frac{1}{N}X^\top Y$, while the ridge estimator takes the form $\hat{\beta}_\lambda^{ridge} = \frac{N}{N+\lambda}\hat{\beta}$, where λ denotes the regularization (penalization) parameter. The RSA coefficient estimator can be expressed as $R\hat{\beta}_R = [R(R^\top X^\top X R)^{-1}R^\top] X^\top Y$ for a random selection matrix R . When the selection probability is uniform across covariates, we have $E_R[R\hat{\beta}_R] = p\hat{\beta}$, where p denotes the common selection probability. In contrast, when the selection probabilities vary across covariates, we obtain $E_R[R\hat{\beta}_R] = diag(\frac{N\beta_1^2}{\sigma^2+N\beta_1^2}, \dots, \frac{N\beta_K^2}{\sigma^2+N\beta_K^2})\hat{\beta}$. This comparison reveals that the selection probability p_j acts as a data-driven shrinkage factor. More generally, when p_j varies across covariates, RSA adaptively shrinks each component of the OLS estimator according to its signal-to-noise

ratio, $\frac{N\beta_j^2}{\sigma^2 + N\beta_j^2} \in [0, 1]$, thereby weighting each coefficient based on its relative importance.

3 Simulation Study

We conduct Monte Carlo simulations to evaluate the finite-sample performance of the proposed RSA method against several widely used benchmarks: RSR (Elliott et al. 2013, Boot & Nibbering 2019), Lasso (Tibshirani 1996), SCAD (Fan & Li 2001), MCP (Zhang 2010), parsimonious model averaging (PMA) (Zhang et al. 2019), Mallows model averaging (MMA) (Hansen 2007), and random forests (RF) (Breiman 2001). Lasso, SCAD, and MCP are standard tools for variable selection in high-dimensional settings, while MMA and PMA aggregate forecasts from multiple models, with PMA offering oracle-like performance when the true model is in the candidate set and remaining asymptotically optimal under misspecification. Both RSR and RF construct ensemble models by aggregating predictions from base learners trained on randomly selected subsets of covariates.

We consider the following linear data-generating process (DGP):

$$y_i = x_i^\top \beta + e_i, i = 1, \dots, N, \quad (3.1)$$

where $x_i \in \mathbb{R}^K$. We vary the sample size N , the number of covariates K , and the sparsity level of β to evaluate performance across different settings.

Throughout this section, we focus on one-step-ahead forecasting and evaluate out-of-sample accuracy using the Mean Squared Forecast Error (MSFE): $MSFE = \frac{1}{N_{test}} \sum_{i=1}^{N_{test}} (\hat{y}_i - x_i^\top \beta)^2$. Additionally, we report the Mean Squared Error (MSE) on the training data to assess in-sample fit: $MSE = \frac{1}{N_{train}} \sum_{i=1}^{N_{train}} (\hat{y}_i - x_i^\top \beta)^2$. The sample size of the training set is set to be twice that of the testing set.

Tuning parameters for all methods are selected via cross-validation when applicable. The

reported results are based on 500 simulation replications. We also employ the Model Confidence Set (MCS) test (Hansen et al. 2011) to formally compare the predictive performance between these methods.

Section 3.1 adapts the setting from Peng et al. (2024) to compare methods under both weak and strong correlation structures, focusing on whether RSA improves upon model selection and model averaging. Sections 3.2 and 3.3 extend the analysis to more general simulations where $K = CN^\alpha$, covering a range of dimensionalities and sparsity levels. Unlike Section 3.1, covariates are randomly ordered to reflect settings where variable importance is unknown, allowing us to identify conditions under which RSA performs well. Section 3.4 explores a more realistic case in which all covariates are predictive to varying degrees, their ordering is unknown, and the sample size is too small to include all variables. The combination of limited sample size and strong correlations presents a demanding setting to assess the robustness of RSA.

3.1 Performance Comparison under Peng et al. (2024)

Table 1: In-sample MSE results.

DGP	ρ	n	p	RSA.opt	RSA.fix	RSR	Lasso	SCAD	MCP	PMA	MMA	RF
poly	0.1	100	66	2.02	2.49	3.77	3.03	3.29	3.32	3.65	2.51	2.40
		300	200	2.09	3.24	4.67	3.42	3.52	3.50	4.91	2.92	3.02
		1000	666	2.43	4.17	5.56	3.97	3.80	3.80	6.29	3.38	3.70
	0.9	100	66	9.85	6.83	5.95	10.41	12.46	12.51	15.75	25.23	15.64
		300	200	6.73	6.56	7.79	10.93	13.94	14.01	24.72	33.61	24.68
		1000	666	6.63	6.65	9.21	12.85	15.92	15.87	35.22	41.86	35.57
exp	0.1	100	66	0.48	0.64	0.90	0.74	0.87	0.88	1.05	0.61	0.58
		300	200	0.50	0.79	1.07	0.78	0.81	0.80	1.20	0.66	0.70
		1000	666	0.49	0.85	1.13	0.74	0.64	0.64	1.30	0.63	0.75
	0.9	100	66	2.59	1.80	1.45	2.78	3.31	3.31	9.71	6.72	4.12
		300	200	1.55	1.55	1.81	2.64	3.35	3.33	12.51	7.95	5.93
		1000	666	1.26	1.24	1.90	2.47	2.97	2.97	11.43	7.80	7.02

Note: “poly” refers to polynomially decaying coefficients, while “exp” denotes exponentially decaying coefficients. RSA.opt represents the RSA method with CV-determined parameters, and RSA.fix refers to the RSA method with fixed parameters, specifically $M = L = 30$ and $p = 0.1$. Values in bold indicate the smallest MSE.

We follow the simulation setup of Peng et al. (2024), while allowing for correlated covariates.

Sample sizes are set to $N \in \{100, 300, 1000\}$ with $K = \lfloor 2N/3 \rfloor$ covariates, where $\lfloor \cdot \rfloor$ denotes the floor function. Covariates are drawn from a multivariate normal distribution with mean zero and covariance $\Sigma_{ij} = \rho^{|i-j|}$ for $\rho \in \{0.1, 0.9\}$. The case $\rho = 0.1$ approximates independent covariates as in Peng et al. (2024), while $\rho = 0.9$ introduces strong dependence, beyond the scope of their theory. The coefficients β_j follow either (i) polynomial decay $\beta_j = j^{-\alpha_1}$ with $\alpha_1 = 0.51$, or (ii) exponential decay $\beta_j = \exp(-j^{\alpha_2})$ with $\alpha_2 = 0.25$. Errors e_i are drawn from $N(0, \sigma_e^2)$, calibrated to yield a signal-to-noise ratio of 0.7, defined as $\frac{Var(x_i^\top \beta)}{Var(x_i^\top \beta) + \sigma_e^2}$.

Table 2: Out-of-sample MSFE results.

DGP	ρ	n	p	RSA.opt	RSA.fix	RSR	Lasso	SCAD	MCP	PMA	MMA	RF
poly	0.1	100	66	2.91	3.37	4.37	4.83	5.03	5.10	4.40	6.55	4.11
				(0.74)	(0.76)	(0.85)	(1.81)	(1.80)	(1.70)	(0.97)	(3.02)	(0.79)
		300	200	2.94	4.02	5.36	5.10	4.97	4.98	5.21	7.64	5.06
				(0.46)	(0.53)	(0.62)	(1.09)	(0.82)	(0.84)	(0.68)	(1.99)	(0.63)
		1000	666	3.33	4.91	6.35	5.61	5.25	5.24	6.37	8.83	6.14
				(0.28)	(0.34)	(0.39)	(0.65)	(0.52)	(0.51)	(0.39)	(1.21)	(0.39)
	0.9	100	66	11.73	7.63	6.58	12.78	15.40	15.73	18.54	65.09	11.46
				(4.30)	(3.06)	(2.77)	(11.08)	(8.20)	(9.80)	(6.46)	(30.61)	(3.79)
		300	200	7.06	6.94	8.53	12.07	15.94	16.00	27.58	87.67	18.12
				(1.74)	(1.84)	(2.17)	(4.91)	(3.95)	(3.96)	(11.36)	(22.50)	(3.14)
		1000	666	7.04	7.07	10.09	14.11	18.10	17.98	37.66	109.07	32.00
				(1.15)	(1.14)	(1.41)	(3.19)	(2.51)	(2.39)	(16.85)	(14.58)	(2.40)
exp	0.1	100	66	0.72	0.88	1.04	1.22	1.36	1.38	1.12	1.60	1.02
				(0.18)	(0.19)	(0.20)	(0.44)	(0.45)	(0.46)	(0.25)	(0.73)	(0.19)
		300	200	0.71	0.98	1.22	1.18	1.17	1.17	1.25	1.69	1.21
				(0.11)	(0.13)	(0.14)	(0.25)	(0.20)	(0.21)	(0.19)	(0.45)	(0.15)
		1000	666	0.66	1.00	1.28	0.98	0.85	0.85	1.32	1.62	1.26
				(0.06)	(0.07)	(0.08)	(0.13)	(0.10)	(0.11)	(0.13)	(0.24)	(0.08)
	0.9	100	66	3.08	2.01	1.59	3.40	4.09	4.13	10.38	17.30	2.98
				(1.13)	(0.79)	(0.71)	(2.94)	(2.19)	(2.45)	(2.32)	(8.11)	(0.99)
		300	200	1.64	1.64	1.98	2.91	3.79	3.77	13.08	20.46	4.08
				(0.43)	(0.43)	(0.52)	(1.18)	(0.97)	(0.94)	(1.86)	(5.41)	(0.73)
		1000	666	1.33	1.31	2.08	2.67	3.29	3.29	11.75	20.10	4.97
				(0.23)	(0.22)	(0.29)	(0.59)	(0.44)	(0.45)	(1.83)	(2.95)	(0.42)

Note: “poly” refers to polynomially decaying coefficients, while “exp” denotes exponentially decaying coefficients. RSA.opt represents the RSA method with CV-determined parameters and RSA.fix refers to the RSA method with fixed parameters, specifically $M = L = 30$ and $p = 0.1$. Values in bold indicate the top performers within the 95% MCS test while values in parentheses represent the standard deviation of the reported MSFEs.

Table 1 presents the MSE results for various methods, with the lowest MSE values highlighted in bold. Under low correlation ($\rho = 0.1$), RSA.opt, where parameters are determined via CV

method, consistently achieves the lowest MSE across all settings. Notably, the MMA method also performs competitively, particularly under the polynomial decay scenario, which is consistent with the findings of Peng & Yang (2022). In contrast, under high correlation ($\rho = 0.9$), RSA.opt outperforms all other methods when the sample size is large, while RSR exhibits the best performance in small-sample settings. The performance of PMA, MMA and RF deteriorates as the correlation increases.

Table 2 provides the corresponding MSFE results, with the best-performing models based on the 95% MCS test shown in bold. Consistent with the in-sample results, RSA.opt achieves the lowest MSFE in all settings where it also attains the lowest MSE. Moreover, RSA.opt exhibits the smallest standard deviations in MSFE, indicating stable predictive performance. RSR also performs well in cases where it yields the lowest MSE. Interestingly, MMA consistently records the highest MSFE across all settings, suggesting poor out-of-sample accuracy. In addition, the MSFE of random forests is at least 1.4 times higher than that of RSA.opt in all settings where RSA.opt performs best.

These simulations highlight RSA’s strong predictive performance, both in- and out-of-sample, comparing to the results in Peng & Yang (2022). While MMA outperforms variable selection under polynomial decay and matches performance under exponential decay, RSA shows consistent robustness across both patterns and outperforms RSR and RF despite their similarities. RSR, however, excels in high-correlation, small-sample settings, likely due to its fixed-size candidate models that reduce estimation variance compared to RSA’s varying-size models. As sample size grows, RSA’s variance decreases, improving its predictive accuracy.

3.2 MSFE Comparison under Polynomially Decaying Coefficients

In this section, we consider DGPs based on Eq. (3.1) to examine scenarios with varying dimensions and sparsity levels. Specifically, we use sample sizes $N \in \{200, 400, 800\}$, and

define the number of covariates as $K = \delta N$, where $\delta \in \{0.1, 0.5, 1, 1.5\}$. The number of nonzero coefficients in β , denoted K^* , is set to K when $\delta = 0.1$ and to $0.3K$ otherwise. This design covers both low- and high-dimensional settings with different levels of sparsity.

The nonzero elements in β are generated according to a polynomial decay structure: $\{j^{-0.51} : j = 1, \dots, K^*\}$ and are randomly placed within the vector β . The remaining coefficients are set to zero. This random placement means the nonzero entries do not follow a strict polynomial decay order within β . Notably, when $\delta \geq 1$, the number of covariates K exceeds the sample size N , making the conventional MMA method inapplicable.

We construct the variance-covariance matrix Σ as $\Sigma_{ij} = \rho^{|i-j|}$ for $i, j = 1, \dots, K$, where $\rho \in \{0.1, 0.9\}$ corresponds to low- and high-correlation settings, respectively. In the Appendix, we also report results based on a random correlation matrix, which reflects the complex dependency structures commonly encountered in empirical applications.

Table 3 reports the MSFE results when the covariates exhibit low correlation ($\rho = 0.1$). In the low-dimensional setting ($K = 20$), MMA achieves the best out-of-sample prediction accuracy. This advantage stems from the fact that MMA's candidate model set includes the true model, enabling it to effectively capture the underlying DGP. As the dimension increases to $K = 100$, variable selection methods such as SCAD and MCP show improved predictive performance. This improvement is due to their ability to exploit the sparsity of the coefficient vector under a low-correlation structure. However, in higher-dimensional settings with sparser coefficients (e.g., $K \geq \delta N, \delta \in \{1, 1.5\}$), RSA.opt consistently outperforms all other methods.

Table 4 presents the MSFE results under high-correlation settings ($\rho = 0.9$). Overall, RSA and RSR demonstrate improved predictive performance while other methods show a decline relative to the low-correlation results in Table 3. Notably, the RSA method with cross-validated parameters consistently outperforms RSR in all cases.

Table 3: MSFE comparison for $\rho = 0.1$ under polynomially decaying coefficients.

N	K	RSA.opt	RSA.fix	RSR	Lasso	SCAD	MCP	PMA	MMA	RF
200	20	0.61 (0.14)	1.49 (0.26)	3.21 (0.45)	0.21 (0.07)	0.21 (0.07)	0.21 (0.07)	0.83 (0.88)	0.21 (0.07)	1.76 (0.27)
	100	1.14 (0.23)	1.86 (0.33)	3.28 (0.48)	1.12 (0.32)	1.06 (0.33)	1.07 (0.33)	3.80 (0.70)	1.42 (0.38)	2.61 (0.41)
	200	2.00 (0.37)	2.64 (0.44)	3.90 (0.54)	2.58 (0.66)	2.48 (0.57)	2.49 (0.58)	4.74 (0.66)	1252.77 (4629.06)	3.57 (0.53)
	300	2.72 (0.44)	3.12 (0.47)	4.20 (0.59)	3.58 (0.87)	3.36 (0.67)	3.34 (0.67)	5.10 (0.73)	2099.73 (11486.63)	4.07 (0.59)
	400	0.98 (0.15)	2.10 (0.26)	3.77 (0.38)	0.24 (0.06)	0.24 (0.06)	0.24 (0.06)	1.56 (1.26)	0.23 (0.06)	2.35 (0.27)
	200	1.39 (0.19)	2.37 (0.29)	3.84 (0.38)	1.24 (0.25)	1.15 (0.24)	1.16 (0.25)	4.66 (0.52)	1.63 (0.30)	3.17 (0.34)
400	400	2.49 (0.30)	3.06 (0.35)	4.34 (0.42)	2.67 (0.56)	2.51 (0.39)	2.51 (0.41)	5.31 (0.52)	3034.59 (13774.41)	3.99 (0.40)
	600	3.01 (0.35)	3.57 (0.41)	4.75 (0.48)	3.60 (0.58)	3.41 (0.47)	3.39 (0.47)	5.77 (0.59)	5598.37 (22194.57)	4.57 (0.49)
	800	1.24 (0.13)	2.66 (0.24)	4.31 (0.31)	0.26 (0.05)	0.26 (0.05)	0.26 (0.05)	3.46 (1.25)	0.25 (0.05)	3.01 (0.24)
	1200	1.64 (0.15)	2.87 (0.25)	4.31 (0.31)	1.36 (0.20)	1.27 (0.17)	1.27 (0.17)	5.28 (0.41)	1.83 (0.23)	3.69 (0.29)
800	800	2.50 (0.21)	3.55 (0.27)	4.86 (0.33)	2.81 (0.36)	2.61 (0.27)	2.60 (0.26)	5.95 (0.42)	6500.56 (31323.1)	4.51 (0.32)
	1200	3.25 (0.26)	4.06 (0.32)	5.25 (0.37)	3.79 (0.46)	3.47 (0.36)	3.47 (0.34)	6.38 (0.45)	21301.89 (134399.61)	5.05 (0.37)

Note: RSA.opt represents the RSA method with CV-determined parameters and RSA.fix refers to the RSA method with fixed parameters, specifically $M = L = 30$ and $p = 0.1$. Values in bold indicate the top performers within the 95% MCS test while values in parentheses represent the standard deviation of the reported MSFEs.

The declined performance of Lasso, SCAD, MCP, PMA, and MMA aligns with theory: high correlation among covariates degrades OLS and variable selection methods by inflating the inverse Gram matrix and hindering identification of relevant predictors. This issue worsens when constructing candidate models in high dimensions. However, strong correlations can mitigate variable selection errors since highly correlated variables act as substitutes, helping maintain prediction accuracy despite different subsets being chosen. The reduction in MSFE for RSA and RSR under high correlation reflects the value of leveraging this structure. RSA's superior performance over RSR and RF stems from its adaptive design, combining models with varying covariate counts and applying a two-round convex weighting scheme. This flexibility allows RSA to remain robust even with severe multicollinearity.

Table 4: MSFE comparison for $\rho = 0.9$ under polynomially decaying coefficients.

N	K	RSA.opt	RSA.fix	RSR	Lasso	SCAD	MCP	PMA	MMA	RF		
200	20	0.77 (0.31)	0.85 (0.34)	2.31 (0.71)	0.89 (0.43)	1.39 (0.54)	1.39 (0.54)	5.17 (4.49)	1.56 (0.50)	1.93 (0.59)		
		1.11 (0.31)	1.12 (0.32)	1.82 (0.47)	1.53 (0.79)	2.10 (0.66)	2.11 (0.68)	15.84 (3.41)	5.88 (1.61)	3.72 (0.75)		
	100	1.98 (0.50)	1.87 (0.49)	2.30 (0.57)	3.03 (1.29)	3.90 (1.08)	3.85 (1.08)	20.01 (3.09)	5374.13 (20179.68)	6.99 (1.17)		
		300	2.46 (0.61)	2.51 (0.63)	2.74 (0.67)	4.38 (1.81)	5.43 (1.36)	5.46 (1.41)	21.77 (3.30)	9661.12 (49016.95)	9.51 (1.56)	
	400	0.91 (0.30)	1.03 (0.35)	2.97 (0.68)	1.08 (0.46)	1.74 (0.53)	1.72 (0.51)	10.95 (9.45)	2.13 (0.52)	3.08 (0.65)		
		200	1.15 (0.23)	1.27 (0.28)	2.07 (0.40)	1.59 (0.57)	2.23 (0.53)	2.22 (0.48)	19.78 (2.47)	6.88 (1.26)	5.70 (0.74)	
		400	1.80 (0.33)	2.01 (0.38)	2.56 (0.45)	2.97 (0.89)	3.92 (0.74)	3.96 (0.74)	22.19 (2.40)	12747.77 (58114.03)	9.65 (1.11)	
		600	2.42 (0.41)	2.59 (0.44)	2.94 (0.49)	4.43 (1.19)	5.60 (0.94)	5.58 (0.98)	23.19 (2.51)	19398.25 (66673.62)	12.11 (1.36)	
		800	0.85 (0.22)	1.28 (0.32)	3.41 (0.60)	1.21 (0.41)	1.91 (0.43)	1.91 (0.43)	27.72 (14.35)	2.54 (0.47)	5.51 (0.70)	
			400	1.17 (0.18)	1.49 (0.22)	2.29 (0.30)	1.60 (0.39)	2.27 (0.36)	2.28 (0.36)	22.06 (1.80)	7.54 (0.94)	8.45 (0.68)
			800	1.88 (0.22)	2.22 (0.28)	2.79 (0.33)	3.10 (0.66)	4.02 (0.51)	4.05 (0.51)	23.66 (1.84)	25391.34 (122901.14)	12.60 (1.00)
			1200	2.45 (0.29)	2.76 (0.33)	3.14 (0.37)	4.57 (0.86)	5.68 (0.72)	5.68 (0.70)	24.35 (1.78)	77271.42 (541851.1)	14.84 (1.10)

Note: RSA.opt represents the RSA method with CV-determined parameters and RSA.fix refers to the RSA method with fixed parameters, specifically $M = L = 30$ and $p = 0.1$. Values in bold indicate the top performers within the 95% MCS test while values in parentheses represent the standard deviation of the reported MSFEs.

3.3 MSFE Comparison under Exponentially Decaying Coefficients

In this section, we adopt a setup similar to that in Section 3.2, but the coefficients now follow an exponential decay pattern $\{\exp(-j^{0.25}) : j = 1, \dots, K^*\}$. This faster decay leads to smaller coefficients and fewer relevant covariates, resulting in a sparser setting than the polynomial decay case in Section 3.2.

Table 5 presents the MSFE results under an exponentially decaying coefficient structure with low covariate correlation ($\rho = 0.1$). Given this strong sparsity and weak correlation, variable selection methods with selection consistency are theoretically expected to perform well. Consistent with this expectation, model selection methods (Lasso, SCAD and MCP) generally outperform RSA when the sample size is large ($N = 800$). Their ability to

Table 5: MSFE comparison for $\rho = 0.1$ under exponentially decaying coefficient.

N	K	RSA.opt	RSA.fix	RSR	Lasso	SCAD	MCP	PMA	MMA	RF
200	20	0.16 (0.04)	0.40 (0.07)	0.72 (0.10)	0.05 (0.02)	0.05 (0.02)	0.05 (0.02)	0.28 (0.26)	0.05 (0.02)	0.44 (0.07)
	100	0.31 (0.06)	0.50 (0.09)	0.76 (0.11)	0.27 (0.08)	0.25 (0.08)	0.25 (0.08)	0.91 (0.14)	0.33 (0.09)	0.66 (0.10)
	200	0.54 (0.10)	0.71 (0.11)	0.92 (0.13)	0.66 (0.17)	0.67 (0.16)	0.67 (0.15)	1.13 (0.16)	298.97 (1104.25)	0.91 (0.13)
	300	0.72 (0.11)	0.82 (0.13)	0.99 (0.14)	0.90 (0.21)	0.90 (0.18)	0.89 (0.19)	1.34 (2.88)	482.05 (2409.93)	1.03 (0.15)
	400	0.27 (0.04)	0.57 (0.07)	0.90 (0.09)	0.06 (0.01)	0.06 (0.01)	0.06 (0.01)	0.55 (0.32)	0.06 (0.01)	0.62 (0.07)
	200	0.38 (0.05)	0.64 (0.08)	0.91 (0.09)	0.30 (0.06)	0.27 (0.06)	0.28 (0.06)	1.12 (0.12)	0.39 (0.07)	0.83 (0.09)
400	400	0.54 (0.07)	0.79 (0.09)	1.02 (0.10)	0.63 (0.13)	0.59 (0.10)	0.60 (0.10)	1.25 (0.12)	717.06 (3257.73)	1.01 (0.10)
	600	0.74 (0.08)	0.88 (0.10)	1.08 (0.11)	0.82 (0.14)	0.77 (0.12)	0.77 (0.12)	1.32 (0.13)	1435.04 (7092.35)	1.11 (0.12)
	800	0.34 (0.03)	0.71 (0.06)	1.03 (0.07)	0.06 (0.01)	0.06 (0.01)	0.06 (0.01)	0.94 (0.25)	0.06 (0.01)	0.79 (0.06)
	1200	0.42 (0.04)	0.75 (0.06)	1.01 (0.07)	0.32 (0.05)	0.28 (0.04)	0.28 (0.04)	1.25 (0.09)	0.43 (0.05)	0.94 (0.07)
800	800	0.56 (0.05)	0.85 (0.07)	1.08 (0.07)	0.58 (0.08)	0.51 (0.06)	0.51 (0.06)	1.33 (0.09)	1450.64 (7001.75)	1.07 (0.08)
	1200	0.72 (0.06)	0.91 (0.07)	1.13 (0.08)	0.72 (0.09)	0.62 (0.07)	0.61 (0.07)	1.37 (0.10)	4478.17 (28146.68)	1.13 (0.08)

Note: RSA.opt represents the RSA method with CV-determined parameters and RSA.fix refers to the RSA method with fixed parameters, specifically $M = L = 30$ and $p = 0.1$. Values in bold indicate the top performers within the 95% MCS test while values in parentheses represent the standard deviation of the reported MSFEs.

accurately identify and retain a small set of relevant covariates leads to superior predictive performance in sparse settings. However, when the sample size N is small with $K \geq N$, RSA.opt demonstrates superior performance. This result highlights the strength of RSA in balancing noise and signal, enabling robust predictions even when variable selection methods struggle due to limited sample size.

Table 6 reports the MSFE results under an exponentially decaying coefficient structure with high covariate correlation ($\rho = 0.9$). Consistent with the findings in Table 4, RSA.opt generally achieves the lowest MSFE values and the smallest standard deviations across most scenarios. Although the coefficients follow an exponential decay pattern, with the largest coefficient being $e^{-1} \approx 0.367$, the high correlation among covariates offers additional

Table 6: MSFE comparison for $\rho = 0.9$ under exponentially decaying coefficient.

N	K	RSA.opt	RSA.fix	RSR	Lasso	SCAD	MCP	PMA	MMA	RF
200	20	0.19 (0.08)	0.21 (0.08)	0.55 (0.17)	0.22 (0.11)	0.35 (0.14)	0.35 (0.14)	1.29 (1.16)	0.39 (0.12)	0.48 (0.14)
		0.28 (0.08)	0.29 (0.08)	0.44 (0.11)	0.40 (0.20)	0.55 (0.16)	0.55 (0.17)	4.07 (0.82)	1.51 (0.41)	0.96 (0.19)
	100	0.49 (0.13)	0.57 (0.13)	0.79 (0.33)	1.03 (0.27)	1.03 (0.30)	5.18 (0.79)	1392.54 (5207.58)	1.83 (0.31)	
		0.62 (0.15)	0.64 (0.16)	0.67 (0.46)	1.13 (0.33)	1.39 (0.35)	1.40 (0.35)	5.51 (0.83)	2395.98 (11621.9)	2.43 (0.40)
	400	0.23 (0.07)	0.27 (0.09)	0.75 (0.18)	0.28 (0.11)	0.46 (0.13)	0.46 (0.14)	2.92 (2.51)	0.56 (0.14)	0.81 (0.17)
		0.29 (0.06)	0.33 (0.07)	0.51 (0.10)	0.42 (0.15)	0.59 (0.13)	0.59 (0.13)	5.14 (0.62)	1.79 (0.33)	1.51 (0.19)
		0.44 (0.08)	0.50 (0.09)	0.61 (0.11)	0.75 (0.24)	0.98 (0.19)	0.97 (0.17)	5.43 (0.58)	3126.09 (14329.43)	2.39 (0.27)
		0.56 (0.09)	0.60 (0.10)	0.67 (0.11)	1.02 (0.28)	1.28 (0.21)	1.28 (0.22)	5.29 (0.57)	4668.08 (18234.6)	2.79 (0.31)
		0.21 (0.05)	0.33 (0.08)	0.86 (0.15)	0.32 (0.10)	0.50 (0.11)	0.50 (0.11)	7.17 (3.77)	0.66 (0.12)	1.43 (0.18)
		0.27 (0.04)	0.37 (0.05)	0.55 (0.07)	0.40 (0.10)	0.57 (0.09)	0.57 (0.09)	5.40 (0.43)	1.85 (0.23)	2.10 (0.17)
	800	0.41 (0.05)	0.49 (0.06)	0.61 (0.07)	0.67 (0.14)	0.86 (0.11)	0.86 (0.12)	5.05 (0.40)	5422.47 (26350.37)	2.71 (0.21)
		0.49 (0.06)	0.56 (0.06)	0.64 (0.07)	0.86 (0.16)	1.05 (0.13)	1.05 (0.13)	4.63 (0.34)	15244.75 (117302.17)	2.82 (0.21)

Note: RSA.opt represents the RSA method with CV-determined parameters and RSA.fix refers to the RSA method with fixed parameters, specifically $M = L = 30$ and $p = 0.1$. Values in bold indicate the top performers within the 95% MCS test while values in parentheses represent the standard deviation of the reported MSFEs.

predictive advantages. By exploiting this structure, RSA maintains stable prediction even when individual signals are weak. In contrast, both model averaging and variable selection methods suffer efficiency loss due to multicollinearity, resulting in worse predictive performance compared to Table 5.

Based on the results in Table 2-6, several key conclusions merge. First, when covariates exhibit low correlation, RSA with cross-validated parameters generally achieves the highest predictive accuracy, both in sample and out of sample, provided that the ratio K/N is not too small, i.e., at least 50% in our simulation settings. This advantage persists even under a random covariance structure. The main exception arises in highly sparse settings, where variable selection methods outperform RSA when the sample size is sufficiently large. This

is because such methods can accurately recover the small number of relevant variables with enough observations. Second, when covariates exhibit high correlation, the RSA method consistently achieves the lowest MSFE values and standard deviations. This superior performance stems from RSA’s ability to leverage shared information among correlated covariates, combined with its two-round convex weighting scheme, which effectively balances model complexity and prediction accuracy.

3.4 MSFE Comparison under Many Relevant Covariates

Sections 3.1 to 3.3 demonstrate RSA’s strong performance in high-dimensional settings with correlated covariates. Here, we examine a practical scenario with many potentially relevant covariates but limited sample size. The relatively small sample size makes it infeasible to include all relevant variables in a single model and undermines the selection consistency of variable selection methods. In contrast, RSA and, to some extent, RSR should be more robust by aggregating predictions from multiple smaller models. We also expect RSA to outperform RSR due to its binomial random subset strategy and two-round convex weighting scheme.

In this section, we set $N \in \{100, 300\}$ and define the number of covariates as $K = \delta N$, where $\delta \in \{1, 1.25, 1.5\}$. The values in coefficient vector β follow either a polynomial decay $\beta_j = j^{-0.51}$ or an exponential decay $\beta_j = \exp(-j^{0.25})$ for $j = 1, \dots, K$. Although all entries in β are nonzero, the exponential decay results in a sparser effective structure. The MSFE results for these two decay patterns are summarized in Tables 7 and 8.

Under low correlation ($\rho = 0.1$), the RSA method consistently outperforms alternative approaches across all sample sizes. In contrast, under high correlation ($\rho = 0.9$), RSA demonstrate superior performance in large-sample cases, whereas RSR yields the best results when the sample size is small. This pattern is consistent with the findings for $N = 100$

and $K = 66$ reported in Table 2. As previously discussed, RSR restricts each candidate model to a fixed number of covariates, whereas RSA allows the number of covariates to vary following a binomial distribution. Consequently, RSA has a positive probability of generating candidate models with a large number of covariates. When the sample size is small, these larger models with strong covariate correlations exhibit high estimation variability, resulting in reduced prediction accuracy. However, as the sample size increases, this variability diminishes, leading to improved predictive performance of RSA.

In conclusion, our comprehensive simulation study demonstrates that the proposed RSA estimator delivers robust and superior out-of-sample predictive performance across a wide range of scenarios. Supplementary result on the corresponding in-sample MSE further indi-

Table 7: MSFE comparison under many relevant covariates: polynomial decay.

ρ	N	K	RSA.opt	RSA.fix	RSR	Lasso	SCAD	MCP	PMA	MMA	RF
0.1	100	100	2.69 (0.67)	3.56 (0.80)	4.61 (0.93)	4.44 (1.54)	4.88 (1.37)	4.87 (1.42)	6.50 (15.31)	898.83 (6474.73)	4.56 (0.95)
		125	3.35 (0.83)	3.85 (0.87)	4.71 (0.96)	5.21 (1.67)	5.37 (1.56)	5.39 (1.53)	21.02 (277.39)	1549.41 (5665.41)	4.85 (1.01)
		150	3.63 (0.85)	4.22 (0.90)	5.03 (1.01)	5.89 (6.55)	5.85 (1.56)	5.77 (1.50)	7.76 (9.62)	8229.52 (153316.30)	5.21 (1.08)
		300	2.92 (0.41)	4.22 (0.54)	5.41 (0.62)	4.56 (0.92)	4.78 (0.71)	4.74 (0.72)	6.75 (0.76)	3319.90 (14965.20)	5.39 (0.62)
		375	3.37 (0.47)	4.47 (0.58)	5.57 (0.65)	5.23 (0.95)	5.28 (0.82)	5.30 (0.82)	6.91 (0.79)	5151.08 (30728.98)	5.68 (0.69)
		450	3.75 (0.53)	4.75 (0.61)	5.76 (0.71)	5.77 (1.02)	5.70 (0.87)	5.68 (0.86)	7.13 (0.86)	5684.13 (43094.06)	5.95 (0.73)
	300	100	7.54 (2.59)	5.33 (1.98)	4.83 (2.11)	9.34 (6.41)	12.08 (4.45)	12.03 (4.45)	56.79 (11.85)	8497.01 (54431.83)	16.87 (4.86)
		125	6.25 (2.34)	6.30 (2.30)	5.00 (2.16)	11.57 (6.62)	14.81 (5.13)	14.76 (5.07)	61.31 (47.51)	15229.04 (62152.35)	19.92 (4.77)
		150	7.09 (2.42)	7.03 (2.37)	5.85 (2.29)	13.85 (8.14)	17.38 (5.85)	17.35 (5.82)	64.19 (57.79)	56559.38 (1032865.60)	23.43 (5.67)
		300	5.25 (1.16)	5.01 (1.12)	5.32 (1.20)	8.50 (3.08)	12.21 (2.37)	12.17 (2.48)	64.96 (7.60)	32901.66 (155784.91)	27.07 (3.56)
		375	5.21 (1.10)	5.76 (1.23)	5.67 (1.26)	10.27 (3.21)	14.46 (2.67)	14.44 (2.63)	65.64 (7.68)	41115.53 (218154.66)	30.73 (4.07)
		450	6.01 (1.26)	6.35 (1.38)	6.12 (1.40)	12.53 (4.11)	17.09 (3.48)	17.15 (3.41)	66.36 (7.33)	59918.21 (620869.72)	33.57 (4.14)

Note: RSA.opt represents the RSA method with CV-determined parameters and RSA.fix refers to the RSA method with fixed parameters, specifically $M = L = 30$ and $p = 0.1$. Values in bold indicate the top performers within the 95% MCS test while values in parentheses represent the standard deviation of the reported MSFEs.

Table 8: MSFE comparison when the number of relevant variables exceeds the sample size: exponential decay.

ρ	N	K	RSA.opt	RSA.fix	RSR	Lasso	SCAD	MCP	PMA	MMA	RF
0.1	100	100	0.69 (0.17)	0.92 (0.20)	1.09 (0.22)	1.14 (0.39)	1.31 (0.35)	1.31 (0.36)	2.00 (9.33)	215.77 (1582.33)	1.13 (0.23)
		125	0.82 (0.20)	0.97 (0.21)	1.11 (0.22)	1.33 (0.71)	1.40 (0.40)	1.42 (0.39)	5.04 (67.87)	359.47 (1292.30)	1.17 (0.24)
		150	0.88 (0.19)	1.04 (0.22)	1.17 (0.24)	1.40 (0.43)	1.47 (0.37)	1.47 (0.37)	2.40 (6.25)	2001.00 (38688.69)	1.24 (0.25)
		300	0.71 (0.10)	0.96 (0.12)	1.18 (0.14)	0.95 (0.20)	0.99 (0.17)	0.99 (0.16)	1.46 (0.16)	721.09 (3283.14)	1.21 (0.14)
		375	0.74 (0.10)	0.98 (0.13)	1.17 (0.13)	1.04 (0.20)	1.06 (0.17)	1.06 (0.17)	1.45 (0.16)	1074.12 (6160.16)	1.23 (0.15)
	300	450	0.80 (0.11)	1.01 (0.13)	1.19 (0.15)	1.12 (0.22)	1.10 (0.18)	1.10 (0.18)	1.46 (0.18)	1148.36 (8067.96)	1.26 (0.16)
		100	1.34 (0.50)	1.34 (0.49)	1.20 (0.53)	2.25 (1.41)	3.05 (1.08)	3.07 (1.13)	14.42 (2.99)	2154.20 (13891.07)	4.31 (1.23)
		125	1.53 (0.57)	1.54 (0.56)	1.21 (0.53)	2.84 (1.62)	3.64 (1.30)	3.60 (1.21)	14.91 (8.08)	3726.38 (15231.68)	4.89 (1.17)
		150	1.68 (0.58)	1.67 (0.56)	1.38 (0.54)	3.26 (1.88)	4.09 (1.45)	4.04 (1.43)	14.52 (2.90)	13739.08 (252244.56)	5.56 (1.35)
		375	0.96 (0.20)	1.01 (0.22)	1.08 (0.24)	1.72 (0.66)	2.40 (0.48)	2.37 (0.46)	12.78 (1.50)	6487.98 (30865.55)	5.31 (0.70)
		450	0.98 (0.20)	1.08 (0.22)	1.08 (0.23)	1.87 (0.54)	2.62 (0.50)	2.62 (0.49)	11.93 (1.40)	7457.24 (39109.44)	5.57 (0.74)

Note: RSA.opt represents the RSA method with CV-determined parameters and RSA.fix refers to the RSA method with fixed parameters, specifically $M = L = 30$ and $p = 0.1$. Values in bold indicate the top performers within the 95% MCS test while values in parentheses represent the standard deviation of the reported MSFEs.

cate that RSA, when tuned via CV, consistently achieves the lowest MSE in settings where it also attains the lowest MSFE, highlighting its strong training performance. Nonetheless, RSA may be suboptimal in certain cases, such as small sample sizes with highly correlated covariates, or large samples with extremely sparse coefficient structures, where alternative methods may perform better. Crucially, these limiting scenarios are readily identifiable in practice, allowing practitioners to make informed decisions about the applicability of RSA. In more complex or ambiguous settings, RSA provides a statistically reliable and computationally efficient baseline for predictive modelling.

4 Empirical Illustration on Asset Return Forecasting

Predicting asset returns remains a central challenge in financial economics, with far-reaching implications for portfolio construction, risk management, and market efficiency. Early studies, such as [Fama & French \(1993\)](#), emphasized the role of fundamental factors, including size (SMB) and value (HML). Since then, a growing body of research has identified hundreds of potential return predictors, often referred to as the “Factor Zoo” ([Cochrane 2011](#)). While factor-based models can exhibit strong in-sample predictive power, many proposed factors lack robustness. Their performance often deteriorates out of sample, particularly after publication ([McLean & Pontiff 2016](#)), or becomes negligible once microcap stocks and liquidity constraints are accounted for ([Chen & Zimmermann 2021](#)).

The proliferation of predictors highlights a key challenge in high-dimensional forecasting: although many covariates may carry valuable signals, incorporating them indiscriminately risks overfitting. Recent work has sought to mitigate this issue by focusing on theoretically motivated factors ([Fama & French 2015](#)) or employing machine learning methods for dimension reduction ([Gu et al. 2020](#)). Consequently, much of the literature has emphasized factor selection ([Feng et al. 2020](#), [Wan et al. 2024](#), [Hwang & Rubesam 2022](#)). In contrast, our approach shifts the focus from selecting a subset of predictors to systematically exploiting the full information contained in the entire set of covariates for return prediction.

We evaluate the performance of RSA relative to competing methods using the high-frequency factor dataset constructed by [Pelger \(2019\)](#), which is well-suited for high-dimensional forecasting. The dataset comprises 332 U.S. stocks and was originally used to extract a set of latent factors via high-frequency principal component analysis. Its high dimensionality and strong factor correlations reflect the challenges RSA is designed to address. To mitigate microstructure frictions inherent in high-frequency data, we aggregate intraday returns into daily observations, yielding 3,270 time series spanning January 2004 to December 2016.

These series are then used to forecast daily S&P 500 returns. To account for potential structural breaks, particularly those associated with the 2008–2009 financial crisis, we exclude the crisis period and divide the sample into pre-crisis (2004–2007) and post-crisis (2010–2016) subperiods.

As shown in Figure 2, the predictive factors exhibit strong correlations in both subperiods. Such multicollinearity can undermine the effectiveness of popular factor selection methods such as Lasso. To be fair, we orthogonalize the predictors prior to estimation. We adopt a rolling-window forecasting framework, using a 252-day estimation window to predict returns up to 22 days ahead, reflecting a realistic investment horizon, approximately one year of past data to forecast one month forward.

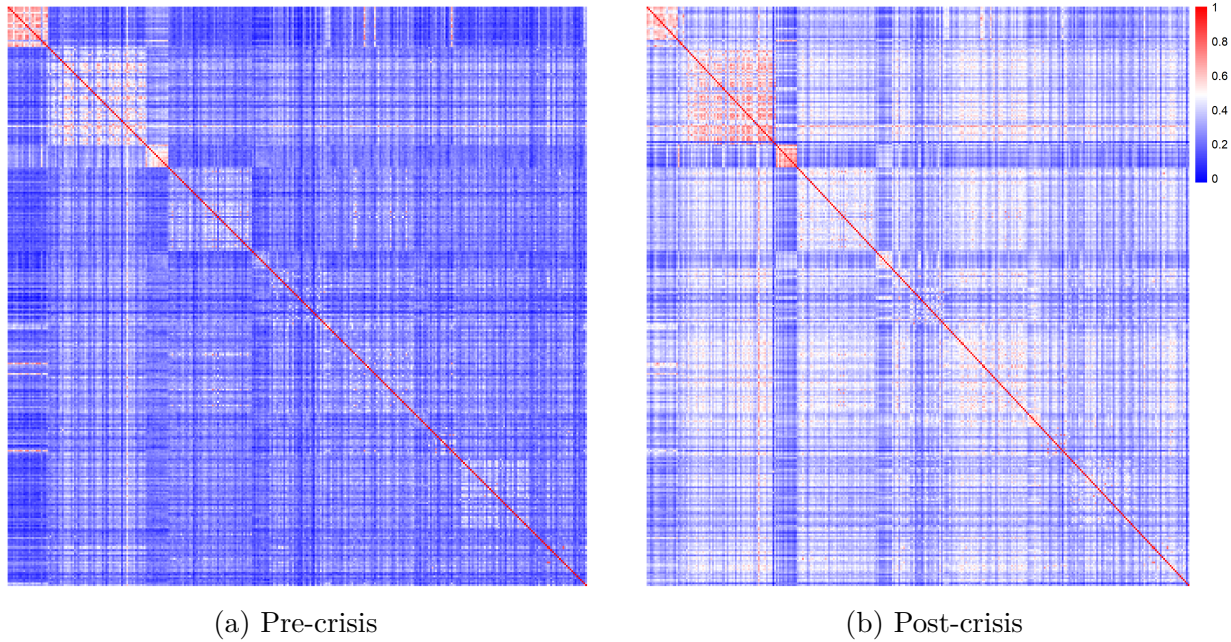


Figure 2: Correlation between original factors

We compare RSA against several alternatives: Lasso, SCAD, and MCP as selection-based methods; RSR and RF due to their conceptual similarity to RSA in ensemble prediction; and PMA as a representative model averaging approach for high-dimensional settings. Predictive performance is assessed using the daily MSFE. The training dataset consisting of 332 orthogonalized factors but only 252 observations, represents the low-correlation,

high-dimensional scenario discussed in Section 3.4, regardless of factor strength. Since RSA with CV-tuned parameters consistently outperforms its fixed-parameter counterpart, our empirical analysis focuses exclusively on the CV-selected configuration.

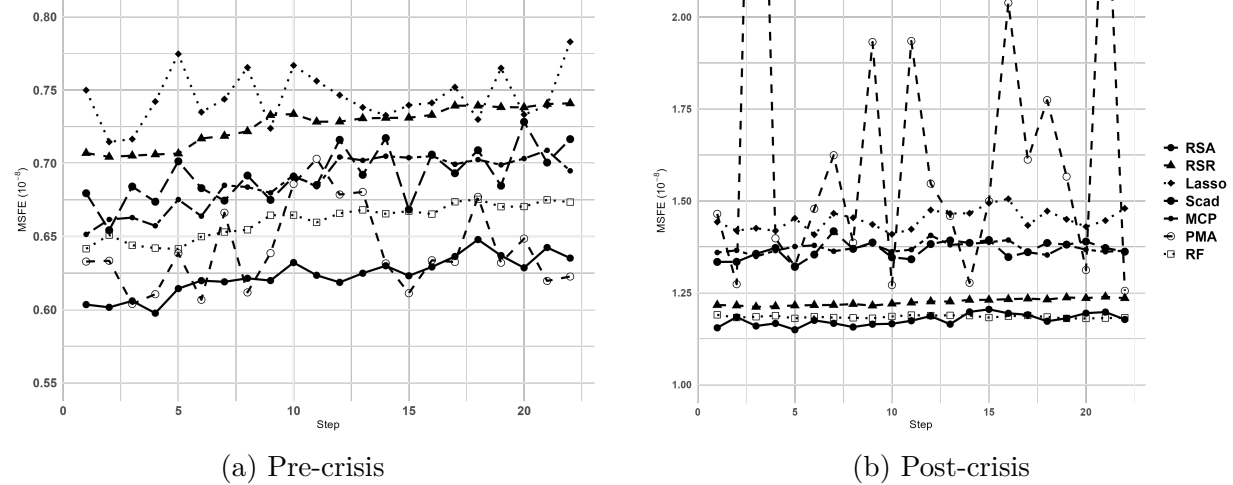


Figure 3: Mean of MSFE for each period.

Figure 3 compares the MSFE of RSA with competing methods during the pre-crisis and post-crisis periods, with standard deviations within each forecast horizon reported in the Appendix. In the pre-crisis period, RSA consistently achieves the lowest or second-lowest MSFE across the 22-day horizon, along with smaller variability both within and across horizons compared to all other methods. In the post-crisis period, macroeconomic shocks, such as the European sovereign debt crisis, increased the volatility of S&P 500 returns, raising prediction errors for all methods. Even so, RSA maintains the lowest and most stable MSFE throughout, whereas RSR and RF remain stable but with slightly higher errors. The selection methods (Lasso, SCAD, MCP) and the model averaging method (PMA) exhibit similar trajectories but with uniformly higher and more volatile MSFE.

RSA’s superior out-of-sample performance does not come at the expense of training error. As shown in the supplementary results, RSA attains comparable or even lower training error than competing methods when using CV-selected tuning parameters. These findings confirm the strong and stable predictive performance of RSA.

5 Conclusions

This paper proposes Random Subset Averaging (RSA), a new ensemble method for high-dimensional forecasting with complex covariate correlations. RSA constructs candidate models via binomial random subset strategy and aggregates them through a two-round convex weighting scheme, striking a balance between model complexity and predictive accuracy, while enhancing predictive stability. We establish its asymptotic optimality under general conditions with data-dependent first-round weights, and derive finite-sample risk bounds under orthogonal designs. Theoretical analysis shows that RSA can outperform both nested model averaging and random subspace methods when selection probabilities are optimally tuned. Simulations and an empirical application further demonstrate RSA’s consistent advantages over variable selection, model averaging, and machine-learning-based ensembles.

While RSA shares conceptual similarities with ensemble methods such as dropout, stacking, and random forests, it is distinguished by its structured two-layer architecture and convex aggregation scheme. These design features not only improve robustness and computational tractability but also provide a foundation for rigorous theoretical guarantees. As a result, RSA offers a principled, computationally feasible, and empirically effective approach to high-dimensional prediction, particularly in settings with model uncertainty or strong covariate multicollinearity. Looking ahead, RSA may be extended to broader modeling frameworks, including classification tasks, generalized linear models, and adaptive or multi-layer ensemble designs.

6 Disclosure statement

The authors declare no conflict of interest.

7 Data Availability Statement

The data that support the findings of this study are openly available in The Journal of Finance at <https://doi.org/10.1111/jofi.12898>.

References

Akaike, H. (1974), ‘A new look at the statistical model identification’, *IEEE Transactions on Automatic Control* **19**(6), 716–723.

Bogdan, M., Van Den Berg, E., Sabatti, C., Su, W. & Candès, E. J. (2015), ‘Slope—adaptive variable selection via convex optimization’, *The Annals of Applied Statistics* **9**(3), 1103.

Boot, T. & Nibbering, D. (2019), ‘Forecasting using random subspace methods’, *Journal of Econometrics* **209**(2), 391–406.

Breiman, L. (2001), ‘Random forests’, *Machine Learning* **45**, 5–32.

Chen, A. Y. & Zimmermann, T. (2021), ‘Open source cross-sectional asset pricing’, *Critical Finance Review* **10**(1), 1–40.

Chen, J. & Chen, Z. (2008), ‘Extended bayesian information criteria for model selection with large model spaces’, *Biometrika* **95**(3), 759–771.

Cochrane, J. H. (2011), ‘Presidential address: Discount rates’, *The Journal of Finance* **66**(4), 1047–1108.

Elliott, G., Gargano, A. & Timmermann, A. (2013), ‘Complete subset regressions’, *Journal of Econometrics* **177**(2), 357–373.

Fama, E. F. & French, K. R. (1993), ‘Common risk factors in the returns on stocks and bonds’, *Journal of Financial Economics* **33**(1), 3–56.

Fama, E. F. & French, K. R. (2015), ‘A five-factor asset pricing model’, *Journal of Financial Economics* **116**(1), 1–22.

Fan, J. & Li, R. (2001), ‘Variable selection via nonconcave penalized likelihood and its oracle properties’, *Journal of the American Statistical Association* **96**(456), 1348–1360.

Feng, G., Giglio, S. & Xiu, D. (2020), ‘Taming the factor zoo: A test of new factors’, *The Journal of Finance* **75**(3), 1327–1370.

Gohain, P. B. & Jansson, M. (2023), ‘Robust information criterion for model selection in sparse high-dimensional linear regression models’, *IEEE Transactions on Signal Processing* **71**, 2251–2266.

Gu, S., Kelly, B. & Xiu, D. (2020), ‘Empirical asset pricing via machine learning’, *The Review of Financial Studies* **33**(5), 2223–2273.

Hansen, B. E. (2007), ‘Least squares model averaging’, *Econometrica* **75**(4), 1175–1189.

Hansen, P. R., Lunde, A. & Nason, J. M. (2011), ‘The model confidence set’, *Econometrica* **79**(2), 453–497.

Ho, T. K. (1998), ‘The random subspace method for constructing decision forests’, *IEEE Transactions on Pattern Analysis and Machine Intelligence* **20**(8), 832–844.

Hwang, S. & Rubesam, A. (2022), ‘Bayesian selection of asset pricing factors using individual stocks’, *Journal of Financial Econometrics* **20**(4), 716–761.

Ishwaran, H. & Kogalur, U. (2023), *Fast Unified Random Forests for Survival, Regression, and Classification (RF-SRC)*. R package version 3.2.3.

URL: <https://cran.r-project.org/package=randomForestSRC>

Liang, H., Zou, G., Wan, A. T. & Zhang, X. (2011), ‘Optimal weight choice for frequentist

model average estimators', *Journal of the American Statistical Association* **106**(495), 1053–1066.

Liew, C. K. (1976), 'Inequality constrained least-squares estimation', *Journal of the American Statistical Association* **71**(355), 746–751.

McLean, R. D. & Pontiff, J. (2016), 'Does academic research destroy stock return predictability?', *The Journal of Finance* **71**(1), 5–32.

Nan, Y. & Yang, Y. (2014), 'Variable selection diagnostics measures for high-dimensional regression', *Journal of Computational and Graphical Statistics* **23**(3), 636–656.

Owrang, A. & Jansson, M. (2018), 'A model selection criterion for high-dimensional linear regression', *IEEE Transactions on Signal Processing* **66**(13), 3436–3446.

Pelger, M. (2019), 'Understanding systematic risk: A high-frequency approach', *The Journal of Finance* .

Peng, J., Li, Y. & Yang, Y. (2024), 'On optimality of mallows model averaging', *Journal of the American Statistical Association* pp. 1–12.

Peng, J. & Yang, Y. (2022), 'On improbability of model selection by model averaging', *Journal of Econometrics* **229**(2), 246–262.

Pluntz, M., Dalmasso, C., Tubert-Bitter, P. & Ahmed, I. (2025), 'A simple information criterion for variable selection in high-dimensional regression', *Statistics in Medicine* **44**(1-2), e10275.

Schwarz, G. (1978), 'Estimating the Dimension of a Model', *Annals of Statistics* **6**(2), 461–464.

Thanei, G.-A., Heinze, C. & Meinshausen, N. (2017), 'Random projections for large-scale regression', *Big and Complex Data Analysis: Methodologies and Applications* pp. 51–68.

Tibshirani, R. (1996), ‘Regression shrinkage and selection via the lasso’, *Journal of the Royal Statistical Society Series B: Statistical Methodology* **58**(1), 267–288.

Wan, A. T., Zhang, X. & Zou, G. (2010), ‘Least squares model averaging by Mallows criterion’, *Journal of Econometrics* **156**(2), 277–283.

Wan, R., Li, Y., Lu, W. & Song, R. (2024), ‘Mining the factor zoo: Estimation of latent factor models with sufficient proxies’, *Journal of Econometrics* **239**(2), 105386.

Yuan, Z. & Yang, Y. (2005), ‘Combining linear regression models: When and how?’, *Journal of the American Statistical Association* **100**(472), 1202–1214.

Zhang, C. H. (2010), ‘Nearly unbiased variable selection under minimax concave penalty’, *Annals of Statistics* **38**(2), 894–942.

Zhang, X. (2021), ‘A new study on asymptotic optimality of least squares model averaging’, *Econometric Theory* **37**(2), 388–407.

Zhang, X., Ullah, A. & Zhao, S. (2016), ‘On the dominance of mallows model averaging estimator over ordinary least squares estimator’, *Economics Letters* **142**, 69–73.

Zhang, X., Zou, G., Liang, H. & Carroll, R. J. (2019), ‘Parsimonious model averaging with a diverging number of parameters’, *Journal of the American Statistical Association* .

Zou, H. (2006), ‘The adaptive lasso and its oracle properties’, *Journal of the American Statistical Association* **101**(476), 1418–1429.

Appendices

A Proofs

Proof of Theorem 2.1. For clarity, denote

$$\begin{aligned}\mathcal{C}_N(\mathbf{w}) &= \|Y - \hat{\mu}_{RSA}(\mathbf{w})\|^2 + 2\sigma^2 \sum_{\ell=1}^L \mathbf{w}_\ell \sum_{m=1}^M \hat{w}_m^{(\ell)} k_m^{(\ell)}, \\ \tilde{\mathcal{C}}_N(\mathbf{w}) &= \|Y - \tilde{\mu}_{RSA}(\mathbf{w})\|^2 + 2\sigma^2 \sum_{\ell=1}^L \mathbf{w}_\ell \sum_{m=1}^M w_m^{(\ell)} k_m^{(\ell)}.\end{aligned}$$

With above defined notations, to establish the claim of the theorem, by Lemma 3 in [Zhang \(2021\)](#) we need to show the following relationships:

$$\sup_{\mathbf{w}} \left| \frac{\mathcal{C}_N(\mathbf{w}) - \mathcal{L}_N(\mathbf{w}) - \|e\|^2}{\mathcal{R}_N(\mathbf{w})} \right| \xrightarrow{p} 0, \text{ and } \sup_{\mathbf{w}} \left| \frac{\mathcal{L}_N(\mathbf{w})}{\mathcal{R}_N(\mathbf{w})} - 1 \right| \xrightarrow{p} 0.$$

On the other hand, the above two relationships are implied by the following relationships:

$$\sup_{\mathbf{w}} \left| \frac{\mathcal{R}_N(\mathbf{w}) - \tilde{\mathcal{R}}_N(\mathbf{w})}{\tilde{\mathcal{R}}_N(\mathbf{w})} \right| \rightarrow 0, \tag{A.1}$$

$$\sup_{\mathbf{w}} \left| \frac{\mathcal{C}_N(\mathbf{w}) - \tilde{\mathcal{C}}_N(\mathbf{w}) - \mathcal{L}_N(\mathbf{w}) + \tilde{\mathcal{L}}_N(\mathbf{w})}{\tilde{\mathcal{R}}_N(\mathbf{w})} \right| \xrightarrow{p} 0, \tag{A.2}$$

$$\sup_{\mathbf{w}} \left| \frac{\mathcal{L}_N(\mathbf{w}) - \tilde{\mathcal{L}}_N(\mathbf{w})}{\tilde{\mathcal{R}}_N(\mathbf{w})} \right| \xrightarrow{p} 0, \tag{A.3}$$

$$\sup_{\mathbf{w}} \left| \frac{\tilde{\mathcal{C}}_N(\mathbf{w}) - \tilde{\mathcal{L}}_N(\mathbf{w}) - \|e\|^2}{\tilde{\mathcal{R}}_N(\mathbf{w})} \right| \xrightarrow{p} 0, \tag{A.4}$$

$$\sup_{\mathbf{w}} \left| \frac{\tilde{\mathcal{L}}_N(\mathbf{w}) - \tilde{\mathcal{R}}_N(\mathbf{w})}{\tilde{\mathcal{R}}_N(\mathbf{w})} \right| \xrightarrow{p} 0. \tag{A.5}$$

In particular, Eqs. (A.1), (A.2), and (A.4) imply the first relationship, while the second relationship follows from Eqs. (A.1), (A.3), and (A.5). Below, we prove each term

individually.

Proof of Eq. (A.1): By calculation, we have

$$\begin{aligned}
\sup_{\mathbf{w}} \frac{|\mathcal{R}_N(\mathbf{w}) - \tilde{\mathcal{R}}_N(\mathbf{w})|}{\tilde{\mathcal{R}}_N(\mathbf{w})} &\leq \sup_{\mathbf{w}} \frac{E \left[\|\hat{\mu}_{RSA}(\mathbf{w}) - \tilde{\mu}_{RSA}(\mathbf{w})\|^2 | X, R \right]}{\tilde{\mathcal{R}}_N(\mathbf{w})} \\
&\quad + 2 \sup_{\mathbf{w}} \frac{E[(\hat{\mu}_{RSA}(\mathbf{w}) - \tilde{\mu}_{RSA}(\mathbf{w}))^\top (\tilde{\mu}_{RSA}(\mathbf{w}) - \mu) | X, R]}{\tilde{\mathcal{R}}_N(\mathbf{w})} \\
&\leq \sup_{\mathbf{w}} \frac{E \left[\|\hat{\mu}_{RSA}(\mathbf{w}) - \tilde{\mu}_{RSA}(\mathbf{w})\|^2 | X, R \right]}{\tilde{\mathcal{R}}_N(\mathbf{w})} \\
&\quad + 2 \sup_{\mathbf{w}} \sqrt{\frac{E \left[\|\hat{\mu}_{RSA}(\mathbf{w}) - \tilde{\mu}_{RSA}(\mathbf{w})\|^2 | X, R \right]}{\tilde{\mathcal{R}}_N(\mathbf{w})}},
\end{aligned}$$

where we utilize the triangular inequality and Cauchy-Schwarz inequality in the first and second steps. Thus to prove Eq. (A.1), it is sufficient to prove $\sup_{\mathbf{w}} \frac{E \left[\|\hat{\mu}_{RSA}(\mathbf{w}) - \tilde{\mu}_{RSA}(\mathbf{w})\|^2 | X, R \right]}{\tilde{\mathcal{R}}_N(\mathbf{w})} \rightarrow 0$.

To prove this, we have

$$\begin{aligned}
&\sup_{\mathbf{w}} \frac{E \left[\|\hat{\mu}_{RSA}(\mathbf{w}) - \tilde{\mu}_{RSA}(\mathbf{w})\|^2 | X, R \right]}{\tilde{\mathcal{R}}_N(\mathbf{w})} \\
&\leq \xi_N^{-1} \sup_{\mathbf{w}} E \left[\|\hat{\mu}_{RSA}(\mathbf{w}) - \tilde{\mu}_{RSA}(\mathbf{w})\|^2 | X, R \right] \\
&= \xi_N^{-1} \sup_{\mathbf{w}} E \left[\left\| \sum_{\ell=1}^L \mathbf{w}_\ell \sum_{m=1}^M [\hat{w}_m^{(\ell)} - w_m^{(\ell)}] P_{X R_m^{(\ell)}} Y \right\|^2 | X, R \right] \\
&\leq \xi_N^{-1} \sum_{\ell=1}^L \sqrt{E[\|\hat{w}^{(\ell)} - w^{(\ell)}\|^4 | X, R]} \sqrt{E \left[\left(\sum_{m=1}^M \|P_{X R_m^{(\ell)}} Y\|^2 \right)^2 \right]} \\
&= O(\xi_N^{-1} r_{N,M}^2 L M N) = o(1).
\end{aligned}$$

Here, we use the relationship that

$$E \left[\|P_{X R_m^{(\ell)}} Y\|^4 \right] \leq E[\|Y\|^4] = O(N^2),$$

where the inequality is due to the fact that $P_{X R_m^{(\ell)}}$ is a projection matrix. Consequently, its

maximal eigenvalue is bounded above by 1.

Proof of Eq. (A.2): By direct calculation, Eq. (A.2) is implied by the following relationships:

$$\sup_{\mathbf{w}} \frac{\left| e^\top \sum_{\ell=1}^L \mathbf{w}_\ell \sum_{m=1}^M [\hat{w}_m^{(\ell)} - w_m^{(\ell)}] P_{X R_m^{(\ell)}} \mu \right|}{\tilde{\mathcal{R}}_N(\mathbf{w})} \xrightarrow{p} 0, \quad (\text{A.6})$$

$$\sup_{\mathbf{w}} \frac{\left| e^\top \sum_{\ell=1}^L \mathbf{w}_\ell \sum_{m=1}^M [\hat{w}_m^{(\ell)} - w_m^{(\ell)}] P_{X R_m^{(\ell)}} e - \sigma^2 \sum_{\ell=1}^L \mathbf{w}_\ell \sum_{m=1}^M [\hat{w}_m^{(\ell)} - w_m^{(\ell)}] k_m^{(\ell)} \right|}{\tilde{\mathcal{R}}_N(\mathbf{w})} \xrightarrow{p} 0. \quad (\text{A.7})$$

For Eq. (A.6), we have

$$\begin{aligned} & \sup_{\mathbf{w}} \frac{\left| e^\top \sum_{\ell=1}^L \mathbf{w}_\ell \sum_{m=1}^M [\hat{w}_m^{(\ell)} - w_m^{(\ell)}] P_{X R_m^{(\ell)}} \mu \right|}{\tilde{\mathcal{R}}_N(\mathbf{w})} \\ & \leq \xi_N^{-1} \sum_{\ell=1}^L \|\hat{w}^{(\ell)} - w^{(\ell)}\| \sqrt{\sum_{m=1}^M (e^\top P_{X R_m^{(\ell)}} \mu)^2} \\ & = O_p(\xi_N^{-1} r_{N,M} L \sqrt{MN}) = o_p(1), \end{aligned}$$

where the last lines follows from the observation that

$$E[(e^\top P_{X R_m^{(\ell)}} \mu)^2 | X, R] = \sigma^2 \text{trace}(\mu^\top P_{X R_m^{(\ell)}} \mu) \leq \sigma^2 \|\mu\|^2 = O(N).$$

For Eq. (A.7), we have

$$\begin{aligned} & \sup_{\mathbf{w}} \frac{\left| e^\top \sum_{\ell=1}^L \mathbf{w}_\ell \sum_{m=1}^M [\hat{w}_m^{(\ell)} - w_m^{(\ell)}] P_{X R_m^{(\ell)}} e - \sigma^2 \sum_{\ell=1}^L \mathbf{w}_\ell \sum_{m=1}^M [\hat{w}_m^{(\ell)} - w_m^{(\ell)}] k_m^{(\ell)} \right|}{\tilde{\mathcal{R}}_N(\mathbf{w})} \\ & \leq \xi_N^{-1} \sum_{\ell=1}^L \|\hat{w}^{(\ell)} - w^{(\ell)}\| \sqrt{\sum_{m=1}^M (e^\top P_{X R_m^{(\ell)}} e - \sigma^2 k_m^{(\ell)})^2} \\ & = O_p \left(\xi_N^{-1} r_{N,M} \sum_{\ell=1}^L \sqrt{\sum_{m=1}^M k_m^{(\ell)}} \right) = O_p(\xi_N^{-1} r_{N,M} L \sqrt{MN}) = o_p(1), \end{aligned}$$

where we use Lemma 2 in [Zhang \(2021\)](#), which implies that $(e^\top P_{X R_m^{(\ell)}} e - \sigma^2 k_m^{(\ell)})^2 = O_p(k_m^{(\ell)})$.

And the last line also follows from the observation that $k_m^{(\ell)} \leq N$ for all m and ℓ .

Proof of Eq. (A.3): We have

$$\begin{aligned} & \sup_w \frac{|\mathcal{L}_N(w) - \tilde{\mathcal{L}}_N(w)|}{\tilde{\mathcal{R}}_N(w)} \\ & \leq \sup_w \frac{\|\hat{\mu}_{RSA}(w) - \tilde{\mu}_{RSA}(w)\|^2}{\tilde{\mathcal{R}}_N(w)} + 2 \sup_w \frac{|(\hat{\mu}_{RSA}(w) - \tilde{\mu}_{RSA}(w))^\top (\tilde{\mu}_{RSA}(w) - \mu)|}{\tilde{\mathcal{R}}_N(w)} \\ & \leq \sup_w \frac{\|\hat{\mu}_{RSA}(w) - \tilde{\mu}_{RSA}(w)\|^2}{\tilde{\mathcal{R}}_N(w)} + 2 \sup_w \sqrt{\frac{\|\hat{\mu}_{RSA}(w) - \tilde{\mu}_{RSA}(w)\|^2}{\tilde{\mathcal{R}}_N(w)}} \sup_w \sqrt{\frac{\tilde{\mathcal{L}}_N(w)}{\tilde{\mathcal{R}}_N(w)}}, \end{aligned}$$

where the first relationship follows from the triangular inequality, and the second relationship follows from the Cauchy-Schwarz inequality. Consequently, it is sufficient to prove the following two relationships:

$$\sup_w \frac{\|\hat{\mu}_{RSA}(w) - \tilde{\mu}_{RSA}(w)\|^2}{\tilde{\mathcal{R}}_N(w)} \xrightarrow{p} 0, \quad (\text{A.8})$$

$$\sup_w \frac{\tilde{\mathcal{L}}_N(w)}{\tilde{\mathcal{R}}_N(w)} \xrightarrow{p} 1. \quad (\text{A.9})$$

In particular, following similar argument as in the proof of Eq. (A.1), we have

$$\begin{aligned} \sup_w \frac{\|\hat{\mu}_{RSA}(w) - \tilde{\mu}_{RSA}(w)\|^2}{\tilde{\mathcal{R}}_N(w)} & \leq \xi_N^{-1} \sup_w \|\hat{\mu}_{RSA}(w) - \tilde{\mu}_{RSA}(w)\|^2 \\ & \leq \xi_N^{-1} \sum_{\ell=1}^L \|\hat{w}^{(\ell)} - w^{(\ell)}\|^2 \left(\sum_{m=1}^M \|P_{X R_m^{(\ell)}} Y\|^2 \right) \\ & = O_p(\xi_N^{-1} r_{N,M}^2 L M N) = o_p(1). \end{aligned}$$

This proves Eq. (A.8). Eq. (A.9) is implied by Eq. (A.5), which we will establish later.

Proof of Eq. (A.4): By direct calculation, it is sufficient to verify the following relationships:

$$\sup_{\mathbf{w}} \frac{|e^\top \mathcal{A}(\mathbf{w}) u|}{\tilde{\mathcal{R}}_N(\mathbf{w})} \xrightarrow{p} 0, \quad (\text{A.10})$$

$$\sup_{\mathbf{w}} \frac{|e^\top \mathcal{B}(\mathbf{w}) e - \sigma^2 \sum_{\ell=1}^L \mathbf{w}_\ell \sum_{m=1}^M w_m^{(\ell)} k_m^{(\ell)}|}{\tilde{\mathcal{R}}_N(\mathbf{w})} \xrightarrow{p} 0, \quad (\text{A.11})$$

where $\mathcal{B}(\mathbf{w}) = \sum_{\ell=1}^L \mathbf{w}_\ell \sum_{m=1}^M w_m^{(\ell)} P_{X R_m^{(\ell)}}$ and $\mathcal{A}(\mathbf{w}) = I - \mathcal{B}(\mathbf{w})$. We first consider Eq. (A.10). For clarity denote $\mathcal{A}_\ell = I - \mathcal{B}_\ell$, where $\mathcal{B}_\ell = \sum_{m=1}^M w_m^{(\ell)} P_{X R_m^{(\ell)}}$. Furthermore, denote $\mathcal{B} = (\mathcal{B}_1^\top, \dots, \mathcal{B}_L^\top)^\top$ and $\mathcal{A} = (\mathcal{A}_1^\top, \dots, \mathcal{A}_L^\top)^\top$. In the following, we also denote $\Phi = (\mu^\top \mathcal{A}_\ell \mathcal{A}_s \mu)_{L \times L} = \mathcal{G}^\top \mathcal{G}$, where $\mathcal{G} = (\mathcal{A}_1 \mu, \dots, \mathcal{A}_L \mu)$. Let $\Psi = \{\sigma^2 \text{trace}(\mathcal{B}_\ell \mathcal{B}_s)\}_{L \times L}$, and $\Psi_0 = \sigma^2 \text{diag}(\text{trace}(\mathcal{B}_1^2), \dots, \text{trace}(\mathcal{B}_L^2))$, respectively. Additionally, note that we have the following bound for $\tilde{\mathcal{R}}_N(\mathbf{w})$:

$$\begin{aligned} \tilde{\mathcal{R}}_N(\mathbf{w}) &= E[\|\tilde{\mu}_{RSA}(\mathbf{w}) - \mu\|^2 | X, R] = \mathbf{w}^\top \mu^\top \mathcal{A} \mathcal{A} \mu \mathbf{w} + \mathbf{w}^\top \mathcal{B} \mathcal{B} \mathbf{w} \\ &= \mathbf{w}^\top (\Phi + \Psi) \mathbf{w} \geq \mathbf{w}^\top (\Phi + \Psi_0) \mathbf{w}, \end{aligned}$$

where the last relation is due to the relationship that $w_m^{(\ell)} \in [0, 1]$ and $\text{trace}(P_{X R_m^{(\ell)}}) \geq 0$. To this end, define $\rho = (e^\top \mathcal{A}_1 \mu, \dots, e^\top \mathcal{A}_L \mu)^\top$, and it is straightforward to verify that $E[\rho | X, R] = 0$, and $\text{Var}(\rho | X, R) = E[(e^\top \mathcal{A}_\ell \mu \mu^\top \mathcal{A}_s e)_{L \times L} | X, R] = \sigma^2 \Phi$. Using Lemma 1 in Zhang (2021), we have

$$\begin{aligned} \sup_{\mathbf{w}} \frac{|e^\top \mathcal{A}(\mathbf{w}) u|^2}{\tilde{\mathcal{R}}_N(\mathbf{w})^2} &= \sup_{\mathbf{w}} \frac{\left| \sum_{\ell=1}^L \mathbf{w}_\ell e^\top \mathcal{A}_\ell u \right|^2}{\tilde{\mathcal{R}}_N(\mathbf{w})^2} \leq \sup_{\mathbf{w}} \frac{(\mathbf{w}^\top \rho)^2}{\tilde{\mathcal{R}}_N(\mathbf{w})} \sup_{\mathbf{w}} \frac{1}{\tilde{\mathcal{R}}_N(\mathbf{w})} \\ &\leq \xi_N^{-1} \sup_{\mathbf{w}} \frac{(\mathbf{w}^\top \rho)^2}{\mathbf{w}^\top (\Phi + \Psi_0) \mathbf{w}} \leq \xi_N^{-1} \rho^\top (\Phi + \Psi_0)^{-1} \rho = O_p(\xi_N^{-1} L) = o_p(1), \end{aligned}$$

where the quadratic term $\rho^\top (\Phi + \Psi_0)^{-1} \rho$ could be bounded as

$$E[\rho^\top (\Phi + \Psi_0)^{-1} \rho | X, R] = \sigma^2 \text{trace}((\Phi + \Psi_0)^{-1} \Phi) = O(L).$$

Next, we prove Eq. (A.11), let $\tau = (\sigma^2 \text{trace}(\mathcal{B}_1) - e^\top \mathcal{B}_1 e, \dots, \sigma^2 \text{trace}(\mathcal{B}_L) - e^\top \mathcal{B}_L e)^\top$.

Again, we have $E[\tau|X, R] = 0$, and by Lemma 2 in [Zhang \(2021\)](#),

$$\text{Var}(\tau|X, R) = E[\tau\tau^\top|X, R] = \{2\sigma^4 \text{trace}(\mathcal{B}_\ell \mathcal{B}_s) + \kappa \text{trace}(\mathcal{B}_\ell * \mathcal{B}_s)\}_{L \times L},$$

where $*$ denotes the Hadamard product, and $\kappa = E[e_i^4] - 3\sigma^4$. Then by Lemma 1 in [Zhang \(2021\)](#), we have

$$\begin{aligned} & \sup_{\mathbf{w}} \frac{\left| e^\top \mathcal{B}(\mathbf{w}) e - \sigma^2 \sum_{\ell=1}^L \mathbf{w}_\ell \sum_{m=1}^M w_m^{(\ell)} k_m^{(\ell)} \right|^2}{\tilde{\mathcal{R}}_N(\mathbf{w})^2} = \sup_{\mathbf{w}} \frac{(\mathbf{w}^\top \tau)^2}{\tilde{\mathcal{R}}_N(\mathbf{w})^2} \\ & \leq \xi_N^{-1} \sup_{\mathbf{w}} \frac{(\mathbf{w}^\top \tau)^2}{\mathbf{w}^\top (\Phi + \Psi_0) \mathbf{w}} \leq \xi_N^{-1} \sup_{\mathbf{w}} \frac{(\mathbf{w}^\top \tau)^2}{\mathbf{w}^\top \Psi_0 \mathbf{w}} \leq \xi_N^{-1} \tau^\top \Psi_0^{-1} \tau. \end{aligned}$$

To bound the quadratic term $\tau^\top \Psi_0^{-1} \tau$ in the above display, consider its expectation

$$\begin{aligned} E[\tau^\top \Psi_0^{-1} \tau|X, R] &= \text{trace} \left(\Psi_0^{-1} \{2\sigma^4 \text{trace}(\mathcal{B}_\ell \mathcal{B}_s) + \kappa \text{trace}(\mathcal{B}_\ell * \mathcal{B}_s)\}_{L \times L} \right) \\ &= \text{trace} \left(\Psi_0^{-1} \text{diag} \{2\sigma^4 \text{trace}(\mathcal{B}_\ell^2) + \kappa \text{trace}(\mathcal{B}_\ell * \mathcal{B}_\ell); \ell = 1, \dots, L\} \right) \\ &\leq \text{trace} \left(\Psi_0^{-1} \text{diag} \{(2\sigma^4 + \kappa) \text{trace}(\mathcal{B}_\ell^2); \ell = 1, \dots, L\} \right) = O(L), \end{aligned}$$

where the second line holds since Ψ_0 is a diagonal matrix, and last line follows from the observation that for any symmetric matrix O , $\text{trace}(O * O) \leq \text{trace}(O^2)$. This implies that Eq. (A.11) holds.

Proof of Eq. (A.5): Once again, Eq. (A.5) is implicitly implied by the following two relationships:

$$\sup_{\mathbf{w}} \frac{\left| e^\top \mathcal{B}(\mathbf{w}) \mathcal{A}(\mathbf{w}) \mu \right|}{\tilde{\mathcal{R}}_N(\mathbf{w})} \xrightarrow{p} 0, \quad (\text{A.12})$$

$$\sup_{\mathbf{w}} \frac{\left| \sigma^2 \text{trace}(\mathcal{B}(\mathbf{w})^2) - e^\top \mathcal{B}(\mathbf{w})^2 e \right|}{\tilde{\mathcal{R}}_N(\mathbf{w})} \xrightarrow{p} 0. \quad (\text{A.13})$$

To establish Eq. (A.12), note that $E[\mathcal{G}^\top \mathcal{B}_\ell e | X, R] = 0$, and

$$Var(\mathcal{G}^\top \mathcal{B}_\ell e | X, R) = E[\mathcal{G}^\top \mathcal{B}_\ell e e^\top \mathcal{B}_\ell \mathcal{G} | X, R] = \sigma^2 trace(\mathcal{B}_\ell \mathcal{G} \mathcal{G}^\top \mathcal{B}_\ell).$$

By Lemma 1 in [Zhang \(2021\)](#), we have

$$\begin{aligned} & \sup_w \frac{|e^\top \mathcal{B}(w) \mathcal{A}(w) \mu|^2}{\tilde{\mathcal{R}}_N(w)^2} = \sup_w \frac{\left| \sum_{\ell=1}^L w_\ell e^\top \mathcal{B}_\ell \mathcal{A}(w) \mu \right|^2}{\tilde{\mathcal{R}}_N(w)^2} \leq \sup_w \frac{\left[\sum_{\ell=1}^L w_\ell |e^\top \mathcal{B}_\ell \mathcal{A}(w) \mu| \right]^2}{\tilde{\mathcal{R}}_N(w)^2} \\ & \leq \sup_\ell \sup_w \frac{|e^\top \mathcal{B}_\ell \mathcal{A}(w) \mu|^2}{\tilde{\mathcal{R}}_N(w)^2} \leq \xi_N^{-1} \sup_\ell \sup_w \frac{|e^\top \mathcal{B}_\ell \mathcal{G} w|^2}{\tilde{\mathcal{R}}_N(w)} \leq \xi_N^{-1} \sup_\ell \sup_w \frac{|e^\top \mathcal{B}_\ell \mathcal{G} w|^2}{w^\top (\Phi + \Psi_0) w} \\ & \leq \xi_N^{-1} \sup_\ell e^\top \mathcal{B}_\ell \mathcal{G} (\Phi + \Psi_0)^{-1} \mathcal{G}^\top \mathcal{B}_\ell e. \end{aligned}$$

To bound the quadratic term $\sup_\ell e^\top \mathcal{B}_\ell \mathcal{G} (\Phi + \Psi_0)^{-1} \mathcal{G}^\top \mathcal{B}_\ell e$, consider its expectation,

$$\begin{aligned} & E[\sup_\ell e^\top \mathcal{B}_\ell \mathcal{G} (\Phi + \Psi_0)^{-1} \mathcal{G}^\top \mathcal{B}_\ell e | X, R] \\ & \leq \sum_{\ell=1}^L E[e^\top \mathcal{B}_\ell \mathcal{G} (\Phi + \Psi_0)^{-1} \mathcal{G}^\top \mathcal{B}_\ell e | X, R] = \sigma^2 \sum_{\ell=1}^L trace(\mathcal{B}_\ell \mathcal{G} (\Phi + \Psi_0)^{-1} \mathcal{G}^\top \mathcal{B}_\ell) \\ & = \sigma^2 \sum_{\ell=1}^L trace((\Phi + \Psi_0)^{-1/2} \mathcal{G}^\top \mathcal{B}_\ell \mathcal{B}_\ell \mathcal{G} (\Phi + \Psi_0)^{-1/2}) \\ & \leq \sigma^2 \sum_{\ell=1}^L \lambda_{\max}(\mathcal{B}_\ell^2) trace((\Phi + \Psi_0)^{-1/2} \mathcal{G}^\top \mathcal{G} (\Phi + \Psi_0)^{-1/2}) \\ & \leq \sigma^2 \sum_{\ell=1}^L trace((\Phi + \Psi_0)^{-1/2} \Phi (\Phi + \Psi_0)^{-1/2}) = O(L^2), \end{aligned}$$

where λ_{\max} denotes the largest eigenvalue. As such, Eq. (A.12) holds under the condition

$$\xi_N^{-1} L^2 \rightarrow 0.$$

For Eq. (A.13), define

$$v_\ell = (\sigma^2 trace(\mathcal{B}_\ell \mathcal{B}_1) - e^\top \mathcal{B}_\ell \mathcal{B}_1 e, \dots, \sigma^2 trace(\mathcal{B}_\ell \mathcal{B}_L) - e^\top \mathcal{B}_\ell \mathcal{B}_L e)^\top.$$

We have $E[v_\ell|X, R] = 0$, and by Lemma 2 in [Zhang \(2021\)](#),

$$\begin{aligned} Var(v_\ell|X, R) &= E[v_\ell v_\ell^\top|X, R] \\ &= \{\sigma^4 \text{trace}(\mathcal{B}_\ell \mathcal{B}_m \mathcal{B}_\ell \mathcal{B}_s) + \sigma^4 \text{trace}(\mathcal{B}_m \mathcal{B}_\ell^2 \mathcal{B}_s) + \kappa \text{trace}((\mathcal{B}_\ell \mathcal{B}_m) * (\mathcal{B}_\ell \mathcal{B}_s))\}_{L \times L}. \end{aligned}$$

Before moving forward, note the following relationships hold:

$$\text{trace}(\mathcal{B}_m \mathcal{B}_\ell^2 \mathcal{B}_m) \leq \lambda_{\max}(\mathcal{B}_\ell^2) \text{trace}(\mathcal{B}_m^2) \leq \text{trace}(\mathcal{B}_m^2), \quad (\text{A.14})$$

where the relationship follows from $0 \leq \lambda_{\max}(\mathcal{B}_\ell) \leq 1$. Similarly, we have

$$\begin{aligned} \text{trace}(\mathcal{B}_\ell \mathcal{B}_m \mathcal{B}_\ell \mathcal{B}_m) &= \text{trace}(\mathcal{B}_\ell^{1/2} \mathcal{B}_m \mathcal{B}_\ell \mathcal{B}_m \mathcal{B}_\ell^{1/2}) \leq \lambda_{\max}(\mathcal{B}_\ell) \text{trace}(\mathcal{B}_m \mathcal{B}_\ell \mathcal{B}_m) \\ &\leq \lambda_{\max}(\mathcal{B}_\ell)^2 \text{trace}(\mathcal{B}_m^2) \leq \text{trace}(\mathcal{B}_m^2), \end{aligned} \quad (\text{A.15})$$

where the first inequality follows from $\text{Tr}(A'BA) \leq \lambda_{\max}(B)\text{Tr}(A'A)$ and $\text{Tr}(AB) = \text{Tr}(BA)$ for symmetric matrices A and B .

By Lemma 1 in [Zhang \(2021\)](#), we have

$$\begin{aligned} &\sup_{\mathbf{w}} \frac{\left| \sigma^2 \text{trace}(\mathcal{B}(\mathbf{w})^2) - e^\top \mathcal{B}(\mathbf{w})^2 e \right|^2}{\tilde{\mathcal{R}}_N(\mathbf{w})^2} = \sup_{\mathbf{w}} \frac{\left| \sum_{\ell=1}^L \mathbf{w}_\ell [e^\top \mathcal{B}_\ell \mathcal{B}(\mathbf{w}) e - \sigma^2 \text{trace}(\mathcal{B}_\ell \mathcal{B}(\mathbf{w}))] \right|^2}{\tilde{\mathcal{R}}_N(\mathbf{w})^2} \\ &\leq \sup_{\mathbf{w}} \frac{\left[\sum_{\ell=1}^L \mathbf{w}_\ell \left| e^\top \mathcal{B}_\ell \mathcal{B}(\mathbf{w}) e - \sigma^2 \text{trace}(\mathcal{B}_\ell \mathcal{B}(\mathbf{w})) \right| \right]^2}{\tilde{\mathcal{R}}_N(\mathbf{w})^2} \\ &\leq \xi_N^{-1} \sup_{\ell} \sup_{\mathbf{w}} \frac{\left| e^\top \mathcal{B}_\ell \mathcal{B}(\mathbf{w}) e - \sigma^2 \text{trace}(\mathcal{B}_\ell \mathcal{B}(\mathbf{w})) \right|^2}{\tilde{\mathcal{R}}_N(\mathbf{w})} \leq \xi_N^{-1} \sup_{\ell} \sup_{\mathbf{w}} \frac{(\mathbf{w}^\top \mathbf{v}_\ell)^2}{\mathbf{w}^\top (\Phi + \Psi_0) \mathbf{w}} \\ &\leq \xi_N^{-1} \sup_{\ell} \sup_{\mathbf{w}} \frac{(\mathbf{w}^\top \mathbf{v}_\ell)^2}{\mathbf{w}^\top \Psi_0 \mathbf{w}} \leq \xi_N^{-1} \sup_{\ell} \mathbf{v}_\ell^\top \Psi_0^{-1} \mathbf{v}_\ell \leq \xi_N^{-1} \sum_{\ell=1}^L \mathbf{v}_\ell^\top \Psi_0^{-1} \mathbf{v}_\ell. \end{aligned}$$

The quadratic term in the above display could be bounded as

$$\begin{aligned}
& \sum_{\ell=1}^L E[v_\ell^\top \Psi_0^{-1} v_\ell | X, R] \\
&= \sum_{\ell=1}^L \text{trace} \left(\Psi_0^{-1} \{ \sigma^4 \text{trace}(\mathcal{B}_\ell \mathcal{B}_m \mathcal{B}_\ell \mathcal{B}_s) + \sigma^4 \text{trace}(\mathcal{B}_m \mathcal{B}_\ell^2 \mathcal{B}_s) + \kappa \text{trace}((\mathcal{B}_\ell \mathcal{B}_m) * (\mathcal{B}_\ell \mathcal{B}_s)) \}_{L \times L} \right) \\
&= \sigma^4 \sum_{\ell=1}^L \text{trace} \left(\Psi_0^{-1} \text{diag} \{ \text{trace}(\mathcal{B}_\ell \mathcal{B}_m \mathcal{B}_\ell \mathcal{B}_m) + \text{trace}(\mathcal{B}_m \mathcal{B}_\ell^2 \mathcal{B}_m); m = 1, \dots, L \} \right) \\
&\quad + \kappa \sum_{\ell=1}^L \text{trace} \left(\Psi_0^{-1} \text{diag} \{ \text{trace}((\mathcal{B}_\ell \mathcal{B}_m) * (\mathcal{B}_\ell \mathcal{B}_m)); m = 1, \dots, L \} \right) \\
&\leq \sigma^4 \sum_{\ell=1}^L \text{trace} \left(\Psi_0^{-1} \text{diag} \{ \text{trace}(\mathcal{B}_\ell \mathcal{B}_m \mathcal{B}_\ell \mathcal{B}_m) + \text{trace}(\mathcal{B}_m \mathcal{B}_\ell^2 \mathcal{B}_m); m = 1, \dots, L \} \right) \\
&\quad + \kappa \sum_{\ell=1}^L \text{trace} \left(\Psi_0^{-1} \text{diag} \{ \text{trace}(\mathcal{B}_m \mathcal{B}_\ell^2 \mathcal{B}_m); m = 1, \dots, L \} \right) \\
&\leq (2\sigma^4 + \kappa) \sum_{\ell=1}^L \text{trace} \left(\Psi_0^{-1} \text{diag} \{ \text{trace}(\mathcal{B}_m^2); m = 1, \dots, L \} \right) \\
&= (2\sigma^4 + \kappa) \sum_{\ell=1}^L \text{trace} \left(\Psi_0^{-1} \Psi_0 \right) = O(L^2),
\end{aligned}$$

where we use the relationship that for any squared matrix O , $\text{trace}(O * O) \leq \text{trace}(O^\top O)$ and Eq. (A.14) – (A.15). As such, Eq. (A.13) holds under the condition $\xi_N^{-1} L^2 \rightarrow 0$. This completes the proof of the theorem. \square

Proof of Theorem 2.2. For clarity, recall that $\hat{\mu}_{RSA} = \sum_{\ell=1}^L \mathbf{w}_\ell \hat{\mu}^{(\ell)}$ and $\hat{\mu}^{(\ell)} = \sum_{j=1}^M w_j^{(\ell)} \hat{\mu}_j^{(\ell)}$.

Additionally, let $A = R(R^\top R)^- R^\top$, so that

$$\hat{\mu}_j^{(\ell)} = X R_j^{(\ell)} (R_j^{(\ell)} X^\top X R_j^{(\ell)})^- R_j^{(\ell)} X^\top Y = X A_j^{(\ell)} \beta + \frac{1}{N} X A_j^{(\ell)} X^\top e.$$

Using this, we obtain $\hat{\mu}_j^{(\ell)} - \mu = X(A_j^{(\ell)} - I)\beta + \frac{1}{N} X A_j^{(\ell)} X^\top e$.

For the first claim of the theorem, we have

$$\begin{aligned}
& E[(\hat{\mu}_{RSA} - \mu)^\top (\hat{\mu}_{RSA} - \mu)] \\
&= E \left\{ \sum_{\ell=1}^L \sum_{h=1}^L \mathbb{W}_\ell \mathbb{W}_h (\hat{\mu}^{(\ell)} - \mu)^\top (\hat{\mu}^{(h)} - \mu) \right\} \\
&= E \left\{ \sum_{\ell=1}^L \mathbb{W}_\ell^2 (\hat{\mu}^{(\ell)} - \mu)^\top (\hat{\mu}^{(\ell)} - \mu) \right\} + E \left\{ \sum_{\ell \neq h} \mathbb{W}_\ell \mathbb{W}_h (\hat{\mu}^{(\ell)} - \mu)^\top (\hat{\mu}^{(h)} - \mu) \right\}, \quad (\text{A.16})
\end{aligned}$$

We analyze each term in Eq. (A.16) separately. First, we have

$$\begin{aligned}
& E \left[(\hat{\mu}^{(\ell)} - \mu)^\top (\hat{\mu}^{(\ell)} - \mu) \right] \\
&= E \left[\sum_{j=1}^M \sum_{q=1}^M w_j^{(\ell)} w_q^{(\ell)} \left(X(A_j^{(\ell)} - I)\beta + \frac{1}{N} X A_j^{(\ell)} X^\top e \right)^\top \left(X(A_q^{(\ell)} - I)\beta + \frac{1}{N} X A_q^{(\ell)} X^\top e \right) \right] \\
&= E \left[\sum_{j=1}^M w_j^{(\ell)} w_j^{(\ell)} \left(X(A_j^{(\ell)} - I)\beta + \frac{1}{N} X A_j^{(\ell)} X^\top e \right)^\top \left(X(A_j^{(\ell)} - I)\beta + \frac{1}{N} X A_j^{(\ell)} X^\top e \right) \right] \\
& \quad (\text{A.17})
\end{aligned}$$

$$+ E \left[\sum_{j \neq q} w_j^{(\ell)} w_q^{(\ell)} \left(X(A_j^{(\ell)} - I)\beta + \frac{1}{N} X A_j^{(\ell)} X^\top e \right)^\top \left(X(A_q^{(\ell)} - I)\beta + \frac{1}{N} X A_q^{(\ell)} X^\top e \right) \right]. \quad (\text{A.18})$$

We then consider Eq. (A.17). We begin by evaluating

$$\begin{aligned}
& E_{X,R} \left[\left(X(A_j^{(\ell)} - I)\beta + \frac{1}{N} X A_j^{(\ell)} X^\top e \right)^\top \left(X(A_j^{(\ell)} - I)\beta + \frac{1}{N} X A_j^{(\ell)} X^\top e \right) \right] \\
&= N E_R \left[\beta^\top (A_j^{(\ell)} - I)(A_j^{(\ell)} - I)\beta \right] + \sigma^2 K p \\
&= N E_R \left[\beta^\top (I - A_j^{(\ell)})\beta \right] + \sigma^2 K p \\
&= N(1-p)\beta^\top \beta + \sigma^2 K p,
\end{aligned}$$

where the cross terms vanish in the first equality due to $E[e|X] = 0$, and the first equality

is due to

$$\begin{aligned}
E_{e,X,R} \left[e^\top X A_j^{(\ell)} X^\top X A_j^{(\ell)} X^\top e \right] &= E_{e,X,R} \text{trace} \left[e^\top X A_j^{(\ell)} X^\top X A_j^{(\ell)} X^\top e \right] \\
&= E_{X,R} \text{trace} \left[X A_j^{(\ell)} X^\top X A_j^{(\ell)} X^\top E(ee^\top | X) \right] \\
&= \sigma^2 E_{X,R} \text{trace} \left[A_j^{(\ell)} X^\top X A_j^{(\ell)} X^\top X \right] \\
&= N^2 \sigma^2 E_R \text{trace} \left[A_j^{(\ell)} A_j^{(\ell)} \right] \\
&= N^2 \sigma^2 \text{trace} E_R \left[A_j^{(\ell)} \right] \\
&= N^2 \sigma^2 K p.
\end{aligned}$$

The second equality follows from

$$(A_j^{(\ell)} - I)(A_j^{(\ell)} - I) = I - A_j^{(\ell)}.$$

For Eq. (A.18), we have

$$\begin{aligned}
&E \left[\left(X(A_j^{(\ell)} - I)\beta + \frac{1}{N} X A_j^{(\ell)} X^\top e \right)^\top \left(X(A_q^{(\ell)} - I)\beta + \frac{1}{N} X A_q^{(\ell)} X^\top e \right) \right] \\
&= E_{e,X,R} \left[\beta^\top (A_j^{(\ell)} - I) X^\top X (A_q^{(\ell)} - I) \beta \right] \\
&\quad + \frac{1}{N} E_{e,X,R} \left[\beta^\top (A_j^{(\ell)} - I) X^\top X A_q^{(\ell)} X^\top e \right] + \frac{1}{N} E_{e,X,R} \left[\beta^\top (A_q^{(\ell)} - I) X^\top X A_j^{(\ell)} X^\top e \right] \\
&\quad + \frac{1}{N^2} E_{e,X,R} \left[e^\top X A_j^{(\ell)} X^\top X A_q^{(\ell)} X^\top e \right].
\end{aligned}$$

Since $A_j^{(\ell)}$ and $A_q^{(\ell)}$ are independent draws, similar to the analysis of the quadratic term, we

obtain

$$\begin{aligned}
E_{e,X,R} \left[\beta^\top (A_j^{(\ell)} - I) X^\top X (A_q^{(\ell)} - I) \beta \right] &= N(1-p)^2 \beta^\top \beta, \\
\frac{1}{N} E_{e,X,R} \left[\beta^\top (A_j^{(\ell)} - I) X^\top X A_q^{(\ell)} X^\top e \right] &= 0, \\
\frac{1}{N^2} E_{e,X,R} \left[e^\top X A_j^{(\ell)} X^\top X A_q^{(\ell)} X^\top e \right] &= \sigma^2 K p^2.
\end{aligned}$$

Thus, we obtain

$$\begin{aligned}
E \left[(\hat{\mu}^{(\ell)} - \mu)^\top (\hat{\mu}^{(\ell)} - \mu) \right] \\
= \left(N(1-p) \beta^\top \beta + \sigma^2 K p \right) \sum_{j=1}^M w_j^{(\ell)} w_j^{(\ell)} + \left(N(1-p)^2 \beta^\top \beta + \sigma^2 K p^2 \right) \sum_{j \neq q} w_j^{(\ell)} w_q^{(\ell)}.
\end{aligned}$$

For notational clarity, define

$$\begin{aligned}
D &= N(1-p) \beta^\top \beta + \sigma^2 K p, \\
F &= N(1-p)^2 \beta^\top \beta + \sigma^2 K p^2, \\
Q &= D \sum_{j=1}^M w_j^{(\ell)} w_j^{(\ell)} + F \sum_{j \neq q} w_j^{(\ell)} w_q^{(\ell)}.
\end{aligned}$$

In the first round, optimizing Q is equivalent to minimizing it subject to the constraint $\sum_{j=1}^M w_j^{(\ell)} = 1$. Using the method of Lagrange multipliers, define the Lagrangian function $L_Q = D \sum_{j=1}^M w_j^{(\ell)} w_j^{(\ell)} + F \sum_{j \neq q} w_j^{(\ell)} w_q^{(\ell)} + \lambda (\sum_{j=1}^M w_j^{(\ell)} - 1)$. The first-order conditions are

$$\begin{aligned}
\frac{\partial L_Q}{\partial w_j^{(\ell)}} &= 2D w_j^{(\ell)} + F \sum_{q:q \neq j}^M w_q^{(\ell)} + \lambda = 2D w_j^{(\ell)} + F(1 - w_j^{(\ell)}) + \lambda = 0, \\
\frac{\partial L_Q}{\partial \lambda} &= \sum_{j=1}^M w_j^{(\ell)} - 1 = 0.
\end{aligned}$$

Solving these equations, we obtain

$$w_j^{(\ell)} = \frac{1}{M},$$

$$\lambda = \frac{F - 2D}{M} - F.$$

Hence, the minimum value of Q is achieved at

$$\begin{aligned} & E \left[(\hat{\mu}^{(\ell)} - \mu)^\top (\hat{\mu}^{(\ell)} - \mu) \right] \\ &= (N(1-p)\beta^\top \beta + \sigma^2 K p) \frac{1}{M} + (N(1-p)^2 \beta^\top \beta + \sigma^2 K p^2) \frac{M-1}{M} \\ &= \frac{1}{M} \left((1-p)N\beta^\top \beta + \sigma^2 K p \right) + \frac{1}{M} \left((1-p)^2(M-1)N\beta^\top \beta + (M-1)\sigma^2 K p^2 \right). \end{aligned}$$

Taking the first-order condition with respect to p , we obtain

$$-N\beta^\top \beta + \sigma^2 K - 2(1-p)(M-1)N\beta^\top \beta + 2p(M-1)\sigma^2 K = 0,$$

Solving for p , the optimal selection probability is given by

$$p = \frac{M}{M-1} \frac{N\beta^\top \beta}{N\beta^\top \beta + K\sigma^2} - \frac{1}{2(M-1)}.$$

With this choice of p , the expectation simplifies to

$$\begin{aligned} & E \left[(\hat{\mu}^{(\ell)} - \mu)^\top (\hat{\mu}^{(\ell)} - \mu) \right] \\ &= \frac{N\beta^\top \beta K \sigma^2}{N\beta^\top \beta + K\sigma^2} + \frac{N\beta^\top \beta K \sigma^2}{(M-1)(N\beta^\top \beta + K\sigma^2)} - \frac{(N\beta^\top \beta + K\sigma^2)}{2M(M-1)} \\ &\asymp \frac{N\beta^\top \beta K \sigma^2}{N\beta^\top \beta + K\sigma^2}, \end{aligned}$$

as $M \rightarrow \infty$.

Next, we consider the cross term $(\hat{\mu}^{(\ell)} - \mu)^\top (\hat{\mu}^{(h)} - \mu)$. The calculations follow similarly, yielding

$$\begin{aligned} & E(\hat{\mu}^{(\ell)} - \mu)^\top (\hat{\mu}^{(h)} - \mu) \\ &= E \left[\sum_{j=1}^M \sum_{q=1}^M w_j^{(\ell)} w_q^{(h)} \left(X(A_j^{(\ell)} - I)\beta + \frac{1}{N} X A_j^{(\ell)} X^\top e \right)^\top \left(X(A_q^{(h)} - I)\beta + \frac{1}{N} X A_q^{(h)} X^\top e \right) \right] \\ &= N(1-p)^2 \beta^\top \beta + K\sigma^2 p^2, \end{aligned}$$

where the second equality follows from

$$E((A_j^{(\ell)} - I)((A_q^{(h)} - I))) = E \left[A_j^{(\ell)} A_q^{(h)} - A_j^{(\ell)} - A_q^{(h)} + I \right] = (1-p)^2 I,$$

due to the independence of the random selection matrices. This further leads to

$$\begin{aligned} E \left[(X(A_j^{(\ell)} - I)\beta)^\top (X(A_j^{(h)} - I)\beta) \right] &= N(1-p)^2 \beta^\top \beta, \\ E[(X(A_j^{(\ell)} - I)\beta)^\top (\frac{1}{N} X A_q^{(h)} X^\top e)] &= 0, \\ E[(\frac{1}{N} X A_q^{(h)} X^\top e)^\top (X(A_q^{(h)} - I)\beta)] &= 0, \\ E[(X(A_j^{(\ell)} - I)\beta)^\top (X(A_q^{(h)} - I)\beta)] &= K\sigma^2 p^2. \end{aligned}$$

Optimizing $E[(\hat{\mu}_{RSA} - \mu)^\top (\hat{\mu}_{RSA} - \mu)]$ with respect to \mathbf{w}_ℓ subject to the constraint $\sum_{\ell=1}^L \mathbf{w}_\ell = 1$, yields the solution $\mathbf{w}_\ell = \frac{1}{L}$. This result is intuitive, as the variability is eliminated after taking the expectation. Consequently, the minimum risk is given by

$$\xi_N \asymp \frac{N\beta^\top \beta K\sigma^2}{N\beta^\top \beta + K\sigma^2}.$$

For the second claim of the theorem, when the selection probability varies across covariates,

we have $E[A] = \text{diag}(\eta_1, \dots, \eta_K)$ for non-negative η_j . This leads to the following results:

$$\begin{aligned}
E_{e,X,R} \left[e^\top X A_j^{(\ell)} X^\top X A_j^{(\ell)} X^\top e \right] &= N \sum_{k=1}^K (1 - \eta_k) \beta_k^2 + \sigma^2 \sum_{k=1}^K \eta_k, \\
E \left[\left(X(A_j^{(\ell)} - I)\beta + \frac{1}{N} X A_j^{(\ell)} X^\top e \right)^\top \left(X(A_q^{(\ell)} - I)\beta + \frac{1}{N} X^\top A_q^{(\ell)} X^\top e \right) \right] \\
&= N \sum_{k=1}^K (1 - \eta_k)^2 \beta_k^2 + \sigma^2 \sum_{k=1}^K \eta_k^2.
\end{aligned}$$

Hence, we obtain

$$\begin{aligned}
E \left[(\hat{\mu}^{(\ell)} - \mu)^\top (\hat{\mu}^{(\ell)} - \mu) \right] \\
= \left(N \sum_{k=1}^K (1 - \eta_k) \beta_k^2 + \sigma^2 \sum_{k=1}^K \eta_k \right) \sum_{j=1}^M w_j^{(\ell)} w_j^{(\ell)} + \left(N \sum_{k=1}^K (1 - \eta_k)^2 \beta_k^2 + \sigma^2 \sum_{k=1}^K \eta_k^2 \right) \sum_{j \neq q} w_j^{(\ell)} w_q^{(\ell)}.
\end{aligned}$$

The optimal weights for each model are $1/M$, and optimizing with respect to η_k yields

$$\eta_k = \frac{M}{M-1} \frac{N \beta_k^2}{N \beta_k^2 + \sigma^2} - \frac{1}{2(M-1)}.$$

Consequently, we obtain

$$\begin{aligned}
E \left[(\hat{\mu}^{(\ell)} - \mu)^\top (\hat{\mu}^{(\ell)} - \mu) \right] \\
= \frac{1}{M} \left(\sum_{k=1}^K (1 - \eta_k) N \beta_k^2 + \frac{1}{N} \sigma^2 \sum_{k=1}^K \eta_k + \sum_{k=1}^K (M-1)(1 - \eta_k)^2 N \beta_k^2 + \frac{1}{N} (M-1) \sigma^2 \sum_{k=1}^K \eta_k^2 \right) \\
= \frac{1}{M} \sum_{k=1}^K \left[(1 - \eta_k) N \beta_k^2 \left(\frac{M \sigma^2}{N \beta_k^2 + \sigma^2} + \frac{1}{2} \right) + \sigma^2 \eta_k \left(\frac{M N \beta_k^2}{N \beta_k^2 + \sigma^2} + \frac{1}{2} \right) \right] \\
\asymp \sum_{k=1}^K \frac{N \beta_k^2 \sigma^2}{N \beta_k^2 + \sigma^2}.
\end{aligned}$$

We now consider $(\hat{\mu}^{(\ell)} - \mu)^\top (\hat{\mu}^{(h)} - \mu)$. The calculation follows similar reasoning:

$$\begin{aligned}
& E \left[(\hat{\mu}^{(\ell)} - \mu)^\top (\hat{\mu}^{(h)} - \mu) \right] \\
&= E \left[\sum_{j=1}^M \sum_{q=1}^M w_j^{(\ell)} w_q^{(h)} \left(X(A_j^{(\ell)} - I)\beta + \frac{1}{N} X A_j^{(\ell)} X^\top e \right) \left(X(A_q^{(h)} - I)\beta + \frac{1}{N} X A_q^{(h)} X^\top e \right) \right] \\
&= N \sum_{k=1}^K (1 - \eta_k^2) \beta_k^2 + \sigma^2 \sum_{k=1}^K \eta_k^2.
\end{aligned}$$

Next, optimizing $E[(\hat{\mu}_{RSA} - \mu)^\top (\hat{\mu}_{RSA} - \mu)]$ with respect to \mathbf{w}_ℓ subject to $\sum_{\ell=1}^L \mathbf{w}_\ell = 1$, gives $\mathbf{w}_\ell = \frac{1}{L}$. Therefore, the minimum risk of $E[(\hat{\mu}_{RSA} - \mu)^\top (\hat{\mu}_{RSA} - \mu)]$ is

$$\xi_N \asymp \sum_{k=1}^K \frac{FG}{F+G} = \frac{1}{N} \sum_{k=1}^K \frac{N\beta_k^2 \sigma^2}{N\beta_k^2 + \sigma^2}.$$

□

Proof of Lemma 2.3. The minimum squared L_2 risk of MA follows from Theorem 1 in Peng & Yang (2022).

We next prove the minimum squared L_2 risk for RPR and RSR. First, define $A = E_R \left[R(R^\top X^\top X R)^{-1} R^\top \right] = \text{diag}(\eta_1^{-1}, \eta_2^{-1}, \dots, \eta_K^{-1})$. Then, for each R , we have $E_R[\hat{\mu}] =$

$XAX^\top Y$. Thus, we have:

$$\begin{aligned}
\xi_N^{RPR} &= \xi_N^{RSR} = E \left[\|X\beta - XAX^\top Y\|^2 \right] \\
&= E \left[\|X\beta - XAX^\top X\beta - XAX^\top e\|^2 \right] \\
&= E[\beta^\top X^\top (I - XAX^\top)^\top (I - XAX^\top) X\beta] + E[e^\top XAX^\top XAX^\top e] \\
&= \sum_{i=1}^K \beta_i^2 N \left(1 - \frac{N}{\eta_i}\right)^2 + \text{tr}(XAXXAX^\top E[ee^\top]) \\
&= \sum_{i=1}^K \beta_i^2 N \left(1 - \frac{N}{\eta_i}\right)^2 + \sum_{j=1}^K \sigma^2 \frac{N^2}{\eta_j^2} \\
&= \sigma^2 \sum_{i=1}^K \left(\frac{N}{\eta_i}\right)^2 + \sum_{j=1}^K \beta_j^2 N \left(1 - \frac{N}{\eta_j}\right)^2.
\end{aligned}$$

For both RPR and RSR, we have $\eta_1 = \eta_2 = \dots = \eta_K = KN/P$. For RPR, this follows from Lemma 1 in [Thanei et al. \(2017\)](#), and for RSR, it follows from the fact that $P([RR^\top]_{ii} = 1) = \frac{P}{K}$. As a result, we have:

$$\xi_N^{RPR} = \xi_N^{RSR} = \sigma^2 \frac{P^2}{K} + \frac{1}{K^2} \sum_{j=1}^K N \beta_j^2 (K - P)^2.$$

The above risk is minimized when setting $P = \frac{K \sum_{j=1}^K N \beta_j^2}{K \sigma^2 + \sum_{j=1}^K N \beta_j^2}$, leading to the desired result. \square

B Additionally numerical results

In this section, we provide additional results from our simulation study and empirical analysis.

Section B.1 outlines the implementation details of the competing methods used in the simulations.

Section B.2 reports the corresponding MSFE comparisons under a random covariance structure, complementing the results in Sections 3.2 to 3.4. This setting captures scenarios where the empirical correlation structure is complex and not directly observable. RSA’s performance remains comparable to that in low-correlation settings, suggesting that its effectiveness extends to more intricate dependence structures.

Section B.3 presents heatmaps of the CV results for the selection probability and the number of candidate models. Across all scenarios, the selection probability p appears to have a more substantial influence, whereas the number of candidate models shows a comparatively modest effect.

Section B.4 reports MSE comparisons corresponding to Sections 3.2 through 3.4. Overall, the results suggest that RSA’s superior out-of-sample performance is not accompanied by an increase in training error, offering additional empirical support for its effectiveness.

Section B.5 presents additional results from the empirical analysis, including asset return volatility in the pre- and post-crisis periods, heatmaps for tuning parameter selection, the standard deviation of MSFE across forecast horizons, and MSE comparisons across methods. Together, these findings further support the practical utility of RSA.

B.1 Implementation detail

The RSR method is implemented following [Elliott et al. \(2013\)](#). Lasso method is implemented via the R package `glmnet`, while SCAD and MCP are implemented using the `ncvreg` package. For MMA, we construct a nested set of candidate models based on the natural ordering of covariates. When it is not directly applicable in high-dimensional settings, we just use the first $N - 2$ covariates to construct the nested models. Notably, when the nonzero coefficients are ordered accordingly, this corresponds to the canonical nested model set described in [Hansen \(2007\)](#). However, when nonzero entries are randomly positioned, the resulting nested model set may not possess desirable properties. For PMA, we construct the nested candidate model set using the solution path of Adaptive Lasso ([Zhang et al. 2019](#)). The random forests method is implemented using the R package `randomForestSRC` ([Ishwaran & Kogalur 2023](#)).

B.2 MSFE comparison under random covariance matrix

In empirical applications, covariates correlations are often complex and unpredictable, motivating our evaluation of model performance under randomly generated covariance structures. Tables B.1 to B.3 report the corresponding MSFE results for Sections 3.2 to 3.4. Table B.1 shows the MSFE results under polynomially decaying coefficients. In this setting, RSA.opt performs comparably to its performance in low-correlation scenarios (Table 3), consistently delivering superior out-of-sample predictive accuracy, especially when both the sample size N and the number of covariates K are large. However, under random covariance structures, RSA.opt requires more observations to outperform competing methods, as evidenced by its lower performance relative to RSA.fix when $N = 200$. This suggests that while RSA.opt is well-suited to handle complex correlation structures, its advantage is more pronounced in larger samples.

Table B.1: MSFE comparison for random covariance matrix (polynomial decay).

N	K	RSA.opt	RSA.fix	RSR	Lasso	SCAD	MCP	PMA	MMA	RF
200	20	0.19 (0.06)	0.27 (0.06)	1.56 (0.25)	0.17 (0.06)	0.19 (0.08)	0.19 (0.08)	0.40 (0.40)	0.15 (0.05)	0.57 (0.12)
	100	0.14 (0.03)	0.17 (0.03)	0.24 (0.04)	0.23 (0.08)	0.22 (0.07)	0.22 (0.07)	0.35 (0.08)	0.29 (0.08)	0.30 (0.05)
	200	0.65 (0.11)	0.57 (0.10)	0.78 (0.12)	0.75 (0.24)	0.70 (0.18)	0.70 (0.17)	1.29 (0.27)	572.77 (2438.50)	0.97 (0.15)
	300	0.77 (0.12)	0.71 (0.12)	0.75 (0.11)	1.16 (0.43)	1.13 (0.26)	1.12 (0.24)	1.95 (0.72)	2529.42 (22585.59)	1.08 (0.18)
	400	0.17 (0.03)	0.33 (0.05)	0.76 (0.09)	0.10 (0.02)	0.10 (0.03)	0.10 (0.03)	0.33 (0.16)	0.09 (0.02)	0.60 (0.07)
	200	0.55 (0.06)	0.48 (0.06)	0.75 (0.08)	0.49 (0.11)	0.44 (0.09)	0.43 (0.09)	1.10 (0.12)	0.73 (0.13)	0.89 (0.09)
400	400	0.26 (0.03)	0.27 (0.03)	0.31 (0.03)	0.41 (0.11)	0.35 (0.06)	0.35 (0.06)	0.60 (0.28)	1805.05 (12264.13)	0.42 (0.05)
	600	0.61 (0.07)	0.62 (0.08)	0.72 (0.07)	0.95 (0.32)	0.78 (0.12)	0.78 (0.12)	1.48 (0.47)	4516.28 (30051.74)	0.97 (0.11)
	800	0.17 (0.02)	0.24 (0.02)	0.38 (0.04)	0.22 (0.04)	0.25 (0.05)	0.25 (0.05)	0.66 (0.33)	0.16 (0.03)	0.45 (0.04)
	400	0.23 (0.02)	0.23 (0.02)	0.30 (0.02)	0.29 (0.06)	0.23 (0.04)	0.23 (0.04)	0.47 (0.04)	0.46 (0.06)	0.39 (0.03)
	800	0.48 (0.04)	0.65 (0.05)	0.84 (0.06)	0.58 (0.08)	0.56 (0.06)	0.56 (0.06)	1.13 (0.09)	1633.76 (5039.92)	1.01 (0.08)
	1200	0.96 (0.08)	0.90 (0.08)	1.06 (0.08)	1.36 (0.29)	1.09 (0.12)	1.10 (0.12)	1.78 (0.31)	9671.02 (69146.84)	1.33 (0.10)

Note: RSA.opt represents the RSA method with CV-determined parameters and RSA.fix refers to the RSA method with fixed parameters, specifically $M = L = 30$ and $p = 0.1$. Values in bold indicate the top performers within the 95% MCS test while values in parentheses represent the standard deviation of the reported MSFEs.

Table B.2 presents the MSFE results under an exponentially decaying coefficient structure. The findings closely mirror those in Table B.1, with RSA exhibiting strong predictive performance, especially in highly sparse settings.

Table B.2: MSFE comparison for random covariance matrix (exponential decay).

N	K	RSA.opt	RSA.fix	RSR	Lasso	SCAD	MCP	PMA	MMA	RF
200	20	0.05 (0.01)	0.07 (0.01)	0.32 (0.05)	0.03 (0.01)	0.04 (0.02)	0.04 (0.02)	0.10 (0.12)	0.03 (0.01)	0.13 (0.02)
	100	0.04 (0.01)	0.04 (0.01)	0.06 (0.01)	0.04 (0.01)	0.05 (0.01)	0.05 (0.01)	0.08 (0.02)	0.05 (0.01)	0.07 (0.01)
	200	0.16 (0.03)	0.15 (0.03)	0.19 (0.03)	0.18 (0.05)	0.18 (0.04)	0.18 (0.04)	0.29 (0.05)	117.91 (506.33)	0.23 (0.03)
	300	0.19 (0.03)	0.18 (0.03)	0.18 (0.10)	0.29 (0.06)	0.28 (0.06)	0.28 (0.06)	0.46 (0.16)	572.23 (4928.26)	0.26 (0.04)
	400	0.04 (0.01)	0.09 (0.01)	0.18 (0.02)	0.02 (0.00)	0.02 (0.01)	0.02 (0.01)	0.08 (0.04)	0.02 (0.00)	0.15 (0.02)
	200	0.15 (0.02)	0.13 (0.02)	0.18 (0.02)	0.11 (0.02)	0.11 (0.02)	0.11 (0.02)	0.25 (0.03)	0.15 (0.03)	0.21 (0.02)
400	400	0.06 (0.01)	0.06 (0.01)	0.07 (0.02)	0.09 (0.02)	0.08 (0.01)	0.08 (0.01)	0.12 (0.02)	298.22 (2026.21)	0.10 (0.01)
	600	0.15 (0.02)	0.15 (0.02)	0.16 (0.08)	0.23 (0.03)	0.20 (0.03)	0.20 (0.03)	0.35 (0.14)	987.05 (6588.30)	0.22 (0.02)
	800	0.04 (0.01)	0.06 (0.01)	0.09 (0.01)	0.05 (0.01)	0.05 (0.01)	0.05 (0.01)	0.15 (0.05)	0.04 (0.01)	0.11 (0.01)
800	400	0.06 (0.00)	0.06 (0.00)	0.07 (0.01)	0.06 (0.01)	0.05 (0.01)	0.05 (0.01)	0.11 (0.01)	0.08 (0.01)	0.09 (0.01)
	800	0.11 (0.01)	0.15 (0.01)	0.19 (0.01)	0.11 (0.02)	0.11 (0.01)	0.11 (0.01)	0.25 (0.02)	315.02 (969.20)	0.23 (0.02)
	1200	0.22 (0.02)	0.20 (0.02)	0.23 (0.06)	0.29 (0.03)	0.23 (0.03)	0.23 (0.03)	0.41 (0.08)	1988.28 (13862.38)	0.29 (0.02)

Note: RSA.opt represents the RSA method with CV-determined parameters and RSA.fix refers to the RSA method with fixed parameters, specifically $M = L = 30$ and $p = 0.1$. Values in bold indicate the top performers within the 95% MCS test while values in parentheses represent the standard deviation of the reported MSFEs.

Table B.3 presents the MSFE result in settings with many relevant covariates. RSA continue to deliver the highest out-of-sample prediction accuracy regardless of signal strength, while RSA with fixed parameters is selected most frequently by the MCS test at 95% significance level.

Table B.3: MSFE comparison under many relevant covariates.

DGP	N	K	RSA.opt	RSA.fix	RSR	Lasso	SCAD	MCP	PMA	MMA	RF
poly	100	100	0.76	0.78	0.68	1.29	1.21	1.23	2.55	1034.57	1.29
			(0.24)	(0.25)	(0.20)	(0.85)	(0.45)	(0.49)	(1.10)	(4327.25)	(0.42)
		125	0.75	0.73	0.80	1.19	1.10	1.09	1.52	329.94	1.05
	150		(0.18)	(0.18)	(0.17)	(0.49)	(0.32)	(0.30)	(3.77)	(1377.63)	(0.24)
			0.91	0.90	0.96	1.38	1.29	1.29	2.49	533.70	1.24
			(0.23)	(0.21)	(0.20)	(0.51)	(0.35)	(0.33)	(7.42)	(2746.59)	(0.26)
	300	300	0.80	0.76	0.91	1.08	0.96	0.96	1.85	1681.07	1.19
			(0.11)	(0.11)	(0.11)	(0.32)	(0.20)	(0.20)	(0.61)	(4548.01)	(0.15)
		375	0.57	0.54	0.58	0.80	0.70	0.70	1.09	4309.65	0.82
exp	100	100	(0.08)	(0.08)	(0.07)	(0.30)	(0.13)	(0.14)	(0.23)	(54691.69)	(0.11)
		125	0.92	0.92	1.07	1.42	1.29	1.30	1.69	5389.49	1.39
			(0.13)	(0.13)	(0.13)	(0.36)	(0.22)	(0.22)	(0.74)	(68462.16)	(0.17)
	150		0.18	0.18	0.16	0.30	0.28	0.28	0.57	227.63	0.29
			(0.05)	(0.06)	(0.04)	(0.18)	(0.10)	(0.10)	(0.27)	(957.58)	(0.09)
			0.18	0.18	0.19	0.30	0.28	0.27	0.37	82.54	0.26
	300	300	(0.04)	(0.04)	(0.04)	(0.12)	(0.08)	(0.08)	(0.91)	(348.94)	(0.06)
		375	0.23	0.22	0.22	0.34	0.33	0.32	0.58	133.14	0.30
			(0.06)	(0.05)	(0.05)	(0.13)	(0.10)	(0.10)	(0.58)	(653.53)	(0.06)
450	200	200	0.20	0.17	0.20	0.25	0.23	0.23	0.40	390.67	0.27
			(0.03)	(0.02)	(0.02)	(0.07)	(0.04)	(0.04)	(0.12)	(1057.08)	(0.03)
	300	300	0.12	0.12	0.13	0.17	0.15	0.15	0.23	876.26	0.18
			(0.02)	(0.02)	(0.02)	(0.07)	(0.03)	(0.03)	(0.05)	(10777.12)	(0.02)

Note: “poly” refers to polynomially decaying coefficients, while “exp” denotes exponentially decaying coefficient. RSA.opt represents the RSA method with CV-determined parameters and RSA.fix refers to the RSA method with fixed parameters, specifically $M = L = 30$ and $p = 0.1$. Values in bold indicate the top performers within the 95% MCS test while values in parentheses represent the standard deviation of the reported MSFEs.

B.3 CV selection for the selection probability and the number of candidate models

B.3.1 CV results for Section 3.1

Figures B.1 and B.2 illustrate the cross-validated performance of the RSA estimator under different choices of selection probability. As shown in both figures, the estimator's performance is highly sensitive to this tuning parameter. Moreover, the optimal selection probability depends on the correlation structure among covariates. When the covariates are highly dependent, a smaller selection probability is generally preferred. This finding aligns with the intuition that strong dependence among covariates can be exploited to enhance predictive accuracy.

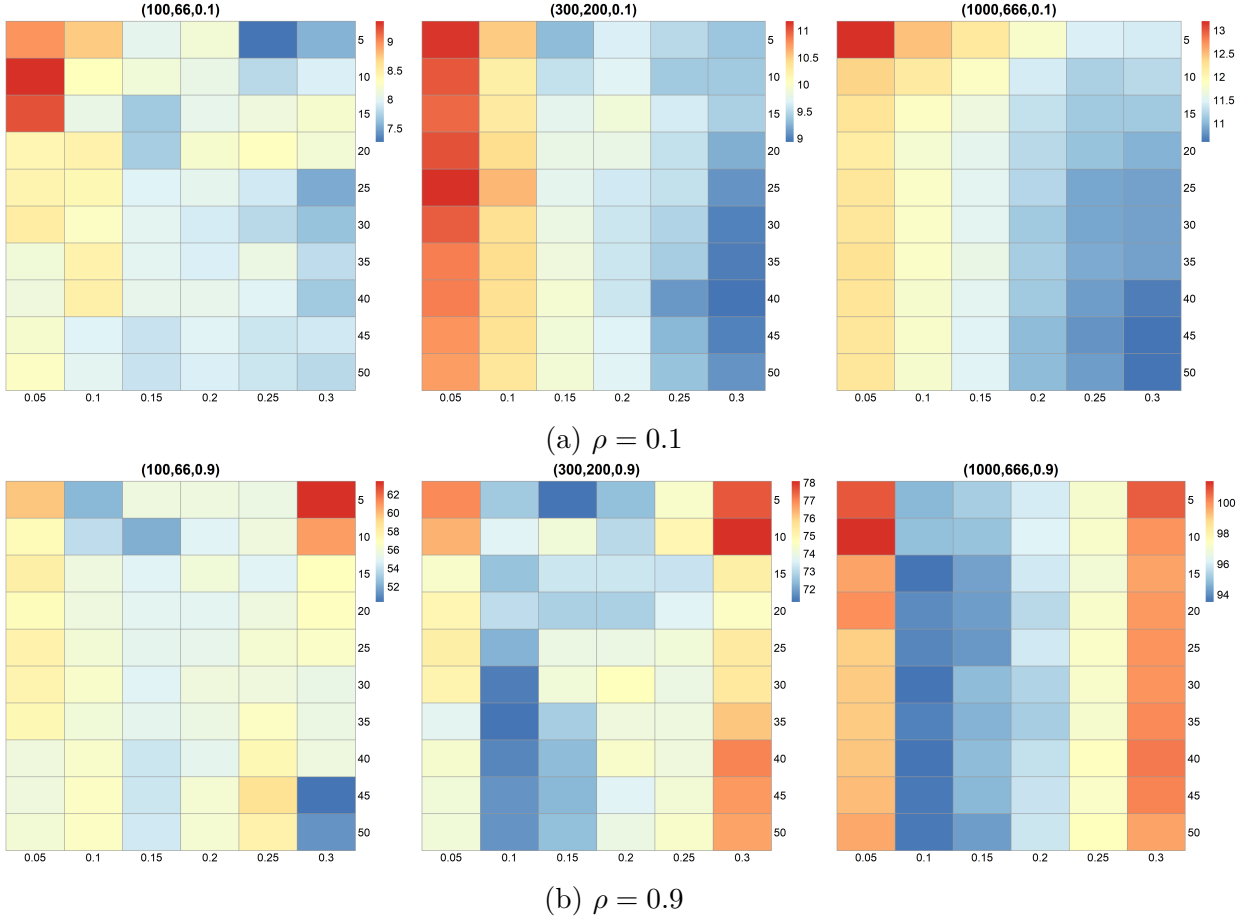


Figure B.1: CV results for Section 3.1: polynomial decay. Values in parenthesis denote (N, K, ρ) . The x -axis represents the selection probability p and the y -axis indicates the number of candidate models M . Dark blue regions correspond to the (p, M) combinations yielding the lowest MSE.

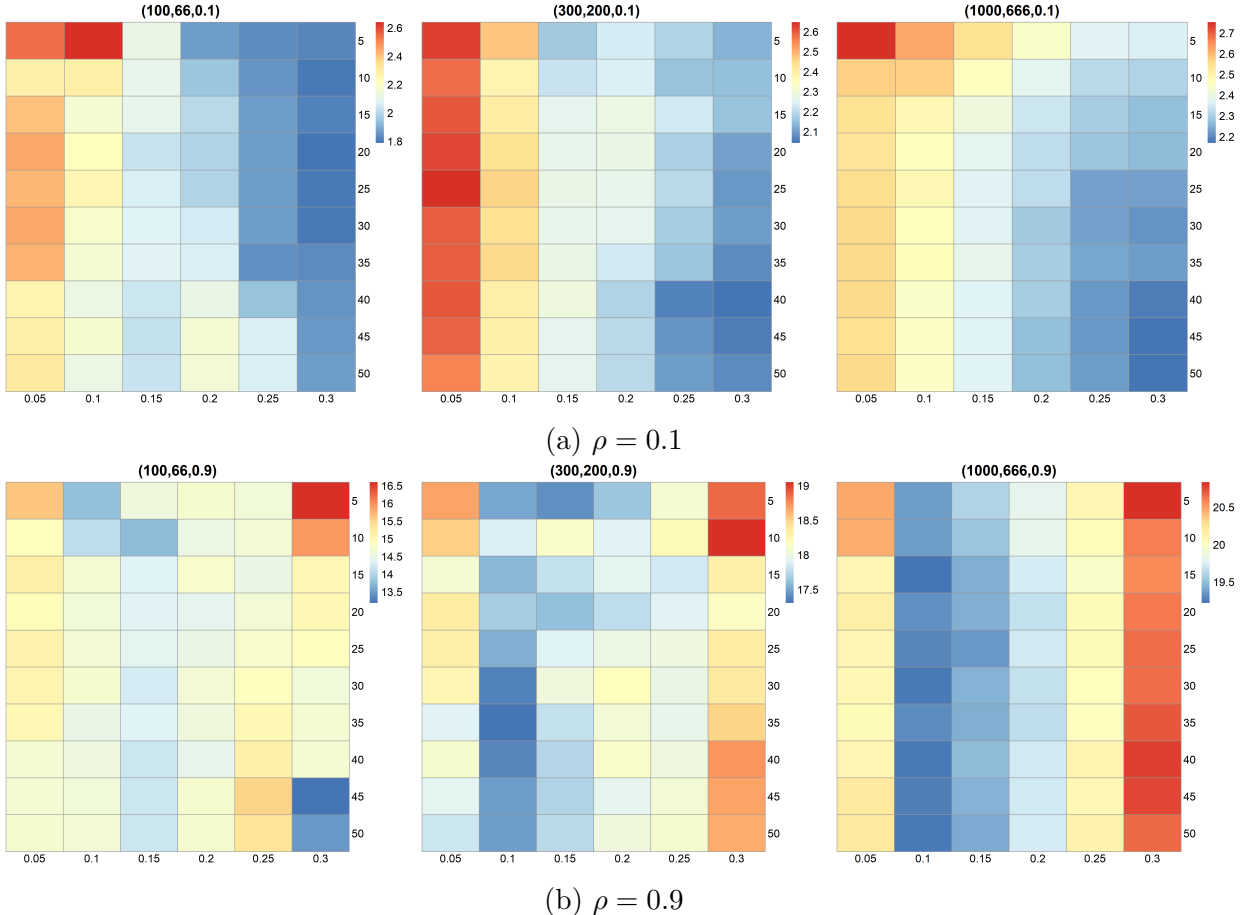


Figure B.2: CV results for Section 3.1: exponential decay. Values in parenthesis denote (N, K, ρ) . The x -axis represents the selection probability p and the y -axis indicates the number of candidate models M . Dark blue regions correspond to the (p, M) combinations yielding the lowest MSE.

B.3.2 CV results for Section 3.2

Figures B.3, B.4, and B.5 report the cross-validation results under three different scenarios: when the covariates are weakly correlated, highly correlated, and randomly correlated, respectively, with polynomially decaying regression coefficients. The results indicate that the selection probability plays a significant role in the performance of the RSA estimator.

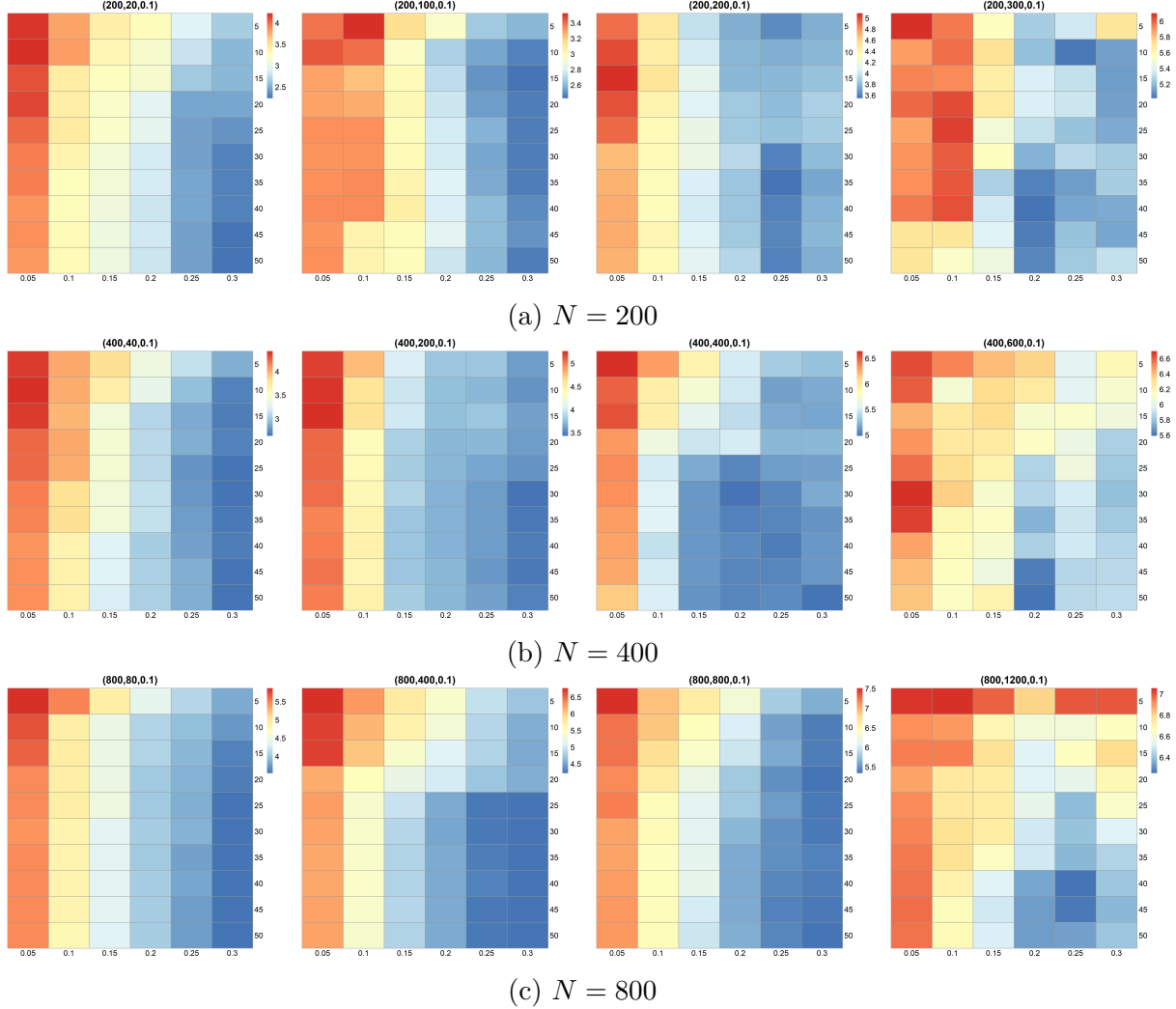


Figure B.3: CV results for Section 3.2: polynomial decay with $\rho = 0.1$. Values in parenthesis denote (N, K, ρ) . The x -axis represents the selection probability p and the y -axis indicates the number of candidate models M . Dark blue regions correspond to the (p, M) combinations yielding the lowest MSE.

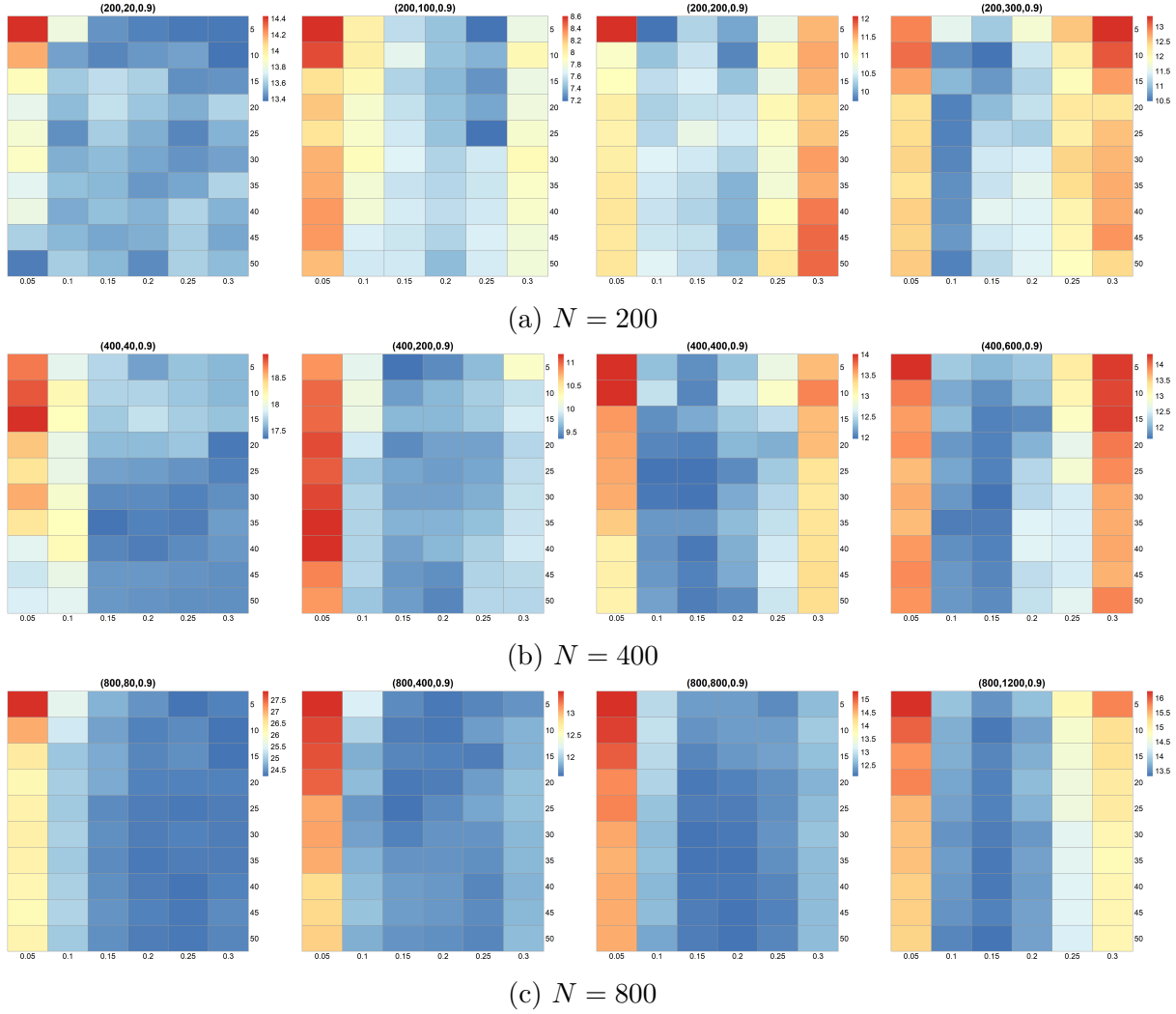


Figure B.4: CV results for Section 3.2: polynomial decay with $\rho = 0.9$. Values in parenthesis denote (N, K, ρ) . The x -axis represents the selection probability p and the y -axis indicates the number of candidate models M . Dark blue regions correspond to the (p, M) combinations yielding the lowest MSE.

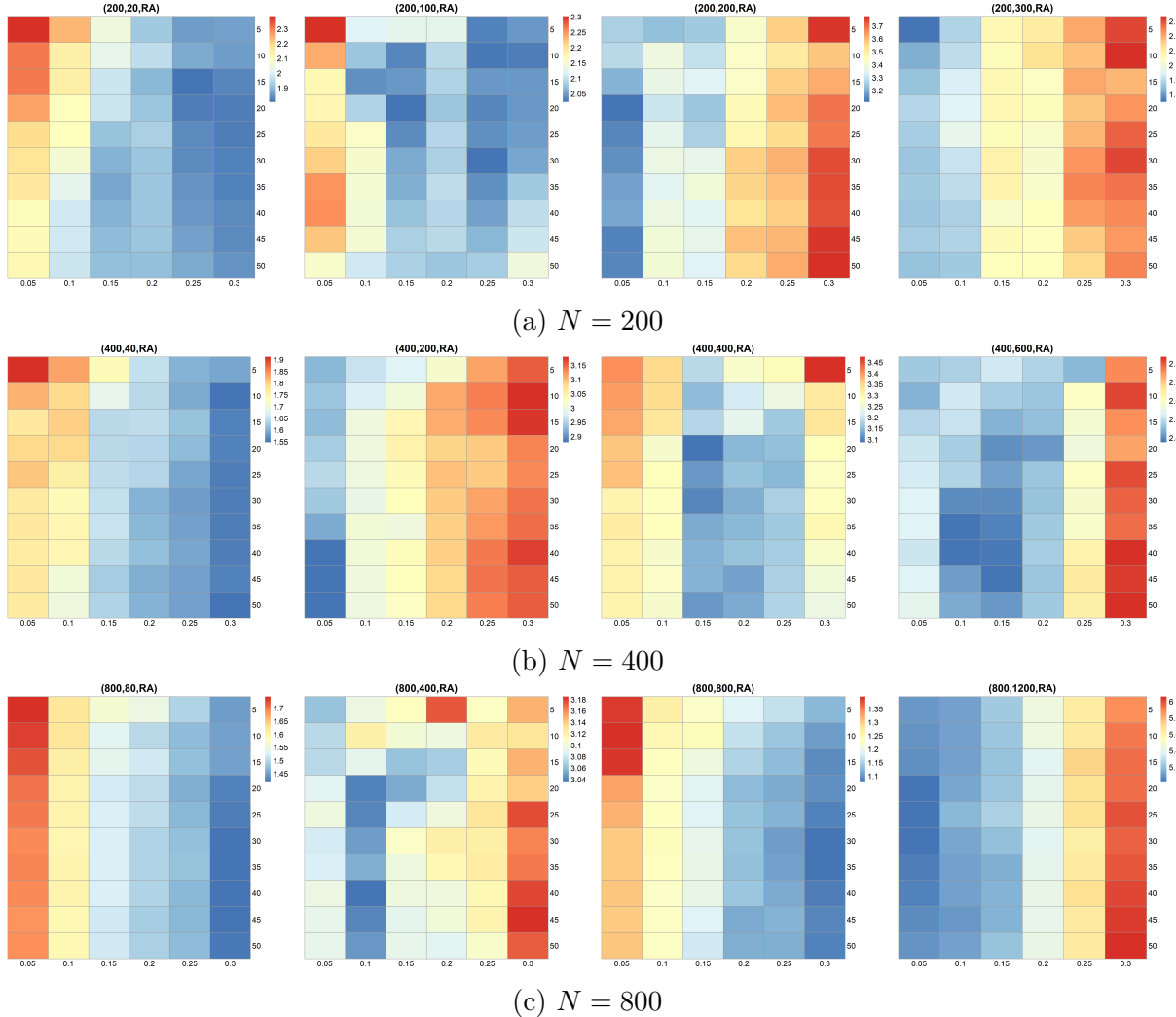


Figure B.5: CV results for Section 3.2: polynomial decay with random covariance structure. Values in parenthesis denote (N, K, ρ) . The x -axis represents the selection probability p and the y -axis indicates the number of candidate models M . Dark blue regions correspond to the (p, M) combinations yielding the lowest MSE.

B.3.3 CV results for Section 3.3

Figures B.6, B.7, and B.8 report the cross-validation results under three different scenarios: when the covariates are weakly correlated, highly correlated, and randomly correlated, respectively, with exponentially decaying regression coefficients. These findings underscore the sensitivity of the RSA estimator to the choice of selection probability across different dependence structures, while also corroborating the importance and effectiveness of the cross-validation procedure.

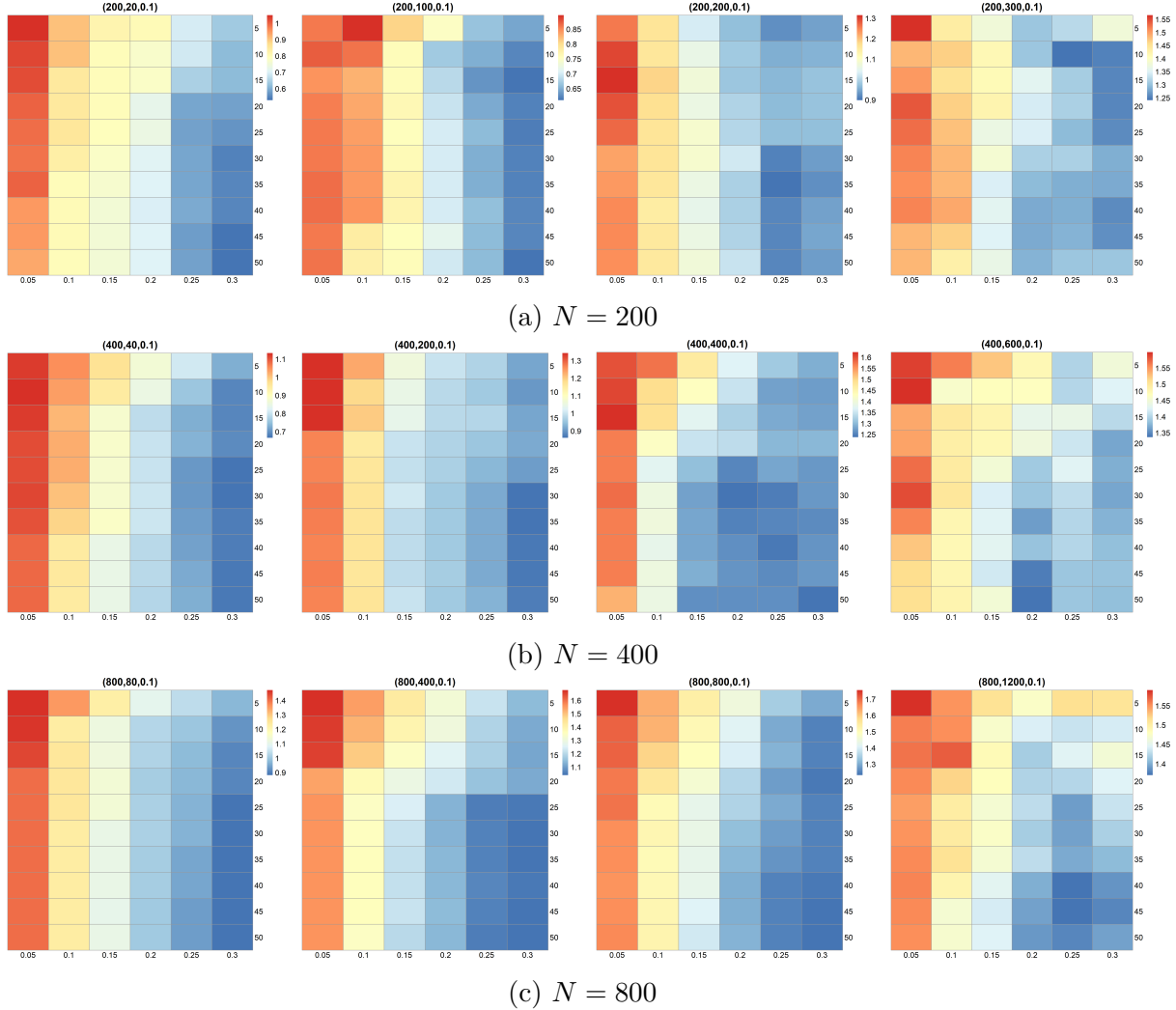


Figure B.6: CV results for Section 3.3: exponential decay with $\rho = 0.1$. Values in parenthesis denote (N, K, ρ) . The x -axis represents the selection probability p and the y -axis indicates the number of candidate models M . Dark blue regions correspond to the (p, M) combinations yielding the lowest MSE.

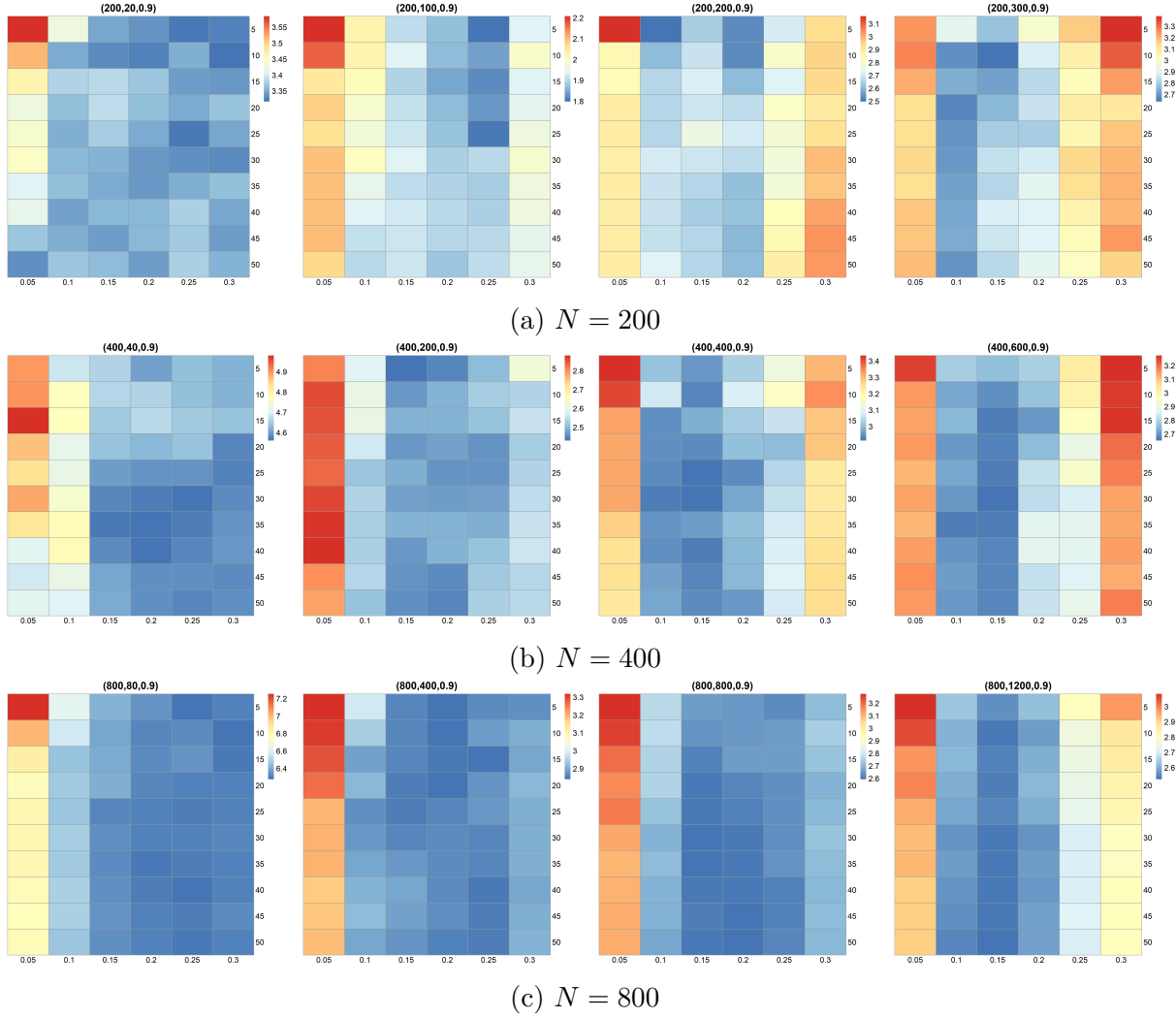


Figure B.7: CV results for Section 3.3: exponential decay with $\rho = 0.9$. Values in parenthesis denote (N, K, ρ) . The x -axis represents the selection probability p and the y -axis indicates the number of candidate models M . Dark blue regions correspond to the (p, M) combinations yielding the lowest MSE.

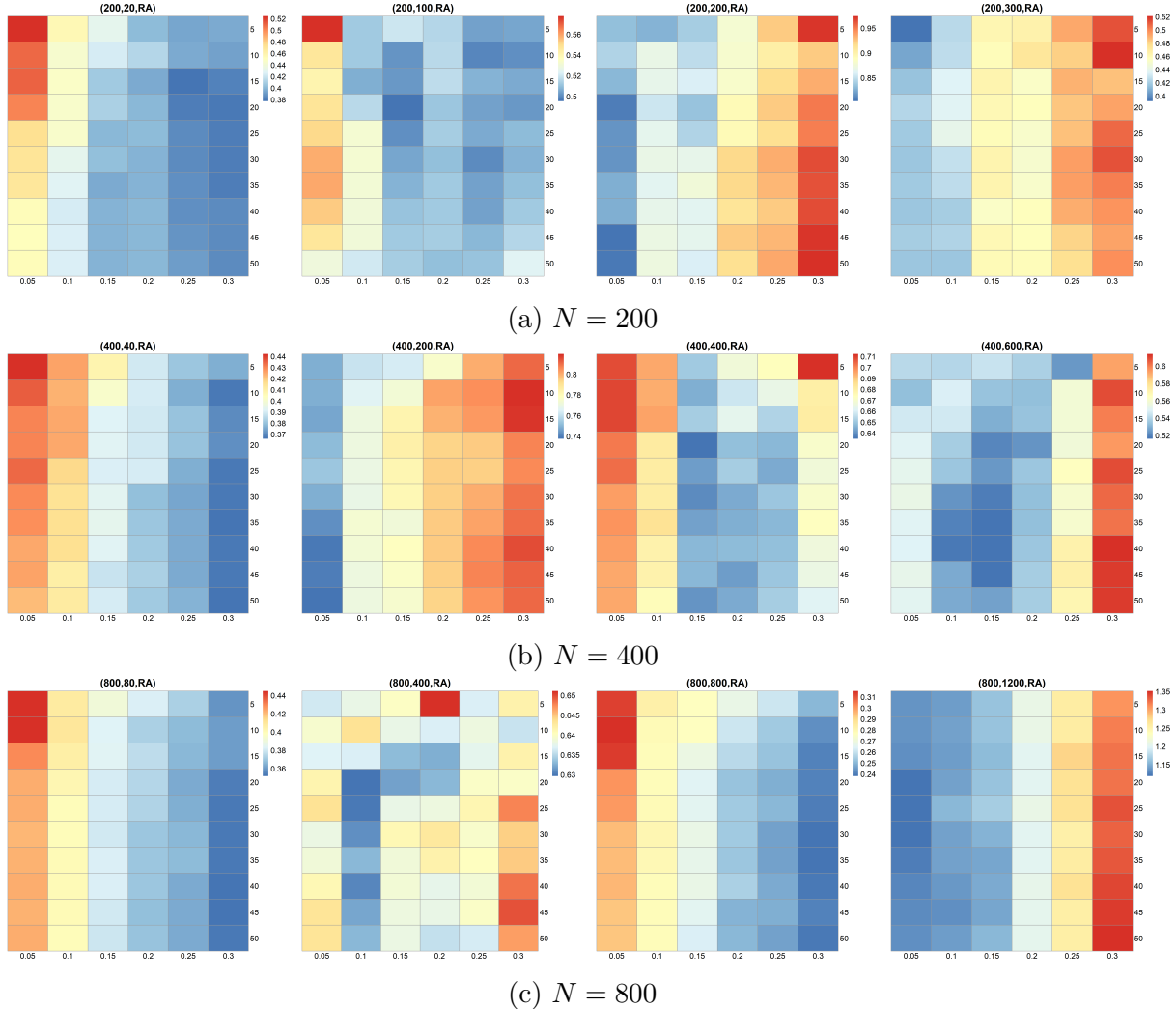


Figure B.8: CV results for Section 3.3: exponential decay with random covariance structure. Values in parenthesis denote (N, K, ρ) . The x -axis represents the selection probability p and the y -axis indicates the number of candidate models M . Dark blue regions correspond to the (p, M) combinations yielding the lowest MSE.

B.3.4 CV results for Section 3.4

Figures B.9–B.14 report the cross-validation results in settings where a large number of covariates are believed to contribute to predictive performance. The findings are consistent with our earlier conclusions and further support the effectiveness of the cross-validation procedure.

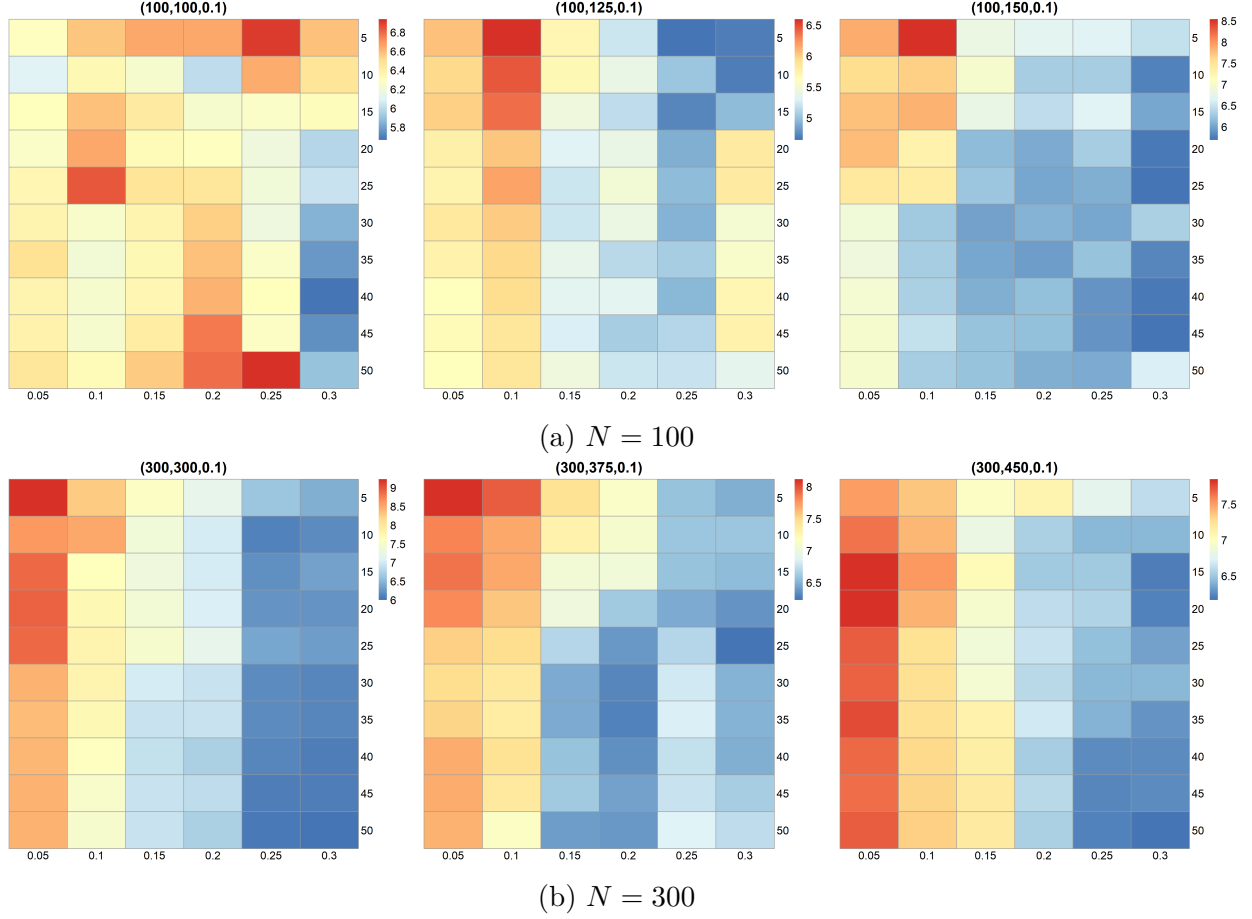


Figure B.9: CV results for Section 3.4: polynomial decay with $\rho = 0.1$. Values in parenthesis denote (N, K, ρ) . The x -axis represents the selection probability p and the y -axis indicates the number of candidate models M . Dark blue regions correspond to the (p, M) combinations yielding the lowest MSE.

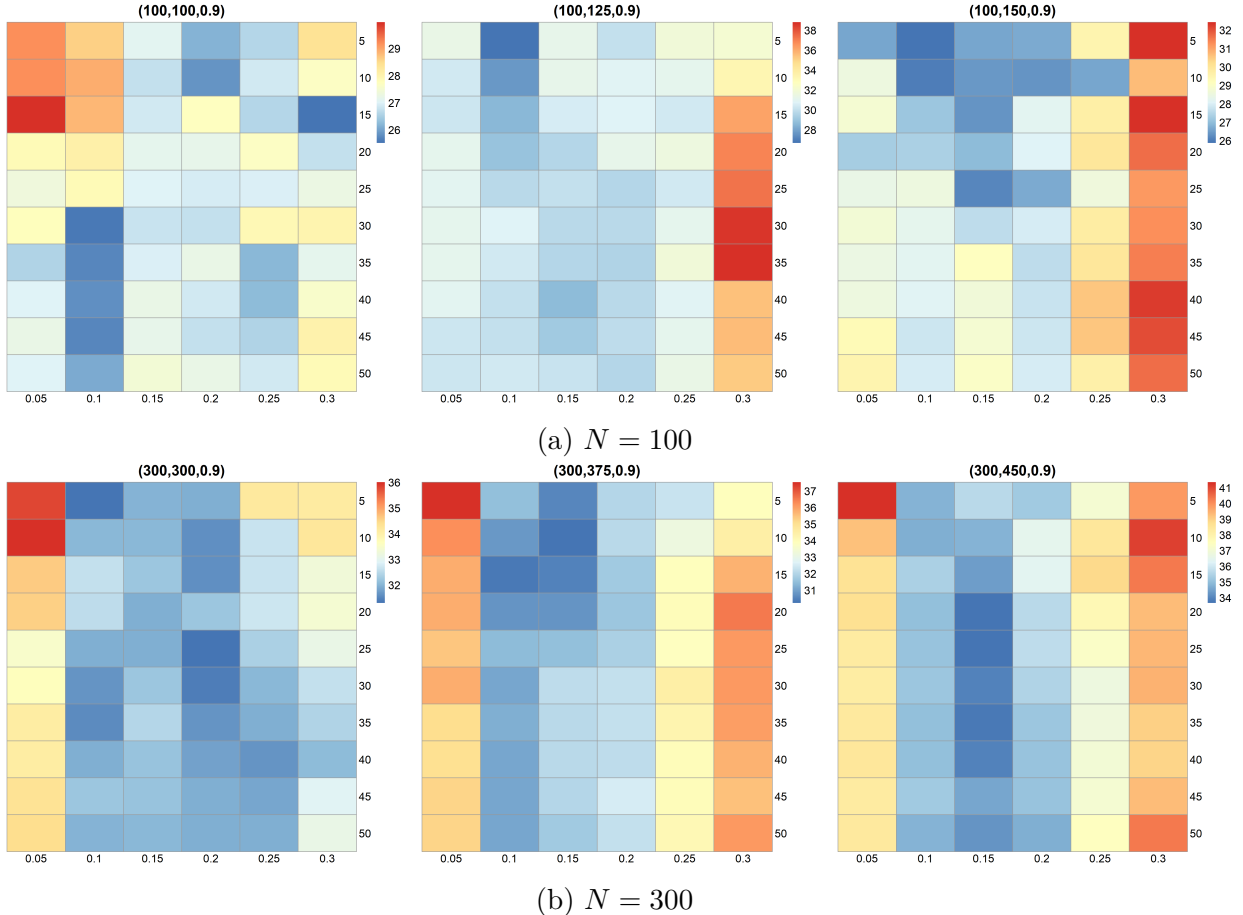


Figure B.10: CV results for Section 3.4: polynomial decay with $\rho = 0.9$. Values in parenthesis denote (N, K, ρ) . The x -axis represents the selection probability p and the y -axis indicates the number of candidate models M . Dark blue regions correspond to the (p, M) combinations yielding the lowest MSE.

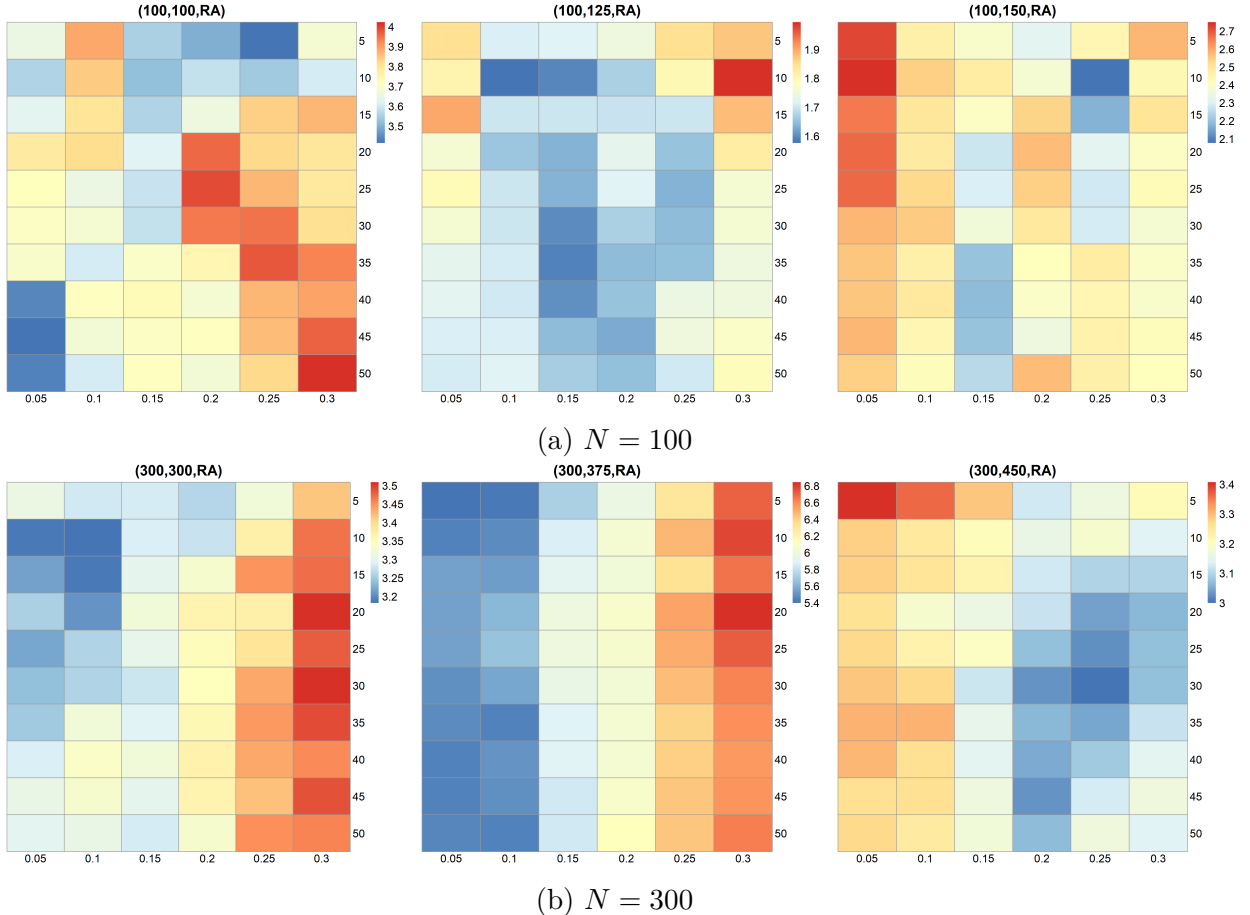


Figure B.11: CV results for Section 3.4: polynomial decay with random covariance structure. Values in parenthesis denote (N, K, ρ) . The x -axis represents the selection probability p and the y -axis indicates the number of candidate models M . Dark blue regions correspond to the (p, M) combinations yielding the lowest MSE.

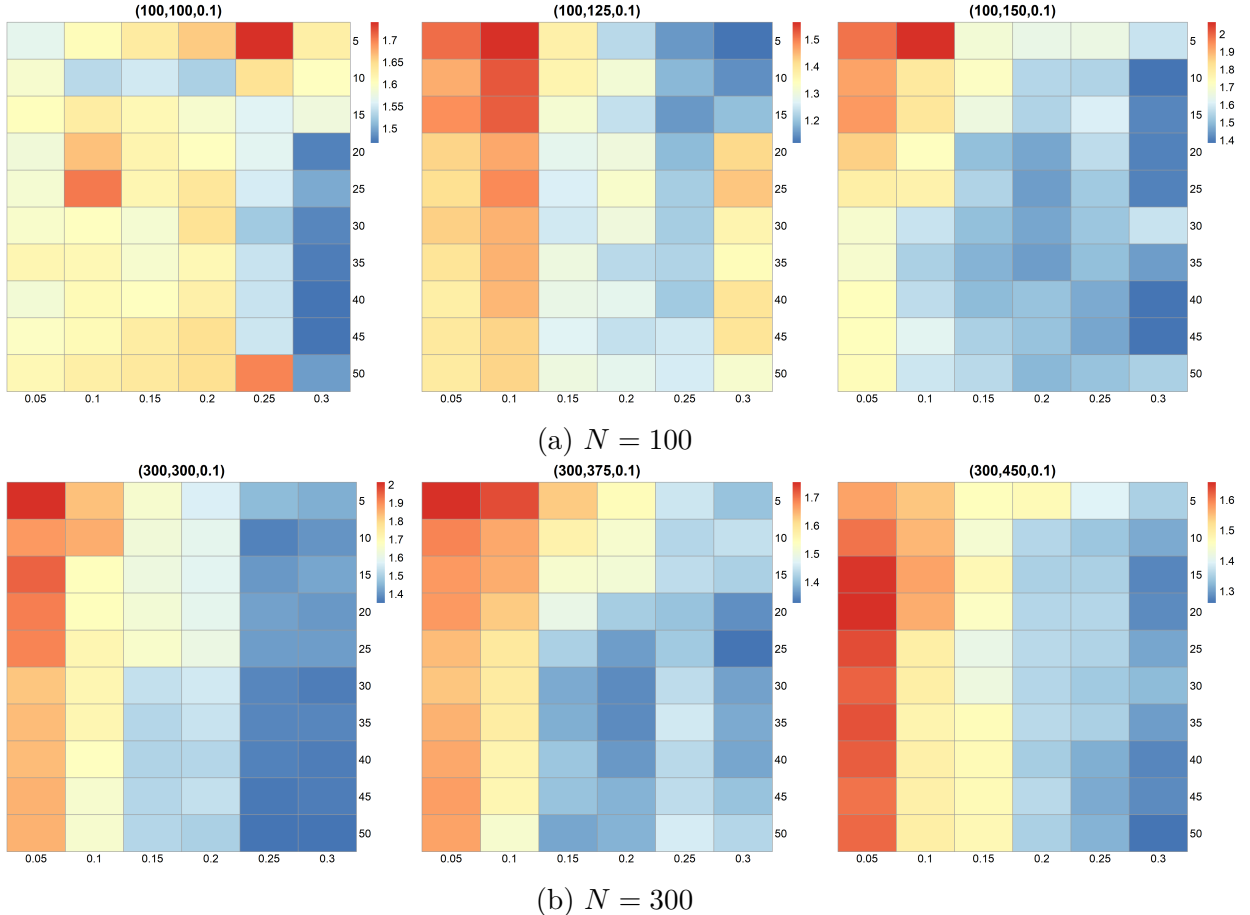


Figure B.12: CV results for Section 3.4: exponential decay with $\rho = 0.1$. Values in parenthesis denote (N, K, ρ) . The x -axis represents the selection probability p and the y -axis indicates the number of candidate models M . Dark blue regions correspond to the (p, M) combinations yielding the lowest MSE.

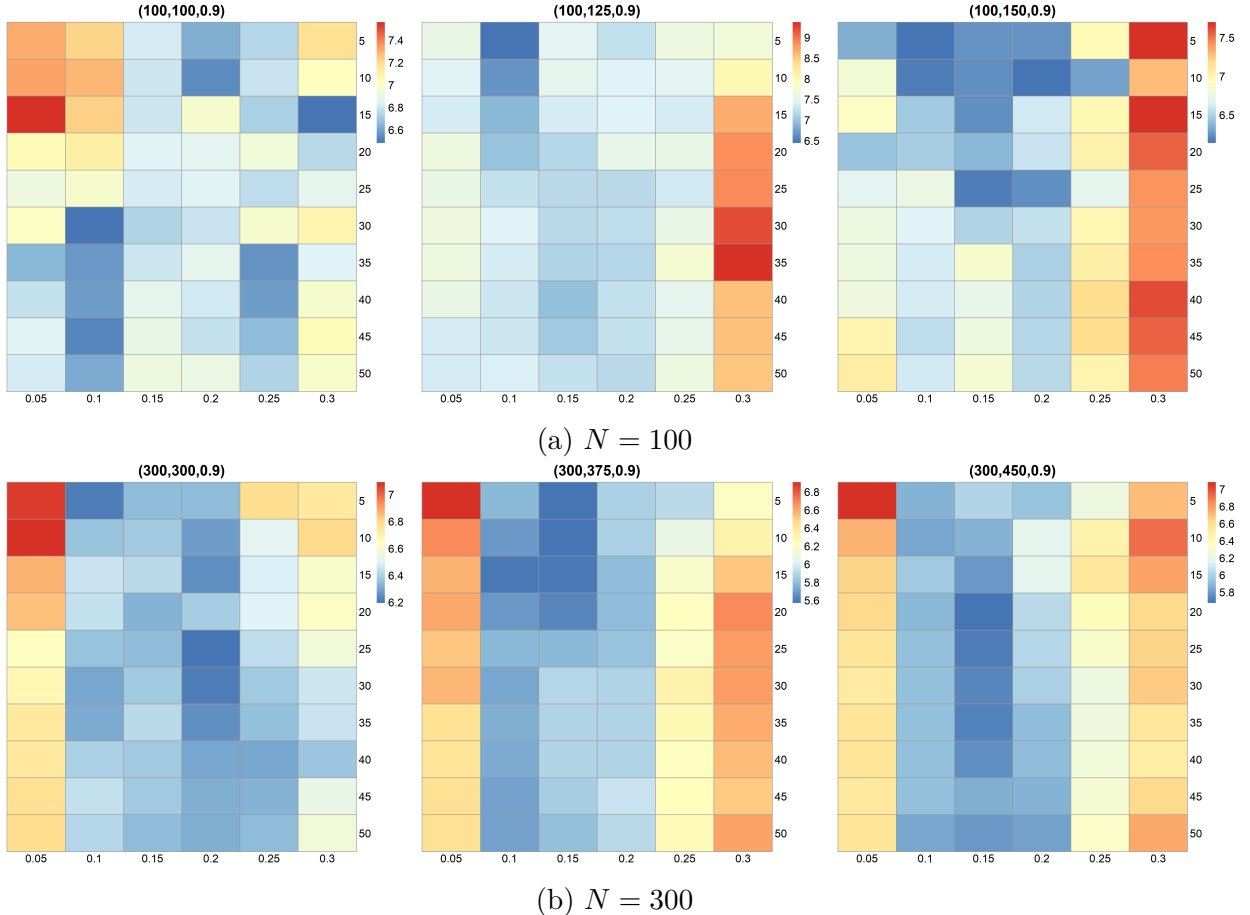


Figure B.13: CV results for Section 3.4: exponential decay with $\rho = 0.9$. Values in parenthesis denote (N, K, ρ) . The x -axis represents the selection probability p and the y -axis indicates the number of candidate models M . Dark blue regions correspond to the (p, M) combinations yielding the lowest MSE.

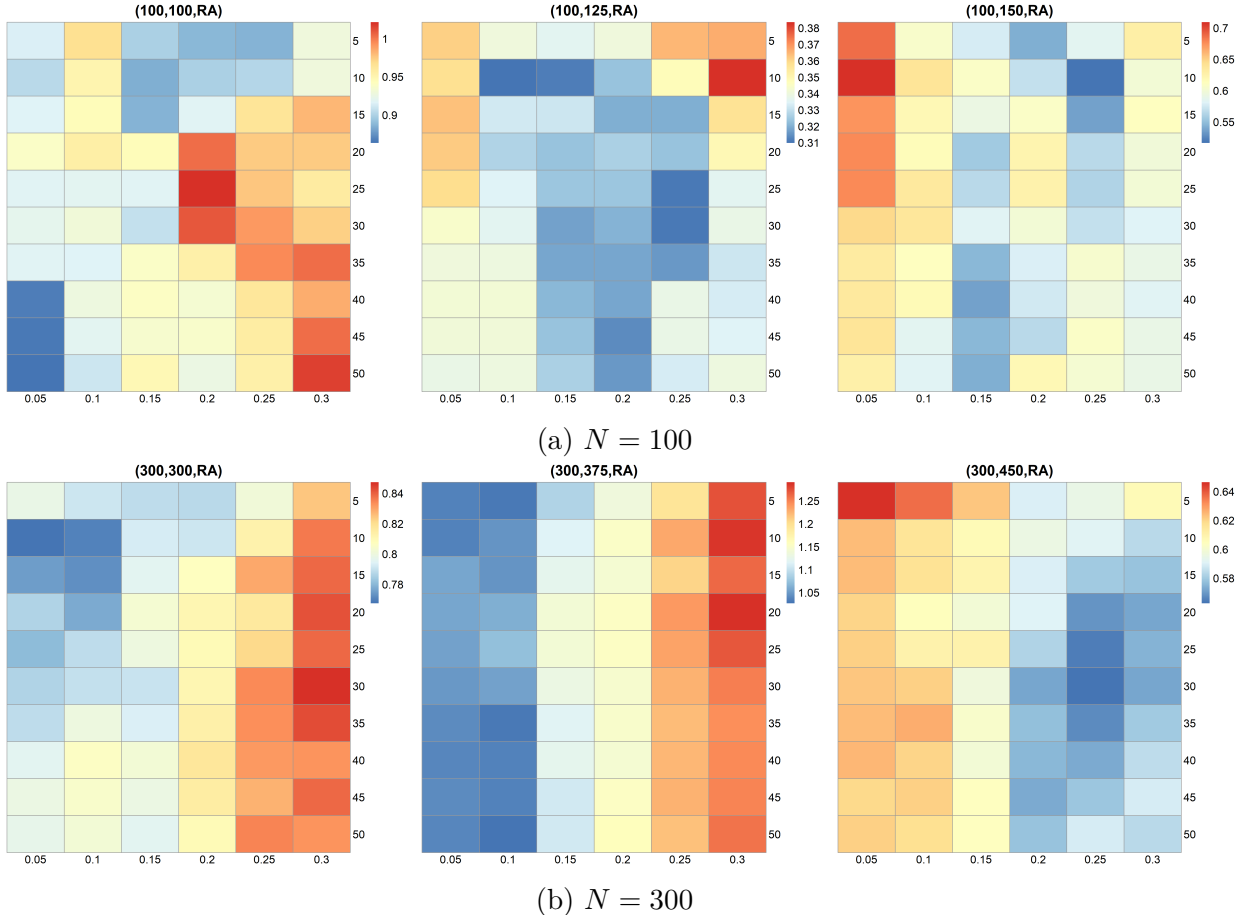


Figure B.14: CV results for Section 3.4: exponential decay with random covariance structure. Values in parenthesis denote (N, K, ρ) . The x -axis represents the selection probability p and the y -axis indicates the number of candidate models M . Dark blue regions correspond to the (p, M) combinations yielding the lowest MSE.

B.4 MSE results in simulations

Tables B.4 to B.7 reports the MSE comparisons for Section 3.2 to 3.4, with the smallest value in each row highlighted in bold. Notably RSA.opt achieves the smallest training error when it has the smallest out-of-sample prediction error.

Table B.4: MSE comparison in Section 3.2: polynomial decay.

ρ	N	K	RSA.opt	RSA.fix	RSR	Lasso	SCAD	MCP	PMA	MMA	RF
0.1	200	20	0.54	1.36	3.15	0.19	0.19	0.19	0.79	0.19	0.88
		100	0.81	1.52	2.95	0.75	0.71	0.71	3.71	0.74	1.09
		200	1.15	1.89	3.11	1.37	1.40	1.41	4.62	2.01	1.37
		300	1.40	2.03	3.06	1.73	1.89	1.87	5.03	2.17	1.53
	400	40	0.88	1.95	3.69	0.21	0.21	0.21	1.47	0.21	1.10
		200	1.00	2.02	3.43	0.85	0.80	0.80	4.59	0.85	1.27
		400	1.59	2.34	3.54	1.51	1.49	1.49	5.32	2.28	1.53
		600	1.61	2.43	3.45	1.88	1.95	1.94	5.71	2.45	1.69
	800	80	1.13	2.52	4.21	0.24	0.24	0.24	3.32	0.23	1.33
		400	1.20	2.52	3.90	0.96	0.89	0.89	5.28	0.97	1.46
		800	1.44	2.81	3.97	1.66	1.60	1.59	5.95	2.55	1.70
		1200	1.62	2.86	3.83	2.04	2.04	2.04	6.35	2.72	1.85
0.9	200	20	0.72	0.80	2.27	0.83	1.26	1.26	4.82	1.39	3.09
		100	0.99	1.02	1.68	1.32	1.72	1.73	15.38	3.15	2.80
		200	1.65	1.58	1.96	2.37	2.88	2.82	19.82	8.63	3.95
		300	2.00	2.00	2.15	3.25	3.71	3.74	21.03	9.16	4.66
	400	40	0.88	1.00	2.90	1.04	1.61	1.59	10.26	1.92	5.03
		200	1.02	1.14	1.88	1.37	1.83	1.82	19.60	3.64	3.64
		400	1.52	1.68	2.15	2.38	2.96	2.98	21.96	9.45	4.78
		600	2.01	2.10	2.35	3.34	3.85	3.83	22.99	9.88	5.47
	800	80	0.82	1.24	3.36	1.16	1.79	1.78	26.50	2.30	7.10
		400	1.05	1.35	2.09	1.41	1.91	1.91	21.90	3.99	4.53
		800	1.65	1.88	2.36	2.50	3.05	3.07	23.51	10.08	5.61
		1200	2.03	2.21	2.50	3.47	3.95	3.96	24.42	10.44	6.18
RA	200	20	0.18	0.24	1.51	0.15	0.17	0.17	0.36	0.14	0.43
		100	0.11	0.14	0.21	0.17	0.18	0.17	0.32	0.16	0.19
		200	0.52	0.43	0.64	0.52	0.52	0.52	1.19	1.04	0.51
		300	0.62	0.54	0.59	0.89	0.90	0.90	1.78	2.05	0.81
	400	40	0.15	0.30	0.74	0.09	0.09	0.09	0.31	0.08	0.35
		200	0.49	0.41	0.68	0.38	0.35	0.35	1.05	0.39	0.49
		400	0.20	0.21	0.26	0.33	0.31	0.31	0.58	0.81	0.32
		600	0.47	0.48	0.56	0.75	0.67	0.67	1.41	2.00	0.78
	800	80	0.16	0.23	0.37	0.20	0.23	0.23	0.64	0.15	0.60
		400	0.20	0.20	0.27	0.25	0.20	0.21	0.46	0.26	0.31
		800	0.29	0.51	0.68	0.37	0.42	0.42	1.11	0.64	0.41
		1200	0.81	0.69	0.82	1.07	0.94	0.94	1.72	2.57	1.05

Note: Values in bold indicate the smallest MSE.

Table B.5: MSE comparison in Section 3.3: exponential decay.

ρ	N	K	RSA.opt	RSA.fix	RSR	Lasso	SCAD	MCP	PMA	MMA	RF
0.1	200	20	0.14	0.36	0.71	0.04	0.04	0.04	0.26	0.04	0.21
		100	0.21	0.41	0.68	0.18	0.16	0.17	0.89	0.17	0.27
		200	0.30	0.50	0.74	0.33	0.36	0.35	1.11	0.48	0.34
		300	0.33	0.52	0.72	0.42	0.47	0.47	1.19	0.52	0.38
	400	40	0.24	0.53	0.88	0.05	0.05	0.05	0.52	0.05	0.28
		200	0.27	0.54	0.82	0.20	0.19	0.19	1.10	0.21	0.32
		400	0.30	0.60	0.83	0.35	0.35	0.35	1.25	0.53	0.37
		600	0.39	0.60	0.79	0.43	0.43	0.43	1.31	0.56	0.40
	800	80	0.30	0.68	1.01	0.06	0.06	0.06	0.91	0.06	0.34
		400	0.31	0.65	0.91	0.22	0.20	0.20	1.25	0.23	0.36
		800	0.32	0.66	0.89	0.36	0.32	0.32	1.33	0.57	0.39
		1200	0.36	0.64	0.82	0.42	0.37	0.38	1.36	0.58	0.41
0.9	200	20	0.18	0.20	0.54	0.21	0.31	0.32	1.19	0.35	0.77
		100	0.25	0.26	0.41	0.34	0.45	0.45	3.95	0.81	0.72
		200	0.43	0.41	0.49	0.62	0.75	0.75	5.15	2.24	1.03
		300	0.50	0.51	0.53	0.83	0.95	0.95	5.32	2.32	1.19
	400	40	0.22	0.26	0.73	0.27	0.42	0.42	2.72	0.51	1.32
		200	0.26	0.30	0.47	0.36	0.49	0.48	5.10	0.95	0.95
		400	0.37	0.42	0.51	0.60	0.73	0.73	5.37	2.31	1.18
		600	0.46	0.48	0.54	0.77	0.88	0.88	5.24	2.25	1.25
	800	80	0.20	0.32	0.84	0.30	0.47	0.47	6.86	0.60	1.84
		400	0.25	0.33	0.50	0.35	0.48	0.48	5.36	0.98	1.12
		800	0.35	0.41	0.51	0.54	0.65	0.65	5.01	2.15	1.20
		1200	0.40	0.44	0.50	0.65	0.74	0.74	4.64	1.98	1.18
RA	200	20	0.04	0.06	0.30	0.03	0.03	0.03	0.09	0.03	0.09
		100	0.03	0.03	0.05	0.03	0.03	0.03	0.07	0.03	0.04
		200	0.13	0.11	0.15	0.12	0.13	0.13	0.27	0.21	0.11
		300	0.15	0.13	0.14	0.22	0.23	0.23	0.43	0.47	0.19
	400	40	0.04	0.08	0.17	0.02	0.02	0.02	0.08	0.02	0.08
		200	0.13	0.11	0.16	0.08	0.08	0.08	0.24	0.08	0.11
		400	0.04	0.05	0.06	0.07	0.07	0.07	0.11	0.13	0.06
		600	0.11	0.12	0.13	0.19	0.17	0.17	0.33	0.47	0.18
	800	80	0.04	0.06	0.09	0.04	0.05	0.05	0.14	0.03	0.13
		400	0.05	0.05	0.06	0.05	0.04	0.04	0.10	0.05	0.06
		800	0.06	0.12	0.16	0.07	0.08	0.08	0.25	0.12	0.09
		1200	0.18	0.15	0.18	0.23	0.20	0.20	0.39	0.56	0.23

Note: Values in bold indicate the smallest MSE.

Table B.6: MSE comparison in Section 3.4: polynomial decay.

ρ	N	K	RSA.opt	RSA.fix	RSR	Lasso	SCAD	MCP	PMA	MMA	RF
0.1	100	100	1.35	2.27	3.68	1.90	2.48	2.49	5.39	2.41	1.75
		125	1.62	2.34	3.56	2.18	2.87	2.85	5.52	2.51	1.85
		150	1.53	2.39	3.56	2.35	3.02	3.08	5.66	2.56	1.93
	300	300	1.60	3.11	4.38	2.12	2.61	2.60	6.67	2.87	2.01
		375	1.68	3.14	4.28	2.36	2.91	2.91	6.88	2.96	2.10
		450	1.71	3.11	4.19	2.54	3.15	3.16	7.07	3.02	2.15
0.9	100	100	6.21	4.49	4.06	7.13	8.61	8.61	52.83	24.35	10.21
		125	5.02	5.17	4.15	8.55	9.88	9.92	54.81	25.24	11.35
		150	5.69	5.80	4.80	9.79	11.25	11.24	57.12	25.58	12.41
	300	300	4.49	4.34	4.56	6.87	8.91	8.94	63.97	27.74	13.76
		375	4.59	4.89	4.76	8.13	10.14	10.09	65.49	28.13	14.78
		450	5.24	5.30	5.03	9.57	11.40	11.46	66.04	28.34	15.39
RA	100	100	0.63	0.64	0.58	1.03	1.00	1.00	2.21	3.45	1.17
		125	0.50	0.48	0.61	0.72	0.76	0.76	1.19	1.17	0.57
		150	0.52	0.55	0.69	0.80	0.91	0.91	1.81	1.23	0.62
	300	300	0.62	0.59	0.75	0.80	0.78	0.78	1.71	1.86	0.79
		375	0.49	0.43	0.47	0.65	0.61	0.61	1.06	2.03	0.75
		450	0.62	0.65	0.81	0.96	1.02	1.01	1.64	1.74	0.81

Note: Values in bold indicate the smallest MSE.

Table B.7: MSE comparison in Section 3.4: exponential decay.

ρ	N	K	RSA.opt	RSA.fix	RSR	Lasso	SCAD	MCP	PMA	MMA	RF
0.1	100	100	0.34	0.58	0.87	0.46	0.67	0.67	1.28	0.57	0.43
		125	0.36	0.58	0.84	0.53	0.76	0.76	1.29	0.59	0.44
		150	0.36	0.58	0.83	0.56	0.79	0.80	1.29	0.59	0.46
	300	300	0.40	0.71	0.95	0.45	0.52	0.53	1.45	0.62	0.44
		375	0.36	0.69	0.90	0.49	0.56	0.56	1.45	0.62	0.45
		450	0.36	0.66	0.87	0.51	0.59	0.59	1.45	0.62	0.45
0.9	100	100	1.13	1.13	1.01	1.74	2.18	2.18	13.42	6.16	2.59
		125	1.23	1.26	1.01	2.10	2.43	2.42	13.40	6.18	2.78
		150	1.35	1.37	1.13	2.32	2.65	2.63	13.57	6.06	2.94
	300	300	0.87	0.87	0.92	1.38	1.75	1.74	12.59	5.46	2.71
		375	0.85	0.91	0.90	1.48	1.84	1.83	11.90	5.11	2.68
		450	0.91	0.92	0.90	1.63	1.92	1.94	11.18	4.80	2.60
RA	100	100	0.15	0.15	0.13	0.24	0.23	0.23	0.50	0.76	0.26
		125	0.12	0.12	0.15	0.18	0.19	0.19	0.28	0.29	0.14
		150	0.13	0.14	0.16	0.20	0.22	0.22	0.45	0.32	0.15
	300	300	0.17	0.14	0.17	0.18	0.18	0.18	0.37	0.43	0.18
		375	0.09	0.09	0.10	0.14	0.13	0.13	0.23	0.43	0.16
		450	0.15	0.15	0.17	0.24	0.25	0.25	0.36	0.47	0.20

Note: Values in bold indicate the smallest MSE.

B.5 Additional results for Section 4

B.5.1 Plot of Log returns for two periods

Figure B.15 displays the log returns during the pre- and post-crisis periods. Due to macroeconomic shocks, such as the European sovereign debt crisis around 2010-2012, S&P 500 log returns exhibits significantly higher volatility in the post-crisis period compared to the pre-crisis period.

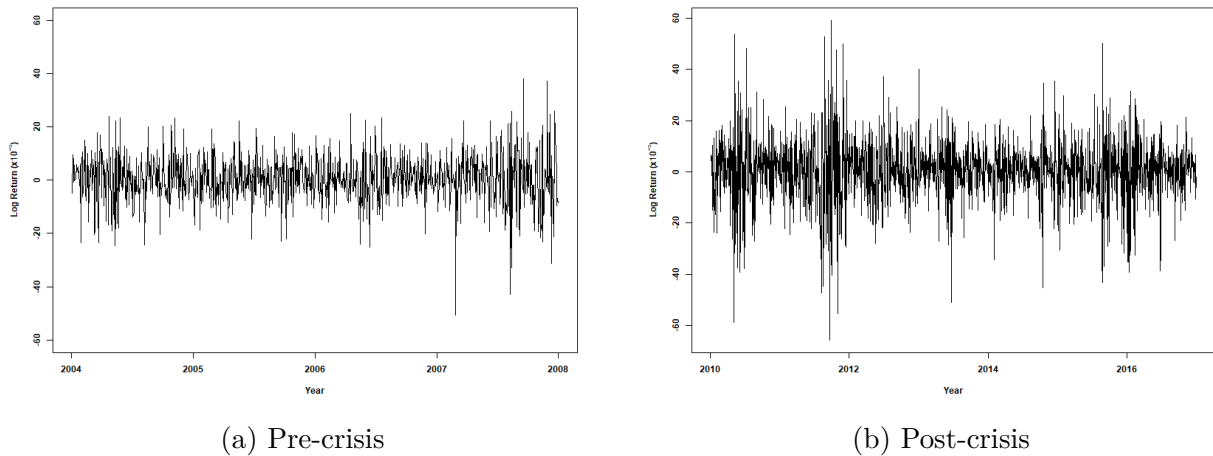


Figure B.15: Log returns of S&P 500 for two periods.

B.5.2 Tuning parameters selected by CV

Based on the CV-selected tuning parameters from the simulation and our preliminary exploration, we set the tuning grid as $p \in [0.01, 0.3]$ with an increment of 0.02 and $M \in [1, 29]$ with an increment of 2 for the pre-crisis period. For the post-crisis period, we use $p \in [0.1, 0.3]$ with an increment of 0.02 and $M \in [1, 29]$ with an increment of 2. Figure B.16 displays the cross-validation results for both periods. Because the factors are orthogonalized, RSA tends to select each factor with a relatively high selection probability, for example, in the post-crisis period, while its performance is not highly sensitive to the number of candidate models. These results closely resemble the CV findings under the

low-correlation setting in Section 3.4.

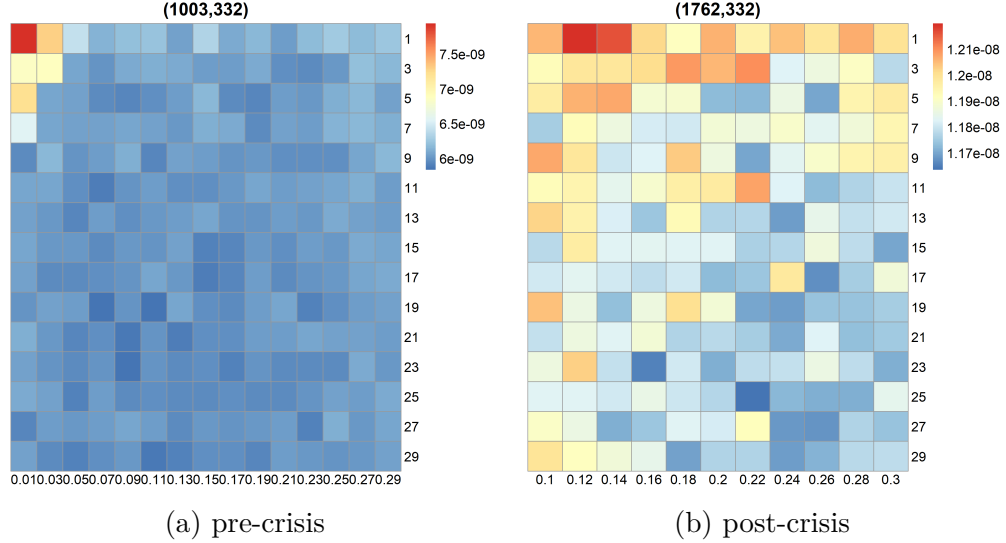


Figure B.16: CV results for Section 4. Values in parenthesis denote (N, K) . The x -axis represents the selection probability p and the y -axis indicates the number of candidate models M . Dark blue regions correspond to the (p, M) combinations yielding the lowest MSE.

B.5.3 Standard deviation of MSFE for different methods

Figure B.17 reports the standard deviation of MSFE for each forecast horizon. In the pre-crisis period, RSA exhibits lower volatility for most horizons, while in the post-crisis period, it consistently achieves the lowest prediction volatility in each horizon.

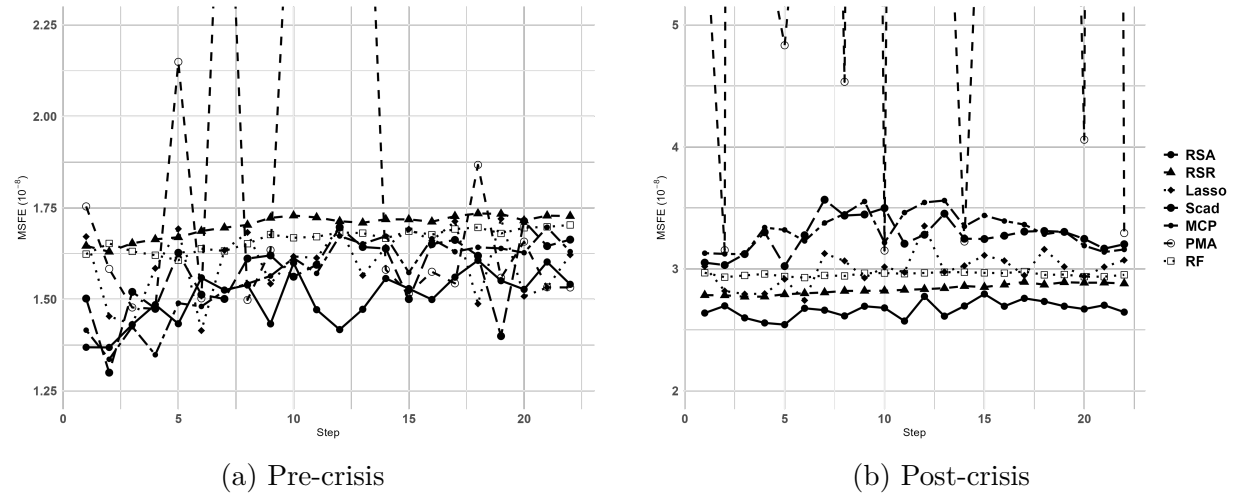


Figure B.17: Standard deviation of MSFE for each forecast horizon.

B.5.4 MSE results for different methods

Table B.8 presents the training error for each subperiod, showing that RSA's superior out-of-sample performance is not achieved at the expense of higher training error.

Table B.8: MSE ($\times 10^{-9}$) comparison for empirical analysis.

Period	RSA	RSR	Lasso	SCAD	MCP	PMA	RF
pre-crisis	3.00	2.90	2.18	3.16	3.20	4.71	1.31
post-crisis	4.56	6.07	5.29	8.14	8.14	9.71	2.93